Analysis of ERBB signalling and the impact of targeted therapeutics using protein microarrays

Inaugural - Dissertation

zur
Erlangung der Doktorwürde der
Naturwissenschaftlich-Mathematischen Gesamtfakultät der
Ruprecht-Karls-Universität
Heidelberg

vorgelegt von
Diplom Biologin Frauke Margarete Henjes
aus Düsseldorf

Tag der mündlichen Prüfung: 29.10.2010

Die vorliegende Arbeit wurde zwischen Oktober 2006 und September 2010 in der Abteilung Molekulare Genomanalyse am Deutschen Krebsforschungszentrum (DKFZ) in Heidelberg durchgeführt.

Gutachter:	Prof. Dr. Werner Buselmaier
	PD Dr. Holger Sültmann

Danksagung

Herrn Prof. Dr. Werner Buselmaier danke ich für die freundliche Übernahme des Erstgutachtens.

Herrn PD Dr. Holger Sültmann möchte ich für die Übernahme des Zweitgutachtens sowie die vielen, guten Ratschläge danken.

Meiner Gruppenleiterin, Frau Dr. Ulrike Korf, danke ich herzlich für die Bereitstellung des Themas, die Betreuung und Unterstützung meiner Arbeit.

Herrn PD Dr. Stefan Wiemann möchte ich für die Leitung der Abteilung nach dem tragischen Tod von Prof. Dr. Annemarie Poustka danken, die es mir ermöglicht hat, meine Arbeit fortzusetzen.

Ein ganz großer Dank geht besonders an Sabrina Schumacher und Corinna Becki sowie Maike Wosch und Daniela Heiss für ihren unermüdlichen Laboreinsatz! Der Proteomicsgruppe danke ich für die gute Zusammenarbeit, besonders Frank Götschel fürs Korrekturlesen und Heiko Mannsperger für die Hilfe bei der RPPA Auswertung. Ein besonderer Dank geht an Christian Schmidt für die tatkräftige Unterstützung bei allem was mit automatización zu tun hat.

Den Mitgliedern des BreastSys Konsortiums unter Koordination von Prof. Dr. Tim Beißbarth möchte ich für die vielen konstruktiven Diskussionen und die gute Zusammenarbeit danken. Christian Bender danke ich für die bioinformatischen Arbeiten, die hilfreichen Diskussionen und die schnelle Hilfe bei der Ausführung der Analysen sowie Stephan Gade für die Hilfe bei allen R- und LaTeX-Problemen. Uli Tschulena und Anja Irsigler danke ich herzlich für die Hilfe bei den Zellzyklusanalysen.

Außerdem danke ich allen Kollegen, die mich während meiner Zeit in Heidelberg unterstützt und begleitet haben, besonders Mark Fellmann, Christian Löbke, Markus und Claudia Ruschhaupt, Stephan Gade, Jan C. Brase und Christian Bender.

Ein herzliches Dankeschön geht an Petra Burmeister, Britta Gepperth, Renate Becker, Simone Kutschera, Maria Riedel und Anika Jöcker für die vielen Unternehmungen und die schöne Zeit in Heidelberg.

Ganz herzlich bedanken möchte ich mich bei Florian Fuchs für seine Unterstützung ganz besonders in den letzten drei Monaten.

Ein besonderer, herzlicher Dank gebührt meinen Eltern, die immer an mich geglaubt und mich bei allen Entscheidungen unterstützt haben.

Für Henning

Contents

Zusammenfassung

Ziel dieser Arbeit war die Analyse der ERBB-Rezeptor anhängigen Signalwege in unterschiedlichen Brustkrebszelllinien und die Etablierung sensitiver Methoden für die quantitative Untersuchung von Signalnetzwerken. Zunächst wurde ein automatisiertes Protokoll für die reproduzierbare Zellstimulation mit Wachstumsfaktoren entwickelt. Des Weiteren wurden Proteinarrays dahingehend angepasst, dass sie für die umfangreiche Analyse von phosphorylierten Proteinen eingesetzt werden konnten, wobei zwei Plattformen angewandt wurden: Microspot Immunoassays und Reverse Phase Protein Arrays. Für die Datenanalyse wurden in Zusammenarbeit mit der Bioinformatik-Gruppe der Abteilung verschiedene Algorithmen entwickelt. Experimente in den ERBB2 überexprimierenden Zelllinien HCC1954 und SKBR3 zeigten, dass die therapeutischen Antikörper gegen ERBB2, Trastuzumab und Pertuzumab, die ligandenabhängige Aktivierung der ERBB Signalkaskaden nicht wirkungsvoll verhindern konnten, und auch durch die Kombination beider Antikörper konnte keine stärkere Inhibition erzielt werden. Im Gegensatz dazu reduzierte die Kombination eines der Antikörper mit dem EGFR Inhibitor Erlotinib signifikant die Liganden induzierte Aktivierung der ERBB Signalkaskaden. Zusätzlich führte die Anwendung der Kombination von Trastuzumab mit Erlotinib auf proliferierenden Zellen zu einer Reduktion der Phosphorylierung des ribosomalen Proteins S6 und des Zellzyklusregulatorproteins RB und damit zu einem Zellzyklusarrest. Daher konnte die Kombination von Erlotinib mit Trastuzumab als potentielle Therapiemöglichkeit für Patientinnen mit ERBB2-positivem Brustkrebs postuliert werden. Der Vergleich der ERBB Signalkaskaden in den Zelllinien MCF7, SKBR3, HCC1954 und BT474 zeigte, dass S6 ein guter Indikator für den Aktivitätsstatus des Signalnetzwerks ist, da S6 durch Signale der ERBB Rezeptorabhängigen PI3K- und der MAPK-Signalkaskaden aktiviert wird. Während diese beiden Signalkaskaden bedingt durch verschiedene Expressionsmuster der Rezeptoren und durch onkogene Mutationen in den Zelllinien unterschiedlich auf die Therapeutika reagierten, spiegelte die Phosphorylierung des Proteins S6 den Einfluss exogener Signale am zuverlässigsten wider.

Summary

This work was focused on the quantitative analysis of time-resolved *in vitro* measurements of ligand-induced ERBB signalling in breast cancer cell lines, as well as the development of experimental methods suitable for the large-scale analysis of signalling networks. First, an automated protocol for the highly reproducible stimulation of cell lines with growth factors was developed. In parallel, protein microarray technologies were advanced to the quantification of phosphoproteins and resulted in two different assay formats: microspot immunoassays and reverse phase protein arrays. In collaboration with the bioinformatics group, data analysis tools were developed for both platforms. Experiments in ERBB2 overexpressing cell lines, HCC1954 and SKBR3, demonstrated that both ERBB2 targeting monoclonal antibodies, trastuzumab and pertuzumab, did not efficiently prevent ligand-induced signalling *in vitro*. Moreover, the combination of both antibody therapeutics did not result in improved efficacy. However, combining a single therapeutic antibody with the EGFR inhibiting small molecule erlotinib significantly downregulated ligand-induced signalling. Furthermore, treatment of proliferating cells with the combination of trastuzumab and erlotinib resulted in a dephosphorylation of the ribosomal protein S6 and the cell cycle regulator protein RB resulting in cell cycle arrest. Thus, the combination of erlotinib with trastuzumab could be postulated as potential therapy for the treatment of ERBB2-positive breast cancer patients. A comparative analysis of ERBB signalling in four cell lines, MCF7, BT474, HCC1954, and SKBR3, revealed that the phosphorylation of the ribosomal protein S6 is a strong predictor to analyse the activation status of signalling networks since the S6 protein integrates signals from the MAPK as well as the PI3K pathway, the two major pathways downstream of ERBB receptors. Due to differential ERBB receptor expression or additional oncogenic mutations, therapeutics affected ERK1/2 and AKT signalling to different extents in the four cell lines whereas the S6 phosphorylation reflected reliably the cellular response on exogenous perturbations.

1 Introduction

1.1 Breast cancer

Cancer is one of the two leading causes of death in western countries. Cancer development is a multistep process and therefore, the cancer risk increases with age. Chromosomal aberrations like copy number variations, translocations, gene amplifications or deletions, and accumulation of mutations are the major causes of cancer. Six essential alterations in cell physiology lead to malignant growth: self-sufficiency in growth signals, insensitivity to growth-inhibitory signals, evasion of apoptosis, limitless replicative potential, sustained angiogenesis, and tissue invasion and metastasis (Hanahan and Weinberg, 2000). While lung cancer is the most frequent cancer in men with 1.09 million new cases in 2008 (16.5% of all diagnosed cancer cases), breast cancer is by far the most frequent cancer type among women with an estimated 1.38 million new cases in 2008 (23% of all diagnosed cancer cases) as delineated by the World Health Organization database (Globocan). Risk factors are among others an increased hormone level caused by childlessness, early menarche, late menopause or hormonal contraception. Mutations of the tumour suppressor genes BRCA1 and BRCA2 are linked to hereditary breast cancer (Hall et al., 1990). Physical activity and low alcohol consumption reduce the cancer risk. Breast cancer is a heterogeneous disease with respect to molecular alterations, cellular composition, and clinical outcome. Based on hierarchical clustering of gene expression data, the first molecular profile of breast cancer was published by Perou et al. (2000). Further analysis of the "intrinsic" gene expression pattern led to the identification of five subtypes with significant clinical implications: luminal A, luminal B, basal epithelial-like, ERBB2-positive, and normal breast-like (Sorlie et al. (2001); Fig. 1.1). Both luminal breast cancer subtypes exhibit a high expression level of the oestrogen receptor (ER) while the basal epithelial-like subtype is characterised by a high level of basal epithelial markers but a low level of ER/luminal-related

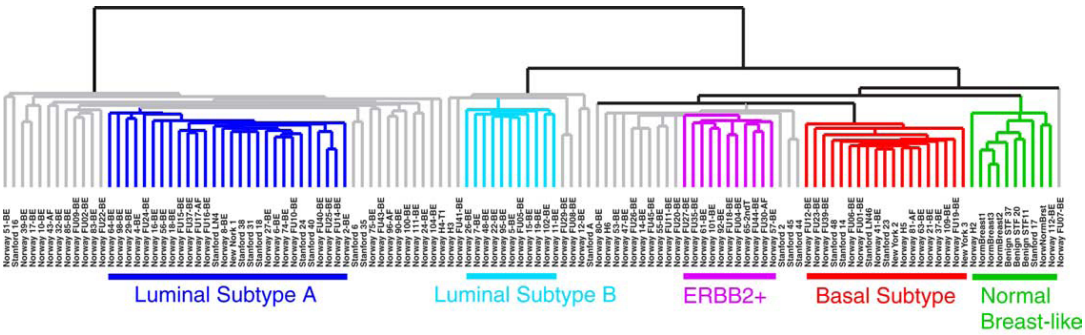

Figure 1.1: Cluster of breast cancer subtypes
Hierarchical clustering of 115 tumour tissues and seven non-malignant tissues. (Figure from Sorlie (2004).)

transcripts. Breast cancer samples related to the ERBB2-positive subtype generally have a high expression level of genes lying in the ERBB2 amplicon at chromosome 17q22.24. The normal breast-like subgroup shows the highest similarity with non-epithelial cells. However, it is still under discussion whether the normal breast-like type presents an important distinct molecular subtype or is due to poor sample quality (Sorlie, 2004). A significant correlation has been observed between the overall survival and chemotherapy sensitivity of the patients and the molecular subclasses (Fig. 1.2). Kaplan Meier survival analysis demonstrated that luminal subtypes are associated with the best clinical outcome. However, a subgroup of ER-positive breast cancer patients, the luminal B subtype, has a high proliferation rate and exhibits similarities in the gene expression level when compared to ER-negative breast cancer patients (Sorlie, 2004). Therefore, tumours classified as luminal B are associated with a poor clinical outcome. Additionally, the luminal B subtype is characterised by a lower expression level of ER/luminal specific genes which may sometimes lead to resistance against adjuvant hormone therapy. ERBB2 belongs to the ERBB family of receptor tyrosine kinases and is overexpressed in 20–30% of breast tumours. The ERBB2-positive subtype is associated with poor prognosis (Slamon et al., 1987) and a short overall survival (Sorlie et al., 2001). The basal breast-like subtype is often associated with the clinical triple-negative tumours which are negative for expression of ER, progesterone receptor and ERBB2. Comparable to the ERBB2-positive subtype, this subtype is also associated with poor prognosis and worse outcome (Dent et al., 2007).

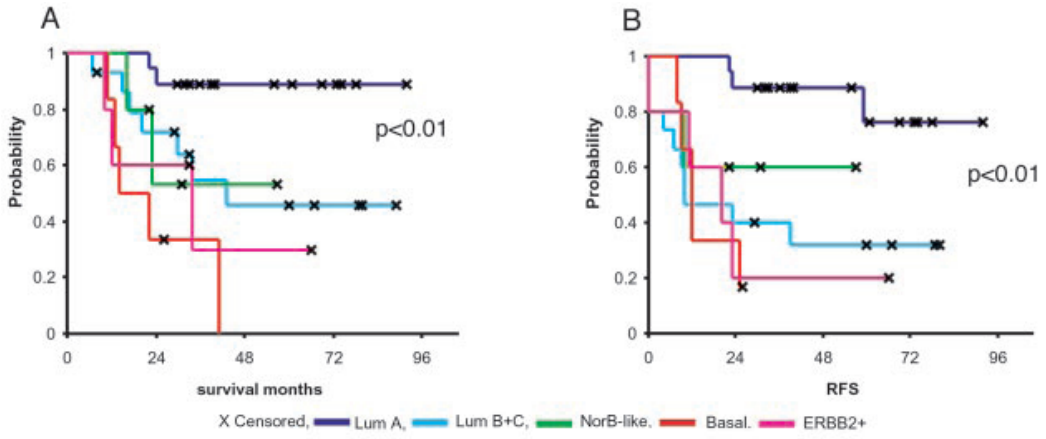

Figure 1.2: Survival depending on breast cancer subtypes
Overall (A) and relapse-free (B) survival analysis of 49 breast cancer patients, uniformly treated in a prospective study. (Figure from Sorlie et al. (2001)).

1.2 Breast cancer therapy

Standard cancer treatment like chemotherapy and radiation target highly proliferating cells by inhibiting cell division or DNA replication. Besides the tumour cells, healthy tissue such as bone marrow, hair follicles, and the digestive tract are strongly affected. Targeted therapies were developed to overcome these severe side effects by blocking exclusively the growth and spread of cancer by disturbing the function of tumour specific molecules and leaving healthy tissue unaffected. Targeted therapeutics mainly fall into the following four categories: tyrosine kinases inhibitors, angiogenesis inhibitors, proteasome inhibitors, and immunotherapeutics. The first targeted therapy was developed against the ER, which is often overexpressed in breast cancer (Ward, 1973). Several so-called selective oestrogen receptor modulators (SERMs) like Tamoxifen, which interfere with the binding of oestrogen to its receptors, are approved for ER-positive breast cancer. Tamoxifen, the first ER-targeting therapeutic agent, was already approved in 1977 for the treatment of advanced breast cancer in postmenopausal women. Herceptin®(trastuzumab), a monoclonal antibody targeting ERBB2, was clinically approved in 1998 for metastatic ERBB2-positive breast cancer in combination with conventional chemotherapy. A further targeted drug for breast cancer therapy is lapatinib, a dual specific tyrosine kinase inhibitor against EGFR and ERBB2, which is approved since 2007 for the treatment of triple positive breast cancer (ER+, EGFR+, ERBB2+) and of advanced metastatic ERBB2-positive breast cancer that has progressed after trastuzumab

treatment applied in combination with capecitabine, a cytostatic agent. Meanwhile, these therapeutics face similar problems as conventional therapeutics like insufficient efficacy. Only one third of the patients respond to trastuzumab therapy and in the end almost all patients develop resistance within the first year of treatment (Esteva et al., 2002). Targeting a single molecule or a single pathway allows the tumour cells to find ways to circumvent drug interference. A strategy to overcome this escape mechanism is to couple toxic substances to tumour-targeting antibodies and thus deliver these directly to the cancer cell (Alley et al., 2010, Krop et al., 2010). Another possibility is the treatment of cancer cells with proapoptotic peptides. These peptides are guided by a second peptide which specifically binds to the vasculature of the tumour (Arap et al., 2002, Zurita et al., 2004). This reduces side effects as well as the likelihood to develop resistance due to target-independent and immediate induction of apoptosis. Today, it is common clinical practice to determine the receptor status in breast cancer to decide for the most appropriate treatment. Only patients with ER-positive tumour are treated with Tamoxifen and ERBB2-positive patients with trastuzumab. However, as not all patients respond to a targeted therapy, it is important to be able to predict which patient will benefit from a certain targeted therapy. A step further will take targeted therapy to personalised medicine which aims at finding the most suitable treatment for a certain patient at the right time.

1.3 ERBB receptor family members

Receptor tyrosine kinases (RTKs) are a group of transmembrane spanning receptors which regulate transduction from extracellular signals into a cellular response. This group of signalling proteins frequently harbours oncogenic mutations or are overexpressed in several cancer entities (Hynes and Lane, 2005). RTKs are divided into 20 groups based on their structure as summarised by Blume-Jensen and Hunter (2001) such as the epidermal growth factor receptor (EGFR) family. The EGFR (or ERBB) family consists of four members, EGFR (ERBB1, HER1) (Ullrich et al., 1984), ERBB2 (HER2, HER-2/neu) (Yamamoto et al., 1986), ERBB3 (HER3) (Kraus et al., 1989, Plowman et al., 1990) and ERBB4 (HER4) (Plowman et al., 1993), which show a high homology to each other. The receptors evolved by two gene duplications from a single receptor in invertebrates to four receptors in vertebrates (Stein and Staros, 2000).

1.3.1 Structure of ERBB receptors

The receptors comprise five regions: an extracellular domain, a transmembrane domain, a juxtamembrane domain, a kinase domain, and a C-terminal regulatory domain. The extracellular domain is further subdivided into four distinct subdomains. In the ligand unbound state, these domains exist in a tethered conformation, and the dimerisation loop is buried. Upon ligand binding, the conformation of these domains changes into an active state. Activated receptors expose the dimerisation loop and are now able to form homo- and heterodimers. The dimerisation as such is independent of the ligand and entirely mediated by receptor interaction (Ferguson et al., 2003, Garrett et al., 2002). The extracellular domain of the ERBB2 is radically different from the other family members. Due to a unique interaction between domain I and III, the receptor resembles the ligand bound conformation (Garrett et al. (2003); Fig. 1.3). Because of this active conformation, the ERBB2 is the preferred dimerisation partner of all other family members (Graus-Porta et al., 1997) and enhances signalling (Karunagaran et al., 1996). Furthermore, ERBB2 has no known ligand (Lemmon, 2009).

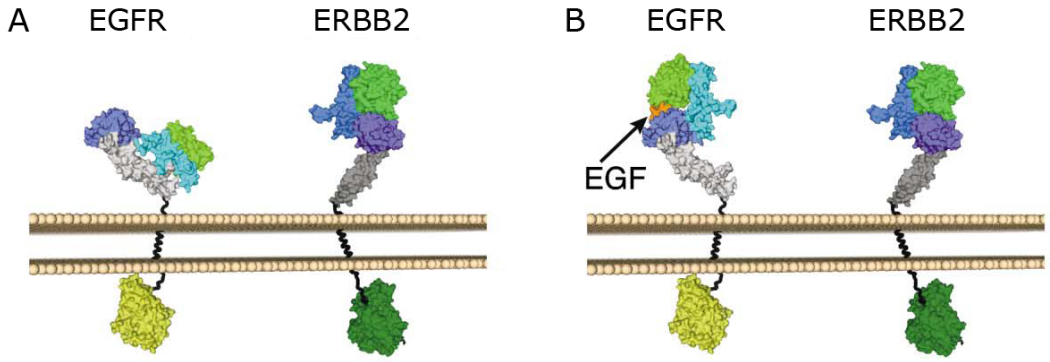

Figure 1.3: Conformation of EGFR and ERBB2
The figure shows the conformation of ERBB2 in comparison with the ligand unbound conformation of EGFR (A) and with the EGF bound conformation (B). (Figure adapted from Franklin et al. (2004).)

1.3.2 ERBB receptor ligands

The EGF-family of peptide growth factors consists of 11 ligands. These ligands are EGF, transforming growth factor alpha (TGF-α), heparin-binding EGF-like

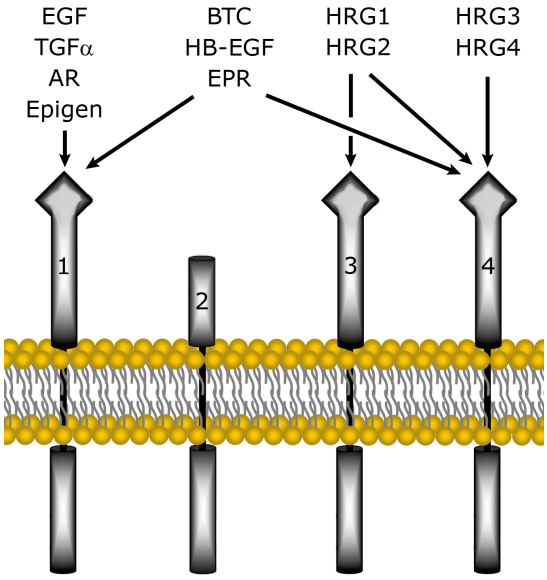

Figure 1.4: The ERBB receptors and their ligands
The figure shows the four ERBB receptors and the 11 ligands grouped according to their binding specificity.

growth factor, (HB-EGF), amphiregulin (AR), betacellulin (BTC), epiregulin (EPR), epigen, and four heregulins (HRG1-4), also called neuregulins. Like the receptors, the ligands evolved from a single ligand in *C. elegans* (Citri and Yarden, 2006). All ligands contain a conserved EGF-like domain and are synthesised as transmembrane precursor molecules (Harris et al., 2003). Release of the ligands is mediated by matrix-metalloproteases (Black et al., 1997). The growth factors are specific for one or two receptors and are divided into four groups based on their specificity. The first group binds specifically to the EGFR, the second group binds to EGFR and ERBB4, the third group binds to ERBB3 and ERBB4, and the fourth group binds specifically to ERBB4 (Fig. 1.4). ERBB ligands are monomeric and induce conformational changes of only the single corresponding receptor. Binding of EGF to EGFR results in EGFR homodimers or EGFR/ERBB2 heterodimers. Binding of HRG1 can result in ERBB3/ERBB2, ERBB3/ERBB4, ERBB4/ERBB4 and ERBB4/ERBB2 dimers. Thus, ligand binding induced receptor activation opens a variety of different dimerisation options. However, several ligands induce certain preferred receptor combinations (Pinkas-Kramarski et al., 1996). While TGF-α preferably leads to the formation of homodimers, EGF induces EGFR/ERBB2 heterodimers (Lenferink et al., 1998), and stimulation with HRG1 mainly results in ERBB2/ERBB3 dimers.

1.3.3 ERBB receptor activation

Receptor dimerisation leads to transphosphorylation of specific tyrosine residues located in the kinase or the C-terminal regulatory domain. Phosphorylation results in full kinase activity of the receptor. Additionally, the phosphotyrosine residues in the C-terminal tail serve as docking sites for adaptor proteins containing SRC-homology 2 (SH2) or phosphotyrosine binding (PTB) domains. Figure 1.5 shows the phosphorylated residues of the four ERBB receptors and the corresponding adaptor molecules. These proteins serve as linkers which pass on the signal from the receptor to distinct downstream signalling pathways. Among the ERBB receptors, there are two receptors with special properties. First, ERBB2 has no own ligand, it enhances and prolongs signalling by exploiting different mechanisms. ERBB2 modulates the dissociation of the receptor-ligand complex of its heterodimerisation partner (Karunagaran et al., 1996). It has also been reported that ERBB2 containing heterodimers evade endocytosis (Wang et al., 1999). While EGFR homodimers are degraded, heterodimers with ERBB2 are recycled back to the cell surface (Lenferink et al., 1998). Overexpression of ERBB2 causes constitutive activation of ERBB2 and ligand-independent activation of EGFR (Worthylake et al., 1999). Second, the ERBB3 receptor has a dead kinase domain (Guy et al., 1994) and is exclusively activated via transphosphorylation. Therefore, ERBB2 and ERBB3 receptors are active only in the context of ligand-activated ERBB heterodimers. ERBB2/ERBB3 dimers are the most prevalent and potent dimers in terms of inducing cell growth and transformation and are therefore regarded as the most tumourigenic heterodimer (Holbro et al., 2003, Wallasch et al., 1995). Members of this family are deregulated in many cancer entities like lung, colon (EGFR), or breast (ERBB2). Thus, ERBB signalling presents one of the most studied and targeted pathogenic signalling network in biology. As described before, the four receptors carry binding sites for a diverse set of SH2 domain containing proteins (Fig. 1.5). These proteins bind to the receptors with different affinities and contribute to the diversity of signalling output. EGFR and ERBB4 mainly possess GRB2 and Shc binding sites which recruit RAS and result in an activation of the mitogen-activated protein kinase (MAPK) pathway. Other direct targets of the EGFR are STAT5 and PLCγ . ERBB3, on the other hand, has at least six binding sites for p85, the regulatory subunit of the phosphoinositide 3-kinase (PI3K). The binding sites on ERBB2 are much more promiscuous (Jones et al., 2006) and this receptor is therefore able to activate both major pathways. Another

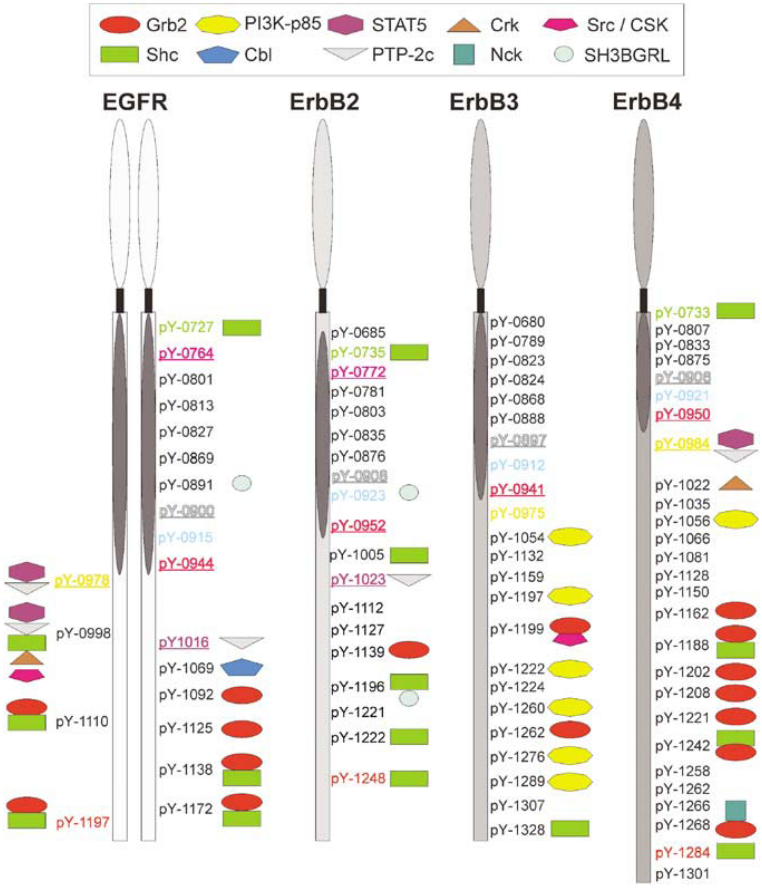

Figure 1.5: Summary of systematic interaction profiling of ERBB receptors

Shown are cytoplasmic phosphotyrosine residues of each receptor. The kinase domains are designated as dark oval. Underlined and coloured residues mark identical sequence regions between the receptors. Most interaction partners are found at the c-terminal end outside the kinase domain. (Picture from Schulze et al. (2005))

factor contributing to the diversity of signalling pathways is the difference in dissociation constants for each adaptor molecule. Jones et al. (2006) showed that the receptors bind different sets of adaptor molecules dependent on the abundance of a certain protein. The ERBB3 network is nearly unaffected by the concentration of adaptor molecules while EGFR and ERBB2 act more promiscuous at high protein expression levels. The overexpression of EGFR and ERBB2 in many cancer types could therefore result in signalling via alternative pathways and not only by inducing stronger signals.

1.4 ERBB signalling pathways

Downstream of the ERBB receptors are two major signalling pathways, the MAPK and the PI3K pathways. The MAPK pathway mainly drives cell proliferation while PI3K activation drives cellular survival and anti-apoptotic signals. Figure 1.6 gives an overview on the major keyplayers of MAPK and PI3K signalling and the crosstalk between the two pathways and the major proteins are described in the glossary.

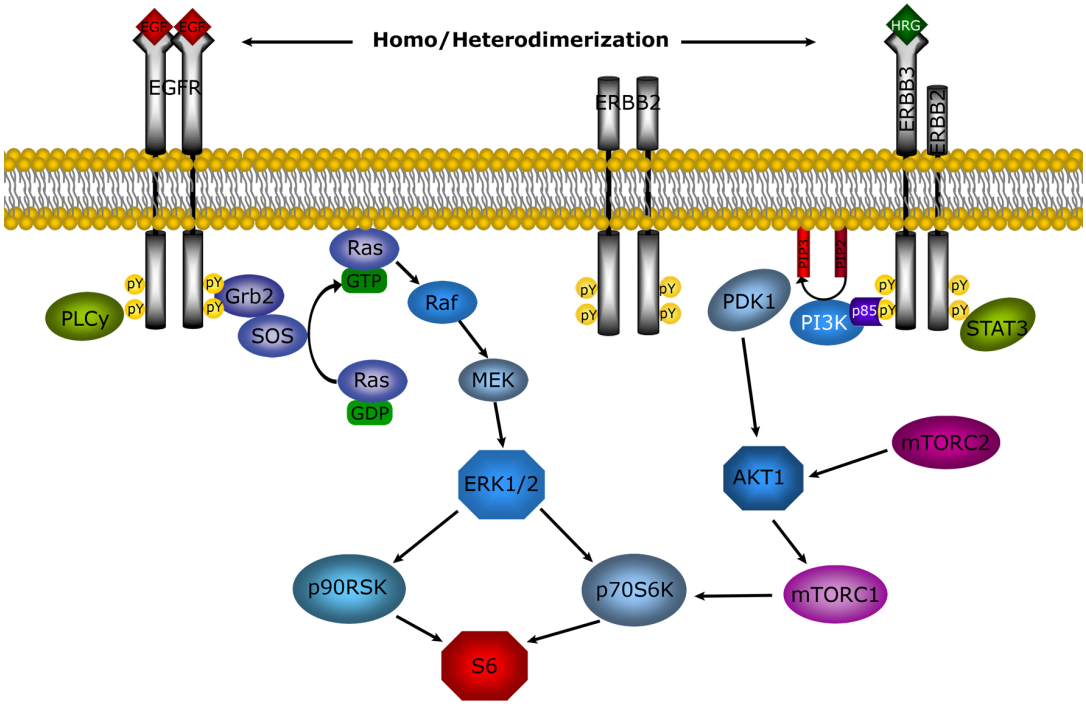

Figure 1.6: ERBB signalling pathway
Schematic overview of downstream proteins involved in ERBB receptor mediated signalling. The arrows do not necessarily represent direct interactions between the proteins.

The guanine nucleotide exchange factor SOS binds to the adaptor molecule GRB2 and is thereby recruited to the activated membrane receptors. RAS, a small membrane-bound monomeric GTP-binding protein, is activated through the SOS-mediated exchange of GDP to GTP. Activated RAS interacts with several effector proteins like RAF and PI3K. The MAPK cascade consists of three components existing in several isoforms. After activation by RAS, RAF translocates into the cytoplasm and phosphorylates the MAPK kinase MEK1/2 which

then leads to the activation of ERK1/2. Signal amplification occurs via the RAF-mediated phosphorylation of MEK1/2, as MEK1/2 is expressed in substantially higher amounts compared to RAF (Santen et al., 2002). MEK1/2 is a dual specific kinase which phosphorylates ERK1/2 at a threonine and a tyrosine residue separated by just a single amino acid and phosphorylation on both amino acids is essential for full ERK1/2 activity. Next, p90RSK is phosphorylated by ERK1/2. The ERK1/2 pathway is deregulated in about one third of all human cancers. Overexpression of the receptors can result in a constitutive activation of this pathway. Besides, members downstream of the receptor are also frequently mutated, especially RAS and B-RAF (Dhillon et al., 2007).

The PI3K consists of two subunits, the regulatory p85 and the catalytical p110 subunit. The p85 subunit directly binds to phosphotyrosines of the activated receptors, mainly ERBB3, and directly leads to activation of the lipid kinase. Next, PI3K phosphorylates phosphatidylinositol-4,5-bisphosphate (PIP_2) to produce phosphatidylinositol-3,4,5-trisphosphate (PIP_3). This is an important second messenger molecule which recruits proteins like PDK1 and AKT to the cell membrane. PDK1 phosphorylates AKT at position T308. AKT then releases inhibition of mTOR by phosphorylating PRAS40 and TSC2. mTOR exists in two complexes: mTORC1, which is rapamycin sensitive, and mTORC2, which is rapamycin insensitive. mTORC2 was identified as PDK2 which phosphorylates AKT at position S473 (Sarbassov et al., 2005). The interplay of PDK1, AKT, and mTORC1 results in phosphorylation of p70S6K which then phosphorylates several effectors associated with translation like the ribosomal protein S6 and eIF4B. A negative regulator of this pathway is PTEN, which dephosphorylates PIP3 and thereby inhibits growth signals and prevents tumour formation. The PI3K pathway is deregulated by activating mutations within different domains of the p110 subunit. Another factor is loss of PTEN which also results in constitutive activation of the PI3K pathway.

1.5 Therapies targeting ERBB receptors

As members of the ERBB receptor family are frequently overexpressed in different cancer entities, mainly due to genomic amplifications, they quickly moved into the focus for development of targeted therapy. In principle, two different molecular strategies, monoclonal therapeutic antibodies and small molecules inhibiting receptor tyrosine kinases, are exploited to produce target specific inhibitors. Nowadays, therapeutics of both categories are clinically approved, and combinatorial therapies are under investigation. Figure 1.7 shows the mode of action of the monoclonal antibodies trastuzumab and pertuzumab, and the small molecule drug erlotinib.

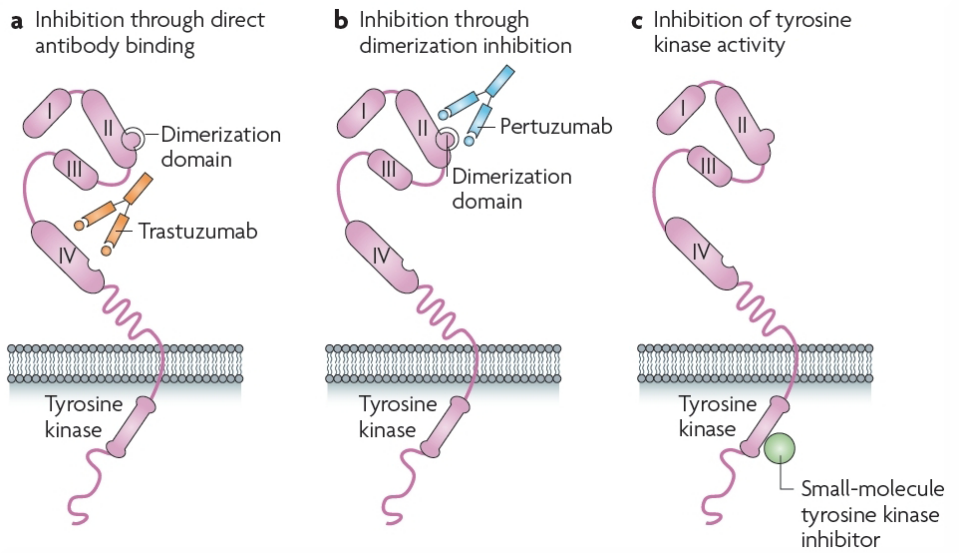

Figure 1.7: Mode of action of trastuzumab, pertuzumab, and erlotinib. The antibody trastuzumab (a) binds to domain IV of ERBB2 extracellular domain. The antibody pertuzumab (b) binds to domain II, the dimerisation loop of ERBB2 and sterically blocks dimerisation. Erlotinib (c) inhibits ATP binding to EGFR tyrosine kinase domain and thereby prevents downstream signalling. (Picture adapted from Baselga and Swain (2009)).

1.5.1 Antibody therapeutics

Trastuzumab is a humanised monoclonal antibody against ERBB2. It was initially approved for the therapy of patients with metastatic breast cancer with

overexpressed ERBB2 in combination with conventional chemotherapy. Its antitumour activity is multifaceted, and the mode of action has not been fully understood. Trastuzumab leads to cell cycle arrest in the G1-phase caused by upregulation of cyclin-dependent kinase (CDK) inhibitor p27 which results in decreased CDK activity (Ye et al., 1999). It has been described that trastuzumab inhibits both the PI3K and MAPK pathways which in turn leads to upregulation of p27 (Yakes et al., 2002). The inhibition of AKT has been shown to be due to an upregulation of PTEN (Nagata et al., 2004). As a humanised IgG1, trastuzumab is bound by the Fcγ receptor III (RIII) and thereby induces antibody-dependent cytotoxicity (ADCC) *in vitro* (Cooley et al., 1999) and *in vivo* (Clynes et al., 2000). Trastuzumab binds to the juxtamembrane region of the ERBB2 receptor (Cho et al., 2003). For that reason, it prevents shedding of the receptor (Molina et al., 2001). Proteolytic cleavage of the receptors results in a truncated ERBB2 called p95. This truncated receptor is constitutively active (Christianson et al., 1998) and no longer subjected to regulation. Initially, it was thought that trastuzumab also leads to an increase in ERBB2 endocytosis or degradation but meanwhile it has been shown that it does not downregulate ERBB2 from the cell surface (Austin et al., 2004). There is still controversy whether the unchanged abundance of ERBB2 is due to endocytosis resistance (Hommelgaard et al., 2004, Longva et al., 2005) or due to enhanced recycling and decreased endocytosis (Austin et al., 2004). Additionally, it was reported that trastuzumab treatmentalso reduced the VEGF receptor expression and led to a vasculature resembling the normal phenotype *in vivo* (Izumi et al., 2002).

Pertuzumab (Omnitarg®) is another humanised monoclonal antibody against ERBB2 (Adams et al., 2006). At the moment, phase III clinical studies are ongoing (NCT01120184). Pertuzumab binds to domain II, the dimerisation domain, and thus prevents binding of ERBB2 to other ERBB receptors (Franklin et al., 2004). It has been reported that pertuzumab is able to inhibit formation of ERBB2/ERBB3 dimers (Agus et al., 2002) and thus to prevent the formation of the most tumourigenic dimer. Pertuzumab has demonstrated its activity *in vitro* and *in vivo* in several tumour entities expressing different levels of ERBB2, including ovarian (Mullen et al., 2007, Takai et al., 2005), breast, prostate (Agus et al., 2002), lung (Sakai et al., 2007) and colorectal cancer (Pohl et al., 2009). In contrast to trastuzumab, which is only active in ERBB2 overexpressing cells, pertuzumab is able to inhibit growth also in cells with normal ERBB2 expression (Sarup et al., 1991).

1.5.2 Small molecule therapeutic agents

Erlotinib (Tarceva®) is a selective inhibitor of the tyrosine kinase domain of EGFR. It is clinically approved since 2005 for the treatment of non-small cell lung cancer (NSCLC) and since 2007 for the treatment of pancreatic cancer. Currently, it is evaluated in several phase II clinical studies for treatment of breast cancer (Dickler et al., 2009). Like many other small molecules targeting the ATP binding site of the receptors, it is not absolute specific for the EGFR but also inhibits other kinases (Karaman et al., 2008).

1.5.3 Resistance to targeted therapies

Targeted therapies aiming at the inhibition of one single molecule are susceptible to resistance. Various breast tumours exhibit innate or acquired resistance towards ERBB2-targeting therapies and resistance is linked to alterations of the PI3K pathway. PTEN is a negative regulator of the PI3K pathway and is the most commonly lost tumour suppressor in human cancer (Liu et al., 2008). In breast cancer, loss of PTEN is associated with poor prognosis (Depowski et al., 2001) and trastuzumab resistance (Nagata et al., 2004). Other factors associated with resistance are gain of enzymatic function mutations of the p110 catalytical subunit of PI3K which results in constitutive activation (Saal et al., 2005) and has been shown to be oncogenic *in vivo* (Bader et al., 2006). Both alterations result in constitutive activation of the PI3K pathway and are therefore reported to correlate with similar prognostic factors (Perez-Tenorio et al., 2007). Additionally, downregulation of p27 is associated with trastuzumab resistance (Nahta et al., 2004). Upregulation or activation of other receptor tyrosine kinases like the IGF-IR (Lu et al., 2001, Nahta et al., 2005), ERBB3 (Sergina et al., 2007, Wang et al., 2008), or MET (Shattuck et al., 2008) are associated with resistance in breast cancer and other cancer entities (Engelman et al., 2007). Studies indicate that the truncated form of ERBB2 which lacks the extracellular domain causes resistance (Xia et al., 2004). One possible explanation is that trastuzumab is not able to bind to the truncated form. Additionally, it has been proposed that trastuzumab instead binds to the shedded extracellular domain and is thereby neutralised (Leary et al., 2009). Finally, the upregulation of ERBB ligands is able to counteract ERBB receptor inhibition. It has been reported that TGF-α is upregulated in tumours which are resistant to therapy

(Valabrega et al., 2005). Chakrabarty et al. (2010) showed that cell lines harbouring both amplified ERBB2 and mutant PI3K revealed higher levels of HRG which results in autocrine activation of ERBB3 and ERBB4. Consistent with this, Eckstein et al. (2008) reported that amphiregulin expression is associated with cisplatin resistance. Overall, overexpression and mutations of kinases or upregulation of receptor ligands were mainly associated with therapy resistance.

Many diseases like cancer are correlated with alterations of protein abundance and function. All cancers carry somatic mutations but only a subset are so-called driver mutations which are implemented in tumour development and confer growth advantage (Pleasance et al., 2010). However, large-scale sequencing studies revealed that the signature of somatic mutations is highly variable. At least 350 cancer genes have been identified so far (Futreal et al., 2004). Another study identified driver mutations in 120 of 518 protein kinase genes (Greenman et al., 2007). An important subclass of mutations confers therapy resistance. Some mutations already exist in resistant subclones and convert to driver mutations once the selective environment changes due to initiation of therapy (Stratton et al., 2009). Although mutations, changes on the transcriptome level, and the fine tuning by micro RNAs influence of cellular behaviour, only transient processes like protein phosphorylation mainly reflect the activity status of a cell. Thus, sequencing and measuring mRNA or miRNA levels are not sufficient to provide information on protein abundance and posttranslational modifications (Tibes et al., 2006). Minor changes of protein abundance, modification or activation can result in a deregulation of the cellular balance between proliferation, differentiation, migration, and apoptosis. Technologies, which allow to measure and quantify small changes in a time-resolved manner, open new possibilities to develop novel therapeutical strategies. The identification of cellular profiles in response to targeting therapeutics may contribute to predict sensitivity or resistance to a certain drug if similar activation profiles can be found in tumours. Consequently, methods for the high throughput analysis of proteins are required to gain insights into the tightly regulated network of cellular signal transduction.

1.6 Protein Microarrays

Protein microarrays are a reliable tool for the quantitative analysis of protein expression and activation of signalling networks (Grubb et al., 2003, Wulfkuhle et al., 2008). Two different approaches were established in the division.

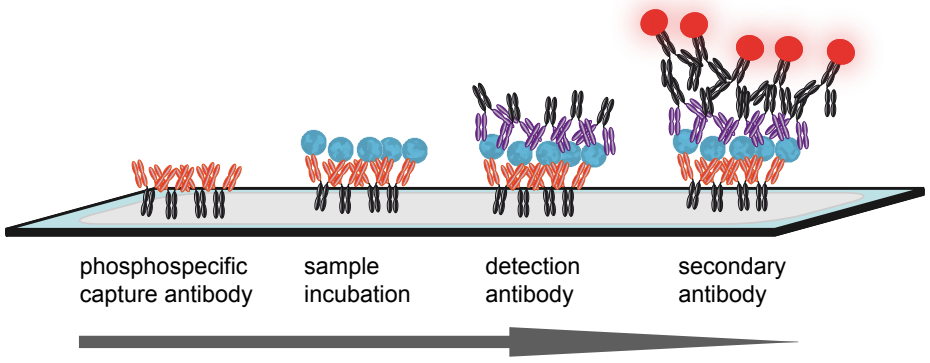

Figure 1.8: Schematic overview of the MIA approach
Capture antibodies are immobilised on nitrocellulose coated glass slides. This antibody binds to the target protein in the lysate which is than detected with a second specific antibody. The complex is visualised by a NIR-labeled secondary antibody.

The first format is the microspot immunoassay (MIA) (Korf et al., 2008a) which allows the determination of several phosphoproteins in parallel from only small sample amounts. A scheme of the procedure is shown in figure 1.8. In general, the MIA is a miniaturised sandwich enzyme-linked immunosorbent assay (ELISA). Two specific antibodies are targeting different epitopes of the same protein. This increases sensitivity and specificity and enables the detection of phosphorylation events of lowly abundant proteins. Capture antibodies are immobilised on nitrocellulose coated glass slides, and a certain set of capture antibodies is spotted on 16 identical subarrays per slide. Six of these subarrays are then incubated with a dilution series of recombinant phosphoproteins of known concentration to generate antibody specific calibration curves for each phosphoprotein. The remaining 10 subarrays are incubated with the protein lysates of interest. With the help of a calibration curve, the concentration of phosphoprotein in the lysate is calculated. Applying MIA allows to determine the absolute quantity of the assessed phosphoproteins. MIAs are a very sensitive

tool, as small amounts of the target phosphoprotein are captured from a sample. A valid antibody pair detects proteins in the pg/ml range, and depending on the abundance of the target protein, only 10–50 µg/ml total protein is needed for the quantification of the target phosphoprotein.

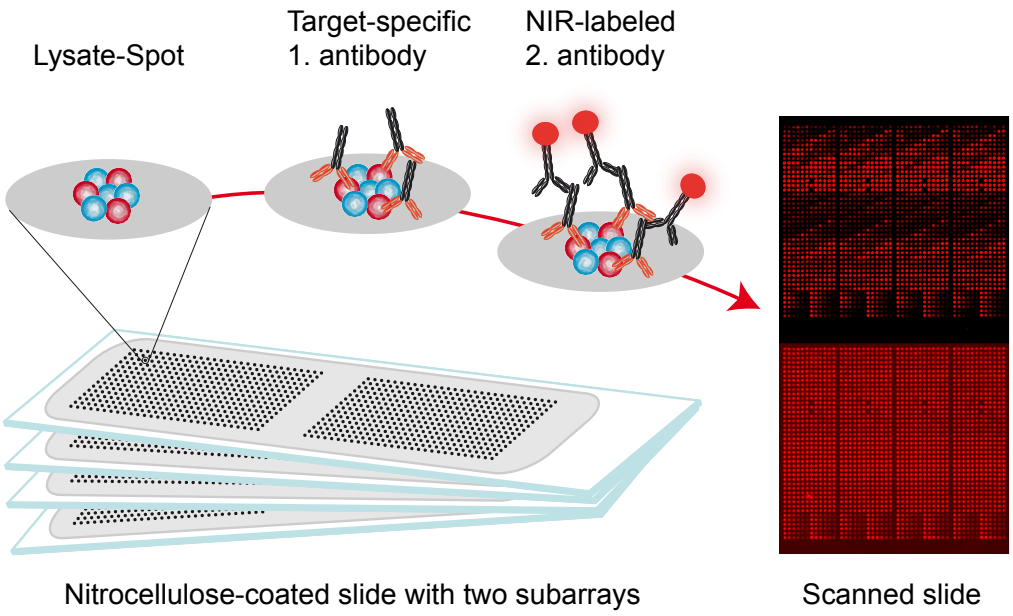

Figure 1.9: Schematic overview of the RPPA approach
Protein lysate is immobilised on nitrocellulose coated glass slides. A specific antibody binds to its target and is visualised by a NIR-labeled secondary antibody.

The second approach are reverse phase protein arrays (RPPAs) (Paweletz et al., 2001). Here, the protein lysates are directly immobilised on nitrocellulose coated glass slides, and more than 2000 samples can be analysed in parallel on one slide. With only a few µl of protein lysate, at least 100 arrays can be printed and analysed. To increase sensitivity, this approach was adapted to detection in the near-infrared range (Loebke et al., 2007). Figure 1.9 shows the workflow of the RPPA. Each array is incubated with a different primary antibody recognising the target protein or phosphorylation site of interest. This complex is visualised by a near-infrared labeled secondary antibody. For normalisation, single arrays are also incubated with total protein dyes. By analysing the signal intensities of individual spots, RPPAs allow the relative quantification of proteins or phosphoproteins within the set of printed lysate samples.

1.7 Aim of the study

The overall aim of the study was the quantitative and time-resolved analysis of ERBB signalling on the systems level in breast cancer cell lines. As prerequisite, experimental methods had to be developed to produce and analyse biological samples on a large scale and to generate data for quantitative modelling. To obtain high quality, quantitative data, protocols had to be adapted to the protein microarray format allowing the targeted analysis of signalling processes. For protein microarray data analysis, appropriate tools had to be developed in parallel. The first aim was to delineate the interplay between signalling processes involving the ERBB3/PI3K and the EGFR/MAPK pathways. The second aim was to examine the impact of the targeted therapeutics trastuzumab, pertuzumab, and erlotinib on ligand-induced pathway activation in ERBB2 overexpressing cell lines to elucidate quantitative differences between all possible combinatorial treatments for the identification of an optimised treatment strategy. Quantitative data will feed into data-driven modelling of network dynamics to identify new points of therapeutic intervention.

2 Materials and methods

2.1 Materials

2.1.1 Chemicals

The chemicals applied in this thesis were purchased from the following companies if not described otherwise:

AppliChem (Darmstadt)	Baker (Groß-Gerau)	BioRad (München)
Fluka (Seelze)	Gerbu (Gaiberg)	Merck (Darmstadt)
PAA (Pasching)	Roth (Karlsruhe)	Sigma (Steinheim)

2.1.2 Equipment

2470 Arrayer	Aushon, Billerica
5100 Cryo 1°C Freezing Container	Thermo Scientific, Karlsruhe
7900HT Sequence Detection System	Applied Biosystems, Darmstadt
Biomek®FX	Beckman Coulter, Krefeld
FACScalubur™	BD, Heidelberg
Incubation chamber	Metecon, Mannheim
Incubator BBD 6220	Heraeus, Hanau
Laminar flow workbench (Hera-safe)	Heraeus, Hanau
Multichannel pipette	Biohit, Rosbach
Multipette plus	Eppendorf, Hamburg
NanoDrop ND-1000 UV/VIS spectrophotometer	NanoDrop Technologies, Wilmington
Odyssey®Infrared Imaging System	LI-COR Bioscience, Lincoln
pH meter	Hanna Instruments, Kehl

Pipetteboy	Integra Biosciences, Fernwald
Pipetteman	Gilson, Langenfeld
PTC-225 Peltier Thermo Cycler	MJ Research
Mini-Protean®II eletrophoresis cell	BioRad, München
Spectra MAX 190	Molecular Devices, Ismaning
SonoPlus	Bandelin, Berlin
Trans-Blot®SD Transfer Cell	BioRad, München
Tube rotator	VWR, Darmstadt
Centrifuges	Biofuge fresco, Heraeus, Hanau
	Multifuge 4KR, Heraeus, Hanau
	Sigma 4K15C, Qiagen, Hilden
	Sorvall RC 5B Plus, Langenselbold

2.1.3 Consumables

10 cm plates	TPP, Darmstadt
6 and 15 cm plates	Greiner Bio-one, Frickenhausen
6-well plates	Nunc, Langenselbold
96-well plates	Greiner Bio-one, Frickenhausen
Cell culture flasks T25, T75, T175	Greiner Bio-one, Frickenhausen
Cell scraper	TPP, Darmstadt
Combitips	Eppendorf, Hamburg
Filtertips (RPT)	Starlab, Ahrensburg
Pasteur pipettes	WU, Mainz
Polypropylene columns (5 ml)	Qiagen, Hilden
Reaction tubes (1.5 ml, 2 ml)	Eppendorf, Hamburg
Serological pipettes	BD, Heidelberg
Tubes (15 ml, 50 ml)	Greiner Bio-one, Frickenhausen

2.1.4 Miscellaneous

Complete, Mini	Roche, Mannheim
Fast Green, FCF	Sigma, Steinheim
Lipofectamine™2000	Invitrogen, Darmstadt
Lysozyme	Sigma, Steinheim
ONCYTE ®Nitrocellulose slides	Grace Biolabs, Bend

peqGold prestained Protein-Marker IV	Peqlab, Erlangen
peqGold prestained Protein-Marker V	Peqlab, Erlangen
PhosSTOP	Roche, Mannheim
PVDF membrane 0.45 µm Immobilon-FL	Millipore, Eschborn
SwellGel Immobilized Glutathione Discs	Pierce, Bonn
Tween®20	Sigma, Darmstadt
Whatman paper (0.34 mm)	Whatman, Dassel

2.1.5 Kits

BCA Protein Assay Kit	Pierce, Bonn
RevertAid™H Minus First Strand cDNA Synthesis Kit	Fermentas, St.Leon-Rot
RNeasy®Mini Kit	Qiagen, Hilden

2.1.6 Recombinant proteins

AKT1/PKBα, active, 14-372	Millipore, Schwalbach
ERK1 (MAPK3), PV3311	Invitrogen, Karlsruhe

2.1.7 Growth Factors

Growth factors were diluted in PBS containing 0.1% BSA to a final concentration of 100 ng/µl.

Betacellulin (BTC)	R&D Systems, Wiesbaden
Epidermal growth factor (EGF)	Sigma, Steinheim
Heregulin-β1 (HRG1-β)	Biocat, Heidelberg

2.1.8 Kinase inhibitors and targeted therapeutics

Table 2.1: Inhibitors, therapeutics, and corresponding concentrations

inhibitor	company	target	stock	applied
erlotinib	Roche	EGFR	12,7 mM	1 µM
gefitinib	Asta Zeneca	EGFR	50 mM	10 µM
LY294002	Calbiochem	PI3K	50 mM	10 µM
PD98059	Calbiochem	MEK1	20 mM	10 µM
pertuzumab	Roche	ERBB2	25 mg/ml	10 µg/ml
rapamycin	US biological	mTORC1	50 mM	10 nM
trastuzumab	Roche	ERBB2	24,7 mg/ml	10 µg/ml

Pertuzumab	10 mM histidine, 240 mM sucrose, 0.02% Tween®20
Trastuzumab	5 mM histidine, 60 mM trehalose, 0.1 mg/ml Tween®20
Erlotinib	6% Captisol

Small molecule inhibitors were dissolved in DMSO.

2.1.9 Buffers, media, solutions

0.25% trypsin EDTA solution	GIBCO, Invitrogen, Darmstadt
7-amino-actinomycin D	Calbiochem, Darmstadt
ABsolut™QPCR ROX (500nM) Mix	ABgene, Schwerte
Antibody Diluent with Background Reducing Components	Dako, Glostrup
DMEM (41966)	GIBCO, Invitrogen, Darmstadt
DMEM (31053)	GIBCO, Invitrogen, Darmstadt
DPBS	GIBCO, Invitrogen, Darmstadt
Fetal Bovine Serum	GIBCO, Invitrogen, Darmstadt
HEPES, 1 M	GIBCO, Invitrogen, Darmstadt
l-glutamine, 200 mM	GIBCO, Invitrogen, Darmstadt
Mammalian Protein Extraction Reagent (M-PER)	Pierce, Bonn
MEM Non-essential amino acids (100x)	GIBCO, Invitrogen, Darmstadt

Nuclease-free Water	Ambion, Darmstadt
Odyssey®Blocking Buffer	Licor Bioscience, Bad Homburg
OptiMEM	GIBCO, Invitrogen, Darmstadt
Ponceau S solution	Sigma, Steinheim
Roti-Load1	Roth, Karlsruhe
Rotiphorese Gel 30	Roth, Karlsruhe
RPMI 1640 (A10491)	GIBCO, Invitrogen, Darmstadt
RPMI 1640 with GlutaMAX™(61870)	GIBCO, Invitrogen, Darmstadt
RPMI 1640 without phenol-red (11835)	GIBCO, Invitrogen, Darmstadt
Sodium pyruvate, 100 mM	GIBCO, Invitrogen, Darmstadt
TEMED	Serva Electrophoresis, Heidelberg
10x PBS (pH 7.4)	1.37 M NaCl 27 mM KCL 18 mM KH_2PO_4 100 mM Na_2PO_4
10x TBS (pH 7.6)	1.37 M NaCl 200 mM Tris

SDS-PAGE

Table 2.2: Composition of polyacrylamid gels

	stacking gel	**running gel**		
		15%	**12.5%**	**7.5%**
Acrylamide	1.33 ml	10 ml	8.3 ml	5 ml
4x gel buffer	2.55 ml	5 ml	5 ml	5 ml
10% SDS (w/v)	100 µl	200 µl	200 µl	200 µl
10% APS	100 µl	100 µl	100 µl	100 µl
TEMED	5 µl	6.7 µl	6.7 µl	6.7 µl
ddH_2O	6 ml	4.7 ml	6.4 ml	9.7 ml

4 x stacking gel buffer	5 M Tris-HCl; pH 6.8
4 x running gel buffer	1.5 M Tris-HCl; pH 8.8
1 x running buffer	25 mM glycine + 0.1% SDS (w/v)
APS	10% in H_2O

Western blotting

Cathode buffer	40 mM aminohexanoic acid, 20% methanol
Anode buffer I	300 mM Tris Base, 20% methanol
Anode buffer II	25 mM Tris Base, 20% methanol
Washing buffer	0.1% Tween®20 in TBS (TBST)
Blocking buffer	Rockland Blocking Buffer 1:2 in TBS 5 mM sodium fluoride 1 mM sodium vanadate
Secondary antibody buffer	Washing buffer + 0.02% SDS (w/v)

Microspot immunoassay

Assay buffer	1% BSA 0.5% NP-40 0.02% SDS (w/v) 50 mM Tris HCl, pH 7.4 150 mM NaCl 1 mM EDTA 5 mM sodium fluoride 1 mM sodium vanadate 1 complete mini/10 ml
Blocking buffer	5% milk (w/v) 0.5% NP-40 50 mM Tris HCl, pH 7.4 150 mM NaCl 1 mM EDTA
Washing buffer	0.1% Tween®20 in PBS (PBST)

Reverse phase protein array

Blocking buffer	Odyssey®Blocking Buffer 1:2 in PBS 5 mM sodium fluoride 1 mM sodium vanadate
Secondary antibody buffer	Washing buffer + 0.5% BSA

Protein expression

Stock solutions	IPTG (1M) 200 mM DTT 200 mM EDTA, pH 8.0 200 mM PMSF 1 M NaCl 1 M Tris-HCl, pH 8.0 1 M $MgCl_2$ 1 M IPTG ampicillin (100 mg/ml) kanamycin (30 mg/ml) lysozyme (50 mg/ml) Benzonase (250 U/µl)
LB medium	10 g tryptone 5 g yeast extract 10 g NaCl ad 1 l ddH_2O, autoclave
LB agar	1.5% agar in LB medium
Lysis buffer	20 mM Tris-HCl, pH 7.5 500 mM NaCl 1% NP-40 1 mM EDTA 1 mM DTT (add freshly)
Elution buffer	10 mM reduced l-glutathione 50 mM Tris-HCl, pH 8.0

In vitro phosphorylation

Kinase assay buffer	50 mM Tris-HCl, pH 7.5 10 mM $MgCl_2$ 1 mM EGTA 0.01% Triton X-100 200 µM ATP (added freshly) 2 mM DTT (added freshly)

2.1.10 Antibodies

Table 2.3: Antibodies used for RPPA and Western blot analysis

target protein	phosphosite	company	catalog number
AKT		CST	9272
AKT		Santa Cruz	sc-1619-r
AKT	S473	CST	9271
AKT	T308	CST	9275
Cyclin D1		CST	2922
EGFR		CST	2646
EGFR		Santa Cruz	sc-03
EGFR	Y992	CST	2235
EGFR	Y1045	CST	2237
EGFR	Y1068	CST	2236
EGFR	Y1086	CST	2220
EGFR	Y1148	CST	4404
EGFR	Y1173	CST	4407
ERBB2		Neomarkers	AB-17
ERBB2	Y877	CST	2241
ERBB2	Y1112	Millipore	04-294
ERBB2	Y1139	abcam	ab53290
ERBB2	Y1221/2	CST	2243
ERBB2	Y1248	Millipore	06-229
ERBB3		Neomarkers	AB-2
ERBB3	Y1197	CST	4561
ERBB3	Y1222	CST	4784
ERBB3	Y1289	CST	4791
ERBB4		Santa Cruz	sc-283
ERBB4		CST	4795
ERBB4	Y1162	Epitomics	2295-1
ERK1/2		Santa Cruz	sc-94
ERK1/2		Millipore	06-182
ERK1/2	T202/Y204	CST	4370
ERK1/2	T202/Y204	CST	9106
GAB1		CST	3232
GAB1	Y307	CST	3234
GSK3α/β		Santa Cruz	sc-7291
GSK3α/β	Y279/216	Epitomics	2309-1

Table 2.3: Antibodies used for RPPA and Western blot analysis

target protein	phosphosite	company	catalog number
MEK		BD	610122
MEK	S217/221	Sigma	M7683
MET		CST	3127
MET	Y1003	CST	3135
MET	Y1234/35	CST	3077
mTOR		CST	2972
mTOR	S2448	CST	2971
mTOR	S2481	Millipore	09-343
NFkB		Santa Cruz	sc-109
NFkB	S536	CST	3033
RSK		CST	9355
SDHA		Santa Cruz	sc-59687
p27		BD	610241
p38		CST	9212
p38	T180/Y182	CST	9211
p70S6K		BD	611261
p70S6K		CST	2708
p70S6K	T389	CST	9206
p70S6K	T389	CST	9234
p70S6K	T241/S424	Epitomics	1135-1
p90RSK	S380	CST	9341
p90RSK	T359S363	CST	9344
PDK1		CST	3062
PDK1	S241	CST	3438
PDK1	S241	CST	3061
PI3K/p85		abcam	ab40755
PI3K/p110		abcam	ab32569
PKCα		abcam	ab32376
PKCα	S657/Y658	abcam	ab23513
PKCα	S657	Millipore	06-822
PLCγ		abcam	ab41433
PLCγ	S1248	CST	4510
PRAS	T246	CST	2997
PTEN		CST	9552
PTEN	T366/S370	Epitomics	2195-1
cRAF	S259	CST	9421

Table 2.3: Antibodies used for RPPA and Western blot analysis

target protein	phosphosite	company	catalog number
cRAF	S289/296/301	CST	9431
RB	S807/811	CST	9308
S6	S235/236	CST	4858
SRC		CST	2123
SRC	Y416	CST	2101
STAT3		Santa Cruz	sc-482
STAT3	S727	CST	9134
STAT3	Y705	CST	9131
STAT5		CST	9310
STAT5	Y694/699	Millipore	05-495

Microspot Immunoassay

Table 2.4: Capture antibodies

target protein	phosphosite	company	catalog number
pAKT1	S473	Millipore	05-669
pAKT1	S473	BD	558368
pAKT1	T308	BD	558316
pAKT1	T308	CST	5106
pERK1/2	T202/Y204	Sigma	M9692
pERK1/2	T202/Y204	CST	9106
pSTAT3	S727	BD	612543

Table 2.5: Detection antibodies

target protein	company	catalog number	dilution
AKT1	Santa Cruz	sc-1619-r	1:400
ERK1/2	Millipore	06-182	1:800
ERK1/2	Santa Cruz	sc-94	1:800
STAT3	CST	9132	1:500

Secondary antibodies

Table 2.6: Secondary antibodies

reactivity	host species	company	label
mouse	goat	Invitrogen	Alexa Fluor®680
rabbit	goat	Invitrogen	Alexa Fluor®680
goat	rabbit	Invitrogen	Alexa Fluor®680
mouse	goat	Pierce	DyLight 680
mouse	goat	Pierce	DyLight 800
rabbit	goat	Pierce	DyLight 680
rabbit	goat	Pierce	DyLight 800

2.1.11 siRNAs

Table 2.7: Applied siRNA from Dharmacon

gene symbol	siRNA ID	antisense sequence 5'-3'
EGFR	J-003114-10	UAUUCCGUUACACACUUUGUU
EGRF	J-003114-11	AUAUUCGUAGCAUUUAUGGUU
EGFR	J-003114-12	AACUGCGUGAGCUUGUUACUU
EGFR	J-003114-13	AGUUAUUGAACAUCCUCUGUU
ERBB2	J-003126-17	UAACCUGUGAUCUCUUCCAUU
ERBB2	J-003126-18	GUAUUGUUCAGCGGGUCUCUU
ERBB2	J-003126-19	CAGUACUCGGCAUUCCUCCUU
ERBB2	J-003126-20	UUGGUUGUGAGCGAUGAGCUU
ERBB3	J003127-10	UAUUGGUUCUCAGCAUCGCUU
ERBB3	J003127-11	UGUCCCGUGAGCACAAUCUUU
ERBB3	J003127-12	CACUUCUCGAAUCCACUGCUU
ERBB3	J003127-13	UUAUAGUUCAACAUGACGAUU
ERBB4	J003128-10	UAUUCGAGUCAAUUCUUGCUU
ERBB4	J003128-11	UAACUAGGUAUCUUUGAGGUU
ERBB4	J003128-12	AAUUUGUCAAUGUUACUGGUU
ERBB4	J003128-13	AAUGUAUACACUCCAGAGCUU

2.1.12 Taqman Gene Expression Assays

The assays used for Taqman analysis listed in table 2.8 were purchased from Applied Biosystems, Darmstadt.

Table 2.8: Taqman Gene Expression Assays

gene symbol	assay ID	gene name
EGFR	Hs00193306_m1	Epidermal growth factor receptor
ERBB2	Hs00170433_m1	v-erb-b2 erythroblastic leukemia viral oncogene homolog 2
ERBB3	Hs00176538_m1	v-erb-b3 erythroblastic leukemia viral oncogene homolog 3
ERBB4	Hs00171783_m1	v-erb-b4 erythroblastic leukemia viral oncogene homolog 4
MET	Hs00179845_m1	met proto-oncogen
GAPDH	Hs99999905_m1	glyceraldehyde-3-phosphate dehydrogenase

2.1.13 Cell culture

All human breast cancer cell lines were purchased from the American Type Culture Collection (ATCC), LGC Prochem, Wesel.

BT474	HTB-20	ductal carcinoma
HCC1954	CRL-2338	ductal carcinoma
MCF7	HTB-22	adenocarcinoma
SKBR3	HTB-30	adenocarcinoma

Growth media

BT474	DMEM 10% FBS 10% NCTC-135 10 µg/ml insuline bovine
HCC1954	RPMI 1640 10% FSB
MCF7	RPMI 1640 with GlutaMAX™ 10% FSB 1 x NEAA 1 mM sodium pyruvate insuline bovine
SKBR3	DMEM 10% FBS 1 x NEAA

Starvation media

BT474	DMEM (phenol-red free) 10% NCTC-135
HCC1954	RPMI 1640 (phenol-red free) 1 mM HEPES 1 mM sodium pyruvate
MCF7	RPMI 1640 (phenol-red free) 1 x NEAA 1 mM sodium pyruvate
SKBR3	DMEM (phenol-red free) 1x NEAA 2 mM l-glutamine 1 mM sodium pyruvate

Freezing medium

	10% DMSO 20% FBS 70% growth medium

2.2 Methods

2.2.1 SDS-PAGE

Discontinuous sodium dodecylsulfate-polyacrylamide gel electrophoresis (SDS-PAGE) was used to separate proteins based on their molecular weight and were performed according to Laemmli (1970). SDS, an anionic detergent, and β-mercaptoethanol denature and dissociate the protein into subunits. β-mercaptoethanol reduces disulfide bonds while SDS binds to hydrophobic regions, unfolds the protein structure and leads to negatively charged proteins whereby the number of incorporated detergent molecules depends mainly on the size of the protein. This results in a uniform charge to mass ratio of 1.4 g SDS per g protein and proteins move in the electric field with a velocity depending on their size and subjected to the sieving effect of the polyacrylamide gel. Polyacrylamide gels consist of a stacking gel and a separating gel. The stacking gel has a large pore size and is used to concentrate the proteins before reaching the separating gel. Protein separation is achieved in the alkaline separating gel with small pore size. Depending on the size of the target protein, gels with differing acrylamide concentrations leading to different pore sizes can be used for optimal resolution.

For sample preparation, protein lysates were mixed 1:4 with 4 x sample buffer and heated for 5 min at 95°C. 20 µg protein per sample was loaded and the gel was run at 120–150 V between 1.5–2 h, depending on the size of the target protein.

2.2.2 Western blotting

The proteins resolved by SDS-PAGE were transferred onto a PVDF membrane by electrophoretic transfer. A semidry approach was employed which consists of three different buffers, anode buffer I, anode buffer II, and cathode buffer. First, the PVDF-membrane was activated in 100% methanol and equilibrated in anode buffer II. Whatman paper was soaked in the three buffers and assembled with the gel and the membrane as shown in figure 2.1. The proteins were transferred for 1 h at 25 V. For proteins above 150 kDa, the transfer was prolonged for 10 min. The transfer of proteins was controlled by staining the membran with Ponceau-S solution, a reversible organic stain. Destaining was achieved with ddH_2O. The membrane was blocked for 1 h with blocking buffer at RT.

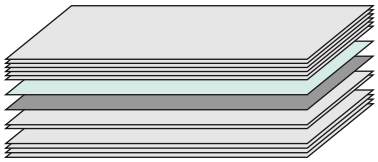

Figure 2.1: Western blot assembly

2.2.3 Immunological protein detection

The antibody against the target protein was diluted 1:1,000 in blocking buffer. The membrane was exposed to the primary antibody dilution over night at 4°C. Following the incubation, the membrane was washed 4 x 5 min with washing buffer. Afterwards, the membrane was incubated with a 1:10,000 secondary antibody dilution for 60 min in a dark box to avoid light exposure. Depending on the host species of the primary antibody, anti-mouse or anti-rabbit secondary antibodies labeled with DyLight 680 or DyLight 800 were used. After washing a second time for 4 x 5 min, the membrane was scanned using the Odyssey®Infrared Imaging System (Odyssey) at 700 and 800 nm allowing the detection of two different proteins on the same Western blot if primary antibodies from different species were used, even if the molecular weight of both proteins was highly similar.

2.2.4 Preparation of recombinant phospho-STAT3

Induction of recombinant GST-tagged STAT3 expression

Bacteria were streaked from glycerol stock onto a LB-plate and incubated over night at 37°C. The next day, 50–60 colonies were collected per plate and inoculated in 10 ml LB medium containing 1% glucose, 15 µg/ml kanamycin, and 100 µg/ml ampicillin. Cultures were grown at 30°C over night at 220 rpm. 500 ml LB medium containing 1% glucose, 15 µg/ml kanamycin, and 100 µg/ml ampicillin were inoculated with 10 ml starter culture. Growth was monitored every hour until the optical density at 600 nm (OD_{600}) reached 0.8. A 1 ml aliquot was taken for pre-induction control. Protein expression was induced with 1 mM isopropyl β-D-1-thiogalactopyranoside (IPTG) and incubation was continued at 30°C for 4 h. Again, a 1 ml aliquot was saved as post-induction control. The cell suspension was cooled down and the cell pellet was harvested by centrifugation at 8,000 x g for 10 min and stored at -20°C.

Protein extraction

The frozen cell pellet was resuspended in 10 ml lysis buffer for protein extraction. Lysozyme (200 µg/ml lysis buffer) was added to the suspension and incubated for 15 min on ice. Afterwards, phenylmethanesulfonylfluoride (PMSF) was added to a final concentration of 100 µM. After sonication for 3 x 10 sec with 50–60% power setting, benzonase (25 U/ml lysis buffer) and 5 mM $MgCl_2$ were added, mixed thoroughly, and incubated for further 20 min on ice. For loading of total protein on SDS-PAGE, 60 µl of the total protein extract solution was mixed with 20 µl 4 x sample buffer and stored at -20°C. To prepare the soluble fraction, protein lysate was centrifuged at 28,000 x g for 20 min at 4°C and cleared from the insoluble particles. A 60 µl aliquot of the supernatant was mixed with 20 µl 4 x sample buffer and stored for SDS-PAGE analysis representing the soluble protein fraction. The supernatant was used for protein purification.

Protein purification

For protein purification, 10 ml of the supernatant yielded by the protein extraction procedure was poured into a purification column and mixed with two SwellGel Immobilized Glutathione Discs. After sealing the column with a lid, the slurry was incubated for 60 min at room temperature on an end-over-end shaker to allow binding of the recombinant fusion protein to the affinity resin. Next, the lid was removed, the tip at the bottom of the column was opened, and the flow-through containing the unbound material was collected for analysis. The slurry was washed 2 times for 10 min each with 10 ml PBS. Both washing fractions were collected for further analysis. After sealing the column tip, 300 µl elution buffer was added and incubated for 5 min. The eluate was captured and the elution procedure was repeated 5 times.

In vitro protein phosphorylation of GST-STAT3 at S727

To phosphorylate STAT3 at serine 727 *in vitro*, the protein kinase ERK1 was used. 2 µl ERK1 active were mixed with 98 µl kinase-assay-buffer. 10 µg GST-STAT3 was added to the ERK1 active dilution and kinase-assay-buffer was added to a final concentration of 25 µg/ml GST-STAT3, mixed, and incubated for 2 h at 30°C. To proof phosphorylation, GST-STAT3 and phosphorylated

GST-STAT3 were analysed on Western blot using phosphospecific antibodies. Phosphorylated GST-STAT3 was aliquoted and stored at -20°C.

2.2.5 Protein microarrays

Printing of antibodies for microspot immunoassays (MIA) and of lysates for reverse phase protein arrays (RPPA) was carried out using the Aushon 2470 Arrayer. This Arrayer is a pin tool spotter which can be equipped with up to 48 solid pins in different alignments. Each pin dips into a single well of a 384-well plate containing the samples. Due to the characteristics of the pins, a small droplet of liquid remains at the tip of the pin. The volume is dependent on the size of the pin. The droplet is then delivered to the slide. Here, the pins had a diameter of 185 µm. This resulted in 1.6 nl per spot with an average spot diameter of 250 µm. To achieve a consistent spot morphology, 0.05% Tween®20 were added to all samples, antibodies and lysates. Tween®20, like any other detergent, lowers the interfacial surface tension and results in a consistant dispersion of the lysate within the spot. For each spotting run, the arrayer generates a so called gal-file which contains the layout of the array and informations regarding the location of each sample on the array.

2.2.6 Microspot Immunoassay

The MIA approach was used to quantify phosphoproteins in cell lysates. Therefore, phosphospecific monoclonal mouse antibodies were used as capture antibodies while polyclonal rabbit antibodies were applied as detection antibodies to bind the captured protein at a different epitope, which is not phosphorylated. In our approach, we only used commercially available antibodies, listed in table 2.4. Each slide was divided into 16 subarrays on which the same set of antibodies was immobilised. Six subarrays were used to create a serial dilution curve, the remaining ten subarrays were used for sample incubation. Figure 2.2 shows the image of a slide with 16 subarrays after performing the detection.

Immobilisation of antibodies

The first step of the MIA procedure was the immobilisation of antibodies on nitrocellulose coated glass slides. To print 16 subarrays per slide, the 2 x 4 pin

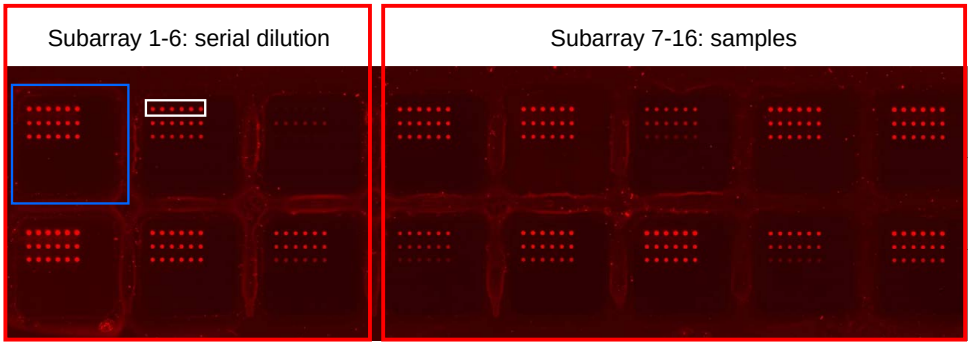

Figure 2.2: MIA slide image
The slide was divided into 16 subarrays (blue). Onto each subarray, three capture antibodies were immobilised in six replicates (white). The slide was incubated with a six-fold serial dilution on subarrays 1-6 and 10 different samples on subarrays 7-16 (red).

and 9 x 9 µm pin spacing configuration of the 2470 Arrayer was used. With this configuration, each capture antibody could be spotted on eight subarrays in parallel. Because spotting was carried out with 8 pins, 3–5 µl of antibody dilution were transferred into 8 wells of one 384-well plate. Figure 2.3 shows the pipetting scheme for three capture antibodies. Prior to spotting, the 384-well plates were centrifuged for 1 min at 700 x g. For low abundant proteins or weak antibodies, two depositions per spot were carried out to double the amount of antibody on the nitrocellulose surface. This resulted in a higher signal intensity. With 3 µl of antibody per well, 36 slides were spotted within 3 h. The spotted slides were stored at 4°C for several weeks.

	1	2	3	4	5	6	7	8	9	10	11	12	13	14	15	16	17	18	19	20	21	22	23	24
A	1	2	1	2	1	2	1	2	3		3		3		3									
B																								
C	1	2	1	2	1	2	1	2	3		3		3		3									
D																								

Figure 2.3: Antibody pipetting layout
Shown is the distribution of three capture antibodies on a 384-well plate for the spotting procedure. Each antibody is dispensed into eight wells.

Sample preparation

For the incubation procedure, the recombinant phosphoproteins and the protein cell lysates had to be denaturated. Therefore, the probes were mixed with 10% SDS to a final concentration of 1% and heated for 5 min at 95°C. To stop the denaturation process, the samples were chilled on ice and centrifuged shortly. To create a standard curve, the recombinant proteins were diluted with assay buffer to generate a six-step two-fold serial dilution. According to the protein of interest, the samples were diluted with assay buffer to a final concentration of 10–50 µg/ml. The concentration of the target protein in the diluted sample has to lie within the range of the dilution series to ensure exact quantification.

Incubation of microspot immunoassays

Ahead of the incubation with the probes, the spotted slides were blocked with blocking buffer for 2–4 hours at 4°C. Before addition of the samples, the slides were mounted into the incubation chamber to create an independent wells on each of the 16 subarrays. 150 µl PBST per well was pipetted with a multichannel pipette to prevent drying. To start the process, the PBST of the first six wells was aspirated off and 200 µl of the standard dilution was transferred into the wells. Afterwards, the PBST from the the last ten wells was aspirated and 200 µl of diluted sample was transferred per well. The slides were incubated over night at 4°C on a rocking platform. The next day, all samples were aspirated off and 150 µl assay buffer was pipetted per well using a multichannel pipette. Slides were washed 3 x 5 min on a rocking platform. After the final washing step, the incubation chamber was disassembled and the slides were placed into a dark box and washed for further 5 min. The following incubation steps were performed in the dark box. Primary antibodies were diluted in assay buffer as listed in table 2.5 and incubated for 2 h at 4°C on a rocking platform. Subsequently, the slides were washed four times in PBST. The Alexa Fluor®680-labeled goat anti-rabbit secondary antibody was diluted 1:5,000 in assay buffer and incubated for 30 min at 4°C on a rocking platform. Afterwards, the slides were washed four times in PBST, one time with ddH_2O, and dried vertically in a slide chamber on paper tissue for at least 30 min and stored in the dark.

Image analysis

The dried slides were scanned using the Odyssey with a laser excitation of 685 nm and a resolution of 21 µm. The images were analysed using the GenePix Pro5.0 software. The software used the gal-files for spot identification and to link the sample annotation to the detected signal intensities. Outliers were flagged and thus discarded from further analysis. The signal intensities of all spots were saved as gpr-files (GenePix result-files).

Data analysis using QuantproReloaded

The analysis of the MIA was performed using the in-house developed R-based software tools Quantpro (Korf et al., 2008b) or QuantproReloaded (Joecker et al., 2010), which was a redesigned software application based on the ideas of Quantpro. In addition to the .gpr-files, Quantpro and QuantproReloaded required a slidedescription and a captureantibody file. The slidedescription file contained the information on the subarrays, for example the specification of the sample, namely calibrator or measurement. Additionally, the dilution factor, the name, and the time point of each sample or the amount of standard protein had to be specified. The captureantibody file contained a list of all capture antibodies printed on the array and the name of the corresponding target protein.

In order to determine the accuracy of a new capture/detection antibody pair using Quantpro, the calibrator measurements were used in a crossvalidation procedure. A linear regression was fitted to 60% of the calibrator measurements and the remaining calibrator measurements were treated as samples of unknown concentration. The absolute deviation from the theoretical concentration was recorded. This was repeated 100 times, and the average deviation was determined.

QuantproReloaded consists of two independent parts. First, the performance analysis employed a cross-validation approach on calibrator data points. The accuracy of the calibrator curve was given for each concentration separately. Different linear and non-linear functions could be chosen to fit the calibrator curve. The example of a calibrator curve and the corresponding performance plot is shown in figure 2.4. After evaluation of the performance plots, the measurement analysis was carried out using the function which had shown the best

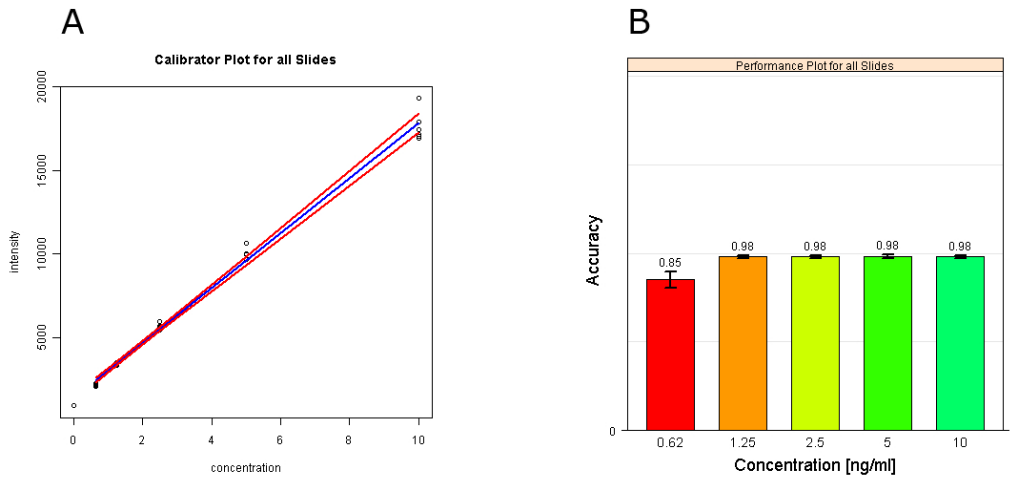

Figure 2.4: Analysis performed using QuantproReloaded
Calibrator plot of pSTAT3 capture antibody BD612653 (A) and the corresponding performance plot (B). The accuracy is calculated for each protein concentration of the serial dilution separately.

performance. Here, the calibrator curve was applied to estimate the concentration of the target analyte in the sample.

2.2.7 Reverse Phase Protein Arrays

Spotting of RPPAs

As the first step with respect to the sample normalisation, the lysates were adjusted to a fixed protein concentration with lysis buffer. Outliers with a low protein concentration were not adjusted. The number of outliers should not exceed 5%. As described before, Tween® 20 was added to a final concentration of 0.05%. Lysates were transferred to a 384-well plate and centrifuged at 700 x g for 1 min. Depending on the number of samples, two or three subarrays were printed per slide. For printing, a print head configuration with 4.5 µm pin spacing was used, equipped with 4 x 4 pins for three subarrays and 4 x 6 pins for two subarrays.

Incubation of RPPAs with antibody solutions

Incubation of the spotted slides with different antibodies was performed in customised incubation chambers. Comparable with the MIA incubation, frames for two or three subarrays were used. The antibody incubation was performed either manually or automated using antibody mediated signal amplification (AMSA) (Brase et al., 2010).

Manual incubation was performed comparable to the procedure described for Western blots. First, slides were blocked over night in blocking buffer at 4°C on a rocking platform. Primary antibody dilutions (1:300) were incubated for 2 h at room temperature on a rocking platform. Afterwards, slides were washed 4 x 8 min in PBST. Next, the slides were incubated with secondary antibody dilution (1:8,000) for 1 h and subsequently washed as described before. After washing the slides in ddH_2O, they were dried vertically in a slide chamber on paper tissue for 30 min.

AMSA detection was performed using the 96-channel head robot Biomek FX to increase the throughput and to minimise experimental variation. Blocking and incubation with primary antibody was performed as described before. Dilutions prepared from anti-rabbit Alexa Flour®680-labeled from goat and anti-goat Alexa Flour®680-labeled antibodies from rabbit (1:8,000) were filled in 96-deep-well plates and incubated alternating for a total of four cycles. For the detection of primary mouse antibodies, anti-mouse Alexa Flour®680 raised in goat was added to the anti-rabbit antibody. Each secondary antibody was incubated for 30 min and slides were washed 4 x 5 min between the incubation steps with washing buffer (PBS + 0.02% SDS (w/v) + 0.02% NP-40). After the last incubated step, slides were washed in ddH_2O and dried as described before.

RPPA image analysis

RPPA slides were scanned using the Odyssey with a laser excitation of 685 nm and a resolution of 21 µm. The images were analysed using the GenePix Pro5.0 software and rawdata was saved as gpr-files. These were used for the further analysis of the data.

RPPA data analysis

In close collaboration with the bioinformatics subgroup of the division and the division Medical Statistics at the University Medical Center Göttingen, an analysis routine was developed tailored towards the requirements of analysing dynamic RPPA data. The scripts needed for the analysis were written in the programming language R (R Development Core Team, 2010) by members of the bioinformatics group. In addition to the gpr-files, two annotation files were needed. The description file contained the specification of every sample sorted by the spot ID as defined by the gal-file. This was used to annotate each spot on each array. The second file, the antibody list, contained the information of antibodies incubated on each subarray. The workflow of the analysis is described in detail in section 3.2. In addition, the R-package "RPPanalyzer" was developed in the division (Mannsperger et al., 2010) and certain features of this package for quality control of the data were used.

Quality control of RPPA data

In order to estimate the quality of the antibodies, dilution series of lysates obtained from stimulated, unstimulated, and starved cells were spotted. First, the raw signal intensities of the dilution series were plotted *versus* the protein concentration of the lysates and the mean of the technical replicates was calculated. Second, a constant model was fitted to the dilution data, as well as linear models. For the linear models, the first, second, and so on dilution step was left out and a linear model fit for each set of dilutions was calculated. The linear models were compared to the constant fit using ANOVA. The one with the smallest p-value was considered as optimal. Furthermore, a 75% confidence intervall (CI) was calculated. This means that with a confidence of 75% the signal intensity of a protein lysate concentration of the dilution series differs significantly from the signal intensity of the next lower protein concentration. The better the antibody, the less data points were excluded from the 75% CI. A second aspect of the quality control was the comparison of the signal intensities of each antibody to the blank signal. The blank corresponded to signal intensities after incubation with secondary antibody without the primary antibody. Antibodies, which revealed the same signal intensities as the blank were omitted from the further analysis. This analysis included the dilution series as well as the samples.

Normalisation of RPPA data

The total protein concentration may differ between the spots due to pipetting and spotting errors. Thus, the antibody signals had to be normalised for the total protein amount per spot as described by Loebke et al. (2007). One slide per spotting run was incubated with the protein dye Fast Green FCF (FCF). This dye can be detected using the Odyssey. The slide was wetted with PBS and incubated in FCF staining solution for 1 h at room temperature on a rocking platform. For destaining, the slide was immersed twice in FCF destaining solution for 30 min each. The slides were scanned at 800 nm and analysed using the GenePix Pro5.0 software as described before. The raw signal intensity (RSI) of each spot was normalised using the signal intensity of FCF readout of each spot (FSI) and the mean of all FCF values ($\overline{\text{FSI}}$) resulting in the normalised signal intensities (NSI) using the following equation.

$$\text{NSI} = log_2\left(\frac{\text{RSI}}{\text{FSI}}\,\overline{\text{FSI}}\right) = log_2(\text{RSI}) - log_2(\text{FSI}) + log_2(\overline{\text{FSI}})$$

Analysis of time-resolved measurements

To smooth the signals and estimate a response over the time, the R-package "gam" (Hastie, 2010) was used to fit smoothing splines (Chambers, 1991) on the time-resolved data. Smoothing splines model the signal over time in a nonparametric way. The output are fits describing the estimated dynamics of the phosphoprotein measurement changes. To calculate if a particular condition had a significant effect, smoothing splines with increasing degrees of freedom were fitted over the median of all biological replicates as explained in section 3.2.3. Afterwards, each model was compared to the constant model fit via analysis of variance (ANOVA). The model with the lowest p-value was chosen as best fit. To find significant differences between two time series experiments, a two-sided two-sample t-test for each time point was performed, using a significance level of alpha=0.05.

2.2.8 Cell culture

The cells were grown in media described in section 2.1.13. Depending on the particular cell size, cells were seeded in differing densities as listed in table 2.9.

Table 2.9: Overview of seeded cell density

Cell lines	Cell density					
	T75	T175	6-well	6 cm	10 cm	14.5 cm
BT474	2×10^6	4×10^6	5×10^5	1.4×10^6	4×10^6	8×10^6
HCC1954	8×10^5	1.8×10^6	2×10^5	5×10^5	2×10^6	4×10^6
MCF7	1×10^6	2.3×10^6	4×10^5	1×10^6	3×10^6	7×10^6
SKBR3	1.2×10^6	2.8×10^6	4×10^5	1.8×10^6	3×10^6	6×10^6

Subculturing of cells

To keep the cells constantly in the exponential growth phase, cells were passaged every two to three (HCC1954) or three to four days (SKBR3, BT474, and MCF7). The medium was completely removed and cells were washed with DPBS. Subsequently, cells were incubated with 2 ml (T75) or 4 ml (T175) of 0.25% trypsin for two (MCF7) to four (HCC1954, SKBR3, and BT474) minutes at 37°C until they detached from the surface. Trypsin was deactivated by addition of 8 ml growth medium, and cells were gently resuspended and counted. Then, the number of cells listed in table 2.9 were transferred into new culture flasks and incubated at 37°C in an atmosphere of 5% CO_2 and 95% humidity.

Freezing and thawing cells

To prepare frozen stocks of the cell lines, actively growing cells were trypsinised, counted and centrifuged at 1,200 rpm for 5 min to remove the medium. Afterwards, cells were resuspended in freezing medium to a quantity of $1.5–2 \times 10^6$/ml and 1 ml was pipetted into each cryo vial. Vials were put into a freezing container to provide the -1°C/min cooling rate and placed into -80°C. For long term storage, cells were transferred to liquid nitrogen.
Cells were thawed in a 37°C waterbath for approximately 2 min and immediately resuspended in prewarmed growth medium. Afterwards, cells were centrifuged for 5 min at 1,200 rpm to remove the freezing medium containing DMSO. The cell pellet was gently resuspended in growth medium, transferred into the culture flask and incubated at 37°C in an atmosphere of 5% CO_2 and 95% humidity.

2.2.9 Growth factor stimulation experiments

High throughput stimulation experiments were carried out in 6-well plates. For Western blot analysis or to gain more lysate, all formates between 6 cm and 14.5 cm plates were used. Cells were seeded according to table 2.9. Cells were cultivated for 24 h and serum-starved in phenol-red free medium for additional 24 h. The stimulation experiments in 6-well plates were carried out using two different protocols.

AUTOMATED cell culture experiments were performed using an automated liquid handling system with an integrated incubator (Biomek FX) to ensure consistency between the biological replicates. The inhibitors and ligands for each experiment were provided in 96-well plates. 50 µl of inhibitor and ligand dilution were added to the cells. For preincubation with inhibitors, the plates were transferred by the system into the incubator for 1 h. For stimulation experiments, the first two time points were left on the deck of the Biomek FX while the further time points were again transferred by the system into the incubator. After the indicated time points (0, 4, 8, 12, 16, 20, 30, 40, 50, 60 min), medium was replaced by ice-cold PBS and plates were placed on ice. Afterwards, PBS was aspirated off and cells were harvested by manual scraping in 40 µl lysis buffer. Lysate were collected on dry ice and stored at -80°C.

MANUAL stimulation in 6-well plates was carried out with a Liquidator^{96}, a manual 96 channel pipette. Therewith, the solutions were applied to each well comparable to the automated system. The plates and the Liquidator^{96} were put on a 37°C preheated pet surgery table. The solution was pipetted using five tips per wells and afterwards the plates were put either to the incubator or were left on the 37°C table, depending on the time of incubation.

Stimulation experiments using other formats than 6-well plates were carried out on the pet surgery table. This was preheated to 37°C. Plates were put on the table and ligands were added using a Multipette. After each time point, medium was discarded, cells were washed with ice-cold PBS and plates were placed on ice. PBS was aspirated off and cells were lysed as described before.

Impact of targeted therapeutics on ERBB signalling

Stimulation experiments were performed in triplicate applying three inhibitors trastuzumab, pertuzumab, and erlotinib at concentrations listed in table 2.1

and two ligands EGF and HRG at a concentration of 5 nM in all possible combinations. Including a control, 0.000008% Tween®20, this resulted in eight experiments per ligand or ligand combination. The layout of the experiments is shown in figure 2.5. Experiments 1–4 were carried out separately for each ligand,

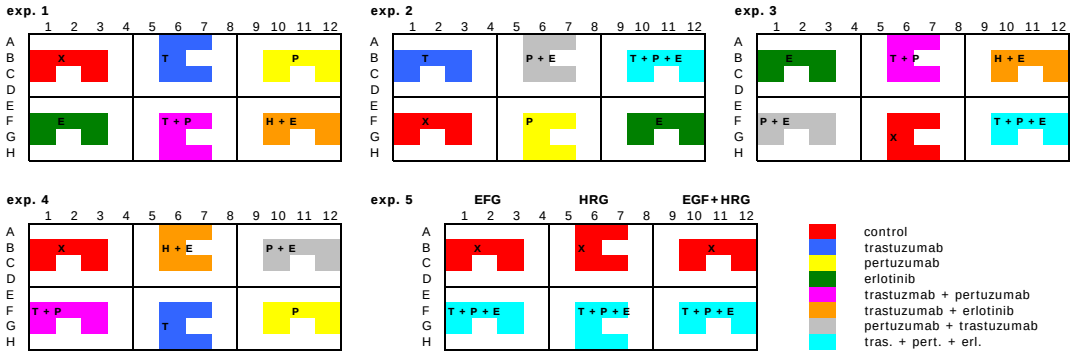

Figure 2.5: Design of stimulation in 6-well format
Layout of inhibitor conditions prepared in 96-well plate for automatical transfer into 6-well plates with growing cells conducted by the Biomek FX. Exp. 1-4 were incubated separately with all the ligand combination. Exp. 5 was accomplished once.

experiment 5 combined three ligand combinations in a single experiment. Altogether, the setup resulted in 13 single experiments performed in 6-well format per cell line. This layout comprised three replicates for all inhibitor conditions and five replicates for the uninhibited controls. Additionally, the impact of the drugs were analysed without addition of a ligand.

2.2.10 siRNA-mediated receptor knockdown

siRNA transfection was performed in the 6-well format. Per well, 2.5 µl Lipofectamine 2000 was added to 147.5 µl OptiMEM, mixed, and incubated for 10 min at room temperature. Afterwards, 300 µl OptiMEM was added. The siRNA stock (20 µM) was diluted 1:100 in sterile, nuclease free H_2O. 150 µl of diluted siRNA was pipetted into each well and 450 µl Lipofectamine 2000/OptiMEM mix was added, mixed, and incubated for 20 min at room temperature. For the mock control, 150 µl sterile, nuclease free H_2O was used instead of siRNA dilution. Meanwhile, cells were trypsinated and counted. 3×10^5 cells were added in 900 µl growth medium to the siRNA/Lipofectamine mixture. Growth medium was renewed 6 h after transfection. After transfection, cells were incubated for 48 h and serum-starved for additional 24 h prior to stimulation.

2.2.11 Preparation of protein extracts

The frozen lysates were thawed on ice and lysis was performed on an end-over-end shaker for 20 min at 4°C. Afterwards, lysates were cleared by centrifugation for 10 min at 16,000 x g. The supernatant was transferred to a fresh, prechilled reaction tube and stored at -20°C and for long term storage at -80°C.

Determination of protein concentration

Total protein concentration was determined using the BCA assay. The microplate procedure was carried out according to protocol whereas only 5 µl instead of 25 µl of each sample of unknown concentration were used (Korf et al., 2008a).

2.2.12 RNA isolation

RNA was isolated using the RNeasy®Kit. Cells were detached by trypsinisation, counted, and pelleted by centrifugation at 1,200 rpm for 5 min. 5×10^5 cells were washed once in PBS and resuspended in 350 µl RLT buffer. 350 µl 70% ethanol was added and the solution was pipetted onto RNeasy®spin columns. Isolation of RNA was performed according to the manufacturers protocol. Elution of RNA was carried out twice by adding 50 µl nuclease-free H_2O. The isolated RNA was stored at -80°C.

Determination of RNA concentration

Total RNA concentration was determined using the NanoDrop ND-1000 UV/VIS spectrophotometer. The absorption of the nucleic acid solution was measured between 230 nm and 280 nm and the concentration was calculated automatically by the software. The absorption maximum of nucleic acids is 260 nm whereas proteins show the maximum absorption at 280 nm. In addition to the concentration, the purity was determined by calculating the ratio of the extinction values at 260 nm/280 nm and 260 nm/230 nm.

2.2.13 First strand synthesis of complementary DNA (cDNA synthesis)

First strand synthesis of complementary DNA (cDNA) was performed applying the ReverdAid™H-Minus First Strand cDNA Synthesis Kit. 400 ng extracted total RNA was mixed with 1 µl oligo$(dT)_{18}$-primer and incubated for 5 min at 70°C in a PCR cycler and subsequently cooled at 4°C. After addition of 8 µl reaction master mix (4 µl 5 x reaction buffer, 2 µl 10 mM dNTPs, 30 units prime RNAse inhibitor and RevertAid™H Minus M-MuLV Reverse Transcriptase), the reaction mix was first heated to 37°C and first strand synthesis was performed for 60 min at 42°C and stopped for 10 min at 70°C. The resulting cDNA solution was directly used for quantitative real-time-PCR.

2.2.14 Quantitative real-time-PCR (TaqMan)

Quantitative real-time-PCR allows the detection of the relative expression of genes with high sensitivity. The probes used for quantification consist of a fluorophore covalently linked to the 5'-end of the oligonucleotide probe and a quencher molecule at the 3'-end. As long as the quencher and the fluorophore are in proximity, the quencher erases the fluorescence emitted by the fluorophore despite exitation. The DNA polymerase exhibits 5'-3' exonuclease activity and degrades the probe which annealed to the template. Degradation of the probes releases the fluorophore and therefore relieves the quenching effect. Thus, fluorescence can be detected by the real-time PCR thermal cycler. Only probes bound to DNA are degraded by the DNA polymerase and therefore the fluorescence detected is directly proportional to the amount of DNA template in the PCR. The increasing fluorescence signal is detected and plotted against the number of PCR cycles.

To perform the Taqman experiment, 20 ng cDNA dissolved in 5 µl H_2O were transferred into a 384-well plate and 6 µl master mix consisting of 5.5 µl 2x PCR buffer and 0.5 µl TaqMan Assay for the probe of interest was added to the well. Each assay reaction was set up in triplicate. The qRT-PCR reaction was executed in the 7900HT Fast Real-Time PCR System. The assay was preheated for 2 min at 50°C and 15 min at 95°C. The reaction cycle of 15 sec 95°C and 1 min 60°C was repeated 40 times.

Quantification of relative gene expression (ΔΔCt method)

The Ct values were determined by the SDS-software. The analysis was performed applying the R-package "ddCt" (Biczok et al., 2010). In a first step, the median of the GAPDH Ct values ($\mathrm{Ct}_{H,j}$) were calculated for each sample triplicate. This value was subtracted from the median Ct values ($\mathrm{Ct}_{i,j}$) of each gene (ΔCt).

$$\Delta\mathrm{Ct}_{i,j} = \mathrm{Ct}_{i,j} - \mathrm{Ct}_{H,j}$$

In a second step, the normalised expression values of a control was subtracted from the normalised expression values ($\Delta Ct_{i,j}$). The "ddCt" package was designed mainly to analyse knockdown experiments. However, this package was applied to analyse the relative amount of gene expression for the four cell lines. As control, the mean expression value of the EGFR for the four cell lines was used as control ($\Delta Ct_{i,R}$). This resulted in ΔΔCt-values.

$$\Delta\Delta\mathrm{Ct}_{i,j} = \Delta\mathrm{Ct}_{i,j} - \Delta\mathrm{Ct}_{i,R}$$

The relative gene expression level of one gene compared to the mean EGFR expression within the four cell lines, normalised to the expression of GAPDH was given by the following equation:

$$\text{expression level}_{i,j} = 2^{-\Delta\Delta\mathrm{Ct}}$$

2.2.15 Cell cycle analysis applying 7AAD

Cell cycle analysis was performed in 6-well format. 2.5×10^5 cells were seeded in 2 ml medium per well and incubated for 24 h. Medium was replaced by 1.2 ml fresh medium and a 1:10 dilution of the therapeutics were added to a final concentration as listed in table 2.1. Cells were incubated for 24 h at 37°C in an atmosphere of 5% CO_2 and 95% humidity. After treatment for 24 h, cells were taken out of the incubated and washed with PBS. To detach the cells, 500 µl trypsin was added and cells were incubated for 3–4 min at 37°C and 5% CO_2. 500 µl medium was added and cells were separated by gently pipetting up and down. Cells were transferred to a 96-well 1.2 ml deep-well-plate and centrifuged at 1450 x g for 5 min at RT. The following steps were performed using the Liquidator[96]. For fixation and permeabilisation, 1 ml icecold 90% methanol was added and carefully resuspended. Afterwards, cells were incubated for 30 min on

ice. Meanwhile, 7AAD solution was prepared by adding 7.5 µl 7AAD to 300 µl PBS per well. Cells were again centrifuged at 1450 x g for 5 min at RT. Supernatant was removed and 300 µl 7AAD staining solution was pipetted per well and cells were resuspended. Plate was covered with foil and left at 4°C for 90 min. DNA content was determind by flow cytometric analysis (FACS Calibur). Analysis of the rawdata to determine the proportion of cells in a specific cell cycle phase was accomplished using the R-package "flowDeconvolutor" (Zhang et al., 2010).

3 Results

3.1 Microspot Immunoassay

The microspot immunoassay (MIA) technology was established for the exact quantification of pERK1/2 in human samples as part of my diploma thesis (Henjes, 2006). To generate an experimental platform suitable for the analysis of ERBB signalling, the assay was extended to the quantification of the phosphoproteins pAKT (S473), pAKT (T308) and pSTAT3 (S727). The readout of the assay was calculated in ng phosphoprotein per µg total protein lysate (ng/µg).

In general, two options exist to detect the phosphorylation status of a protein. Phosphoproteins can be captured either with a phosphoprotein specific antibody and detected with a protein specific antibody or vice versa. Using phosphospecific antibodies in the capture step has major advantages. First, total protein and phosphoprotein concentration can, in principle, be detected within one assay, when a specific antibody for total protein is printed in parallel. This is not possible if a phosphospecific antibody is used in the detection step. Second, the detection with the phosphospecific antibody requires that the phosphoepitope of interest is accessible for the detection antibody. This is critical as protein binding to immobilised antibodies cannot ensure even exposure of all proteins. In addition, polyclonal antibodies can bind to different epitopes on the surface of the captured proteins, which might increase signal intensity. Although phosphoproteins were quantified with high reproducibility using the MIA approach, the corresponding measurements of the total target protein amount were highly variable.

3.1.1 Development of a Microspot Immunoassay

The antibody validation routine comprised several steps to ensure high specificity as well as low cross reactivity among antibodies used in the multiplexed

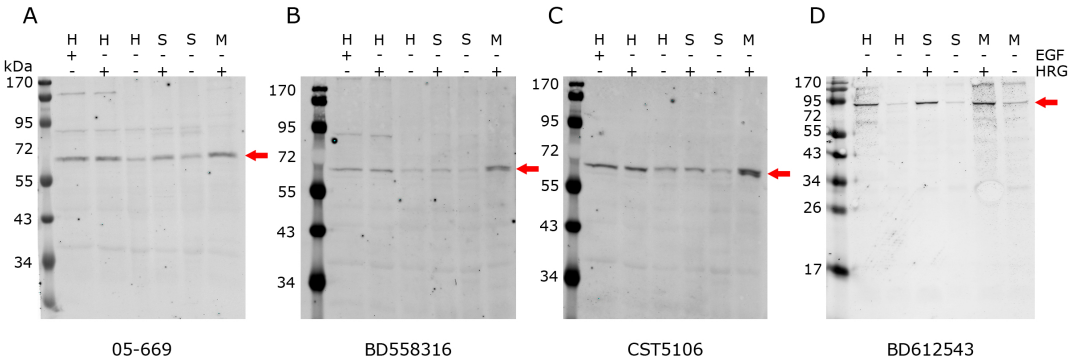

Figure 3.1: Antibody validation by Western blot
Western blot of four capture antibodies A: 05-669 (AKT S473; 60 kDa), B: BD558316, C: CST5106 (pAKT T308; 60 kDa) and D: BD612543 (pSTAT3; 92 kDa) probed on starved and EGF- or HRG-stimulated HCC1954 (H), SKBR3 (S), and MCF7 cells (M). The arrow points to the specific signal.

format. The steps required for assay development are explained in the following section.

Assessment of antibody specificity

As a first step in the development of a new assay, all antibodies were tested by Western blot for their specificities. Phosphospecific antibodies were probed on starved and stimulated breast cancer cell lysates to control if the antibodies detected only the phosphorylated protein present in the stimulated sample (Fig. 3.1). All antibodies caused a stronger signal in the stimulated samples confirming phosphospecificity. To keep the assay format similar to the successfully established pERK1/2 assay, only monoclonal mouse antibodies were used as capture antibodies. The development of the assay for AKT (T308) will be explained in detail. Assays for pAKT (S473) and pSTAT3 (S727) were established accordingly.

Determination of antibody reactivity

Two phosphospecific antibodies against the new target of interest were spotted along with other capture antibodies already established for microspot immunoassays. Next, a serial dilution of recombinant phosphoprotein was incubated on the mounted slide as described in section 2.2.6. Several detection antibodies

were tested, alone and in combination with already established detection antibodies. In general, the signal intensities of the capture antibody had to show a linear correlation with the protein concentration. The quality of an antibody pair was evaluated as described in section 2.2.6.

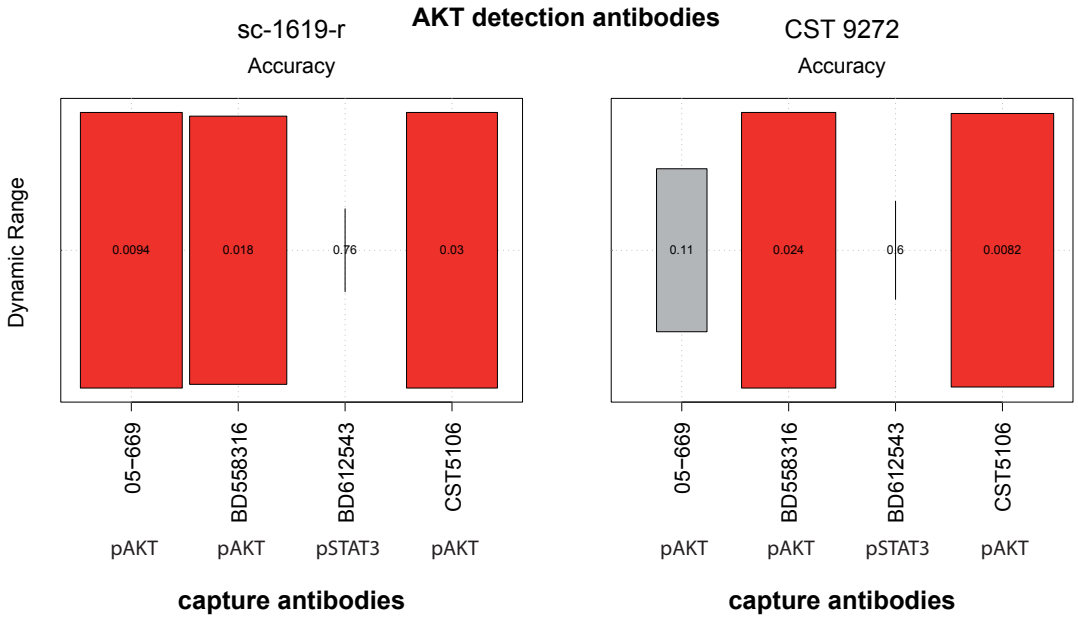

Figure 3.2: Performance plot
Analysis of reactivity between the capture antibodies for AKT-S473 (05-669), AKT-T308 (BD558316, CST5106) and STAT3 (BD612543) with recombinant pAKT and the AKT detection antibodies sc-1619-r and CST9272. The higher the accuracy, the broader the box of the antibody pair. A broad, red box indicated a reliable combination of capture and detection antibody, a small, grey box indicates low accuracy and a small dynamic range, and no box indicated that the antibody pair did not detect the phosphoprotein.

In the initial experiment, the slide was divided into two equal parts comprising eight pads each. Six subarrays were incubated with a five-step two-fold serial dilution of recombinant pAKT and assay buffer as a negative control. Two additional subarrays were incubated with MCF7 cell lysates, HRG-stimulated and unstimulated. The first part of the slide was then incubated with sc-1619-r as detection antibody, and the second part with CST9272. Figure 3.2 shows the resulting performance plots generated by Quantpro. First of all, the performance plots revealed that the pSTAT3 capture antibody did neither cross react with recombinant pAKT nor with the AKT detection antibodies. This was an

Table 3.1: Antibody combinations tested to newly establish a AKT (T308) assay

capture antibodies		detection antibodies		
		AKT		STAT3
		sc-1619-r	CST9272	CST9132
BD558316	AKT (T308)	good	good	no signal
CST5106	AKT (T308)	background	background	no signal
05-669	AKT (S473)	good	not working	no signal
BD612543	STAT3 (S727)	no signal	no signal	good

important requirement for the combination of both phosphoproteins within a single assay. Second, the three pAKT capture antibodies showed a good performance with the detection antibody sc-1619-r, but the capture antibody 05-669 did not work well in combination with CST9272. For both detection antibodies, CST5106 revealed a high background signal, however, since the correlation between protein concentration and signal intensity was linear, a good performance plot was obtained for both detection antibodies. According to these results, the AKT detection antibody sc-1619-r was used for the further development of the assay, as it showed good performance with all capture antibodies. Then, a serial dilution of both recombinant phosphoproteins, pAKT and pSTAT3, were incubated in parallel and a mixture of the detection antibodies CST9132 (STAT3) and sc-1619-r (AKT) was applied. In this experiment, the pSTAT3 capture antibody showed a good performance plot as a linear correlation between signal intensity and the protein concentration was also obtained for pSTAT3 (data not shown).

As second validation step, the potential crossreactivity between recombinant pSTAT3 and the AKT capture and detection antibodies was assessed. A serial dilution of recombinant pSTAT3 and two protein lysates, as described before, were applied to each half of the slide. In the first setup, sc-1619-r as AKT detection antibody was incubated and in the second part, both detection antibodies were mixed. The performance plot indicated no correlation between pSTAT3 and the AKT antibodies, whereas the pAKT capture antibody CST5106 resulted in a very high signal intensity, even for the negative control. For this reason, CST5106 was not suitable for the MIA platform and was discarded from the assay and BD558316 was used to capture AKT (T308). On the other hand, the high specificity of the pSTAT3 detection was confirmed since no crossreactivity

with the pAKT capture antibodies was observed. Table 3.1 summarises the identification of suitable pAKT (T308) antibody pairs to integrate the quantification of pAKT (T308) into the existing assay for pAKT (S473) and pSTAT3.

As a final validation experiment, selected antibody pairs were examined using biological samples obtained from dynamic measurements of MCF7 cells stimulated with HRG. Taking into account the highly different abundance of the phosphoprotein of interest, two separate MIAs were established in which different dilutions of the lysates are applied. The first MIA quantifies pERK1/2 and pAKT (S473) and the second assay the less abundant phosphoproteins pAKT (S473), pAKT (T308) and pSTAT3 (S727) (table 3.2).

Table 3.2: Antibody combinations used for the two microspot immunoassays

capture	**detection antibodies**		
antibodies	**ERK1/2**	**AKT**	**STAT3**
Assay 1:	sc-94 / 06-182	sc-1619-r	
M9692	pERK1/2		
CST9106	pERK1/2		
05-669		pAKT S473	
Assay 2:		sc-1619-r	9132
05-669		pAKT S473	
BD558361		pAKT T308	
BD612543			pSTAT3 S727

3.2 Reverse Phase Protein Arrays

Reverse phase protein arrays (RPPA) are a tool for quantitative measurements of protein abundance and activation. Specificities and sensitivities of the antibodies were examined thoroughly, since protein quantification relies on a single antibody. RPPAs were used to analyse signalling networks on the protein level. Before analysing the time-resolved measurements, the quality of the experimental data had to be validated carefully. During the advancement of the RPPA technology, additional steps of quality control were introduced which were required to analyse the generated high amount of data.

3.2.1 Antibody validation

For the reliability of RPPA analysis, it was crucial, that all antibodies were very specific. Therefore, the first step of the antibody validation routine was screening new antibodies for specificity towards the respective target proteins using the Western blot technique. Figure 3.3 shows the Western blots of two antibodies specific against pPKCα. The antibody 06-822 showed a single specific

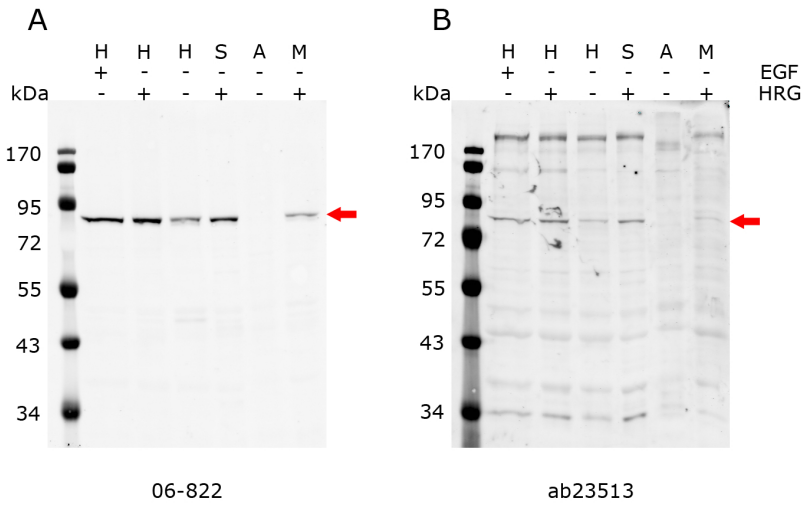

Figure 3.3: Antibody validation by Western blot
Two antibodies against pPKCα (S657) (82 kDa) 06-822 (A) and ab23513 pPKCα (S657/Y658) (B) probed on EGF or HRG stimulated and unstimulated cell lysates from HCC1954 (H), SKBR3 (S), A431 (A), and MCF7 (M) cells. The arrow points at the specific signal.

band and was positively validated for RPPA. In contrast, ab23513 revealed in addition a prominent unspecific band and high background and therefore this antibody was not used for RPPA analysis.

To establish antibodies suitable for the quantification of downstream targets of ERBB signalling, all antibodies validated as specific on Western blot were analysed on RPPA. To achieve this, dilution series prepared from lysates of HCC1954, SKBR3, and BT474 cells under steady-state and stimulated conditions were spotted, and 45 antibodies against different proteins and phosphosites from the ERBB signalling network were applied (table 3.3). Before lysis, cells were serum-starved for 24 h and stimulated with EGF or HRG for 10 min to induce protein phosphorylation.

Table 3.3: Antibody qualities evaluated based on dilution series

target	phosphosite	company	catalog number	quality
AKT	T308	CST	4056	high
AKT	S473	CST	4058	high
AKT	S473	CST	9271	high
AKT	T308	CST	9275	high
EGFR		Santa Cruz	sc-03	high
EGFR		CST	2646	high
EGFR	Y1068	CST	2236	moderate
EGFR	Y1173	CST	4407	high
EGFR	Y845	CST	2231	high
EGFR	Y992	CST	2235	moderate
EGFR	Y1045	CST	2237	low
EGFR	Y1148	CST	4404	moderate
EGFR	Y1086	CST	2220	moderate
ERBB2		Neomarkers	AB-17	high
ERBB2		CST	2165	high
ERBB2	Y1139	abcam	ab53290	moderate
ERBB3		Neomarkers	AB-2	high
ERBB3	Y1197	CST	4561	high
ERBB3	Y1222	CST	4784	moderate
ERK1/2	T202/Y204	CST	9106	high
GAB1		CST	3232	high
GAB1	Y307	CST	3234	high
MEK		BD	610122	high
MEK1/2	S217/221	Sigma	M7683	high

Table 3.3: Antibody qualities evaluated based on dilution series

target	phosphosite	company	catalog number	quality
MET		CST	3127	low
MET	Y1003	CST	3135	low
MET	Y1234/35	CST	3077	low
NFkB		Santa Cruz	sc-109	high
NFkB	S536	CST	3033	high
p90RSK	S380	CST	9341	high
p90RSK	T359S363	CST	9344	high
PDK1		CST	3062	high
PDK1	S241	CST	3061	high
PKC		abcam	ab32376	high
PKC	S657/Y658	abcam	ab23513	high
PLCγ		abcam	ab41433	high
PLCγ	S1248	CST	4510	high
PTEN	T366/S370	Epitomics	2195-1	high
RSK		CST	9355	high
SDHA		Santa Cruz	sc-59687	high
SRC	Y416	CST	2101	high
SRC		CST	2123	high
STAT3	Y705	CST	9131	moderate
STAT3	S727	CST	9134	high
STAT3		Santa Cruz	sc-482	high

34 of the 45 antibodies tested revealed a linear correlation between lysate concentration and signal intensity and a high dynamic range. Phosphospecific antibodies also showed different signal intensities between the dilution series with stimulated and unstimulated lysates, indicating the phospho-specificity of the antibodies. However, a few antibodies showed a linear correlation but the intensity range was very low. A linear correlation but low signal intensity might be due to the fact that the target protein is of low concentration as observed for the phospho-EGFR antibodies. Those antibodies were used with caution and quality was validated on each new sample set. Besides showing a linear correlation and a high dynamic range, the resulting data had to reflect the actual protein expression or activation status of the samples. This was not possible for the MET and pMET and the corresponding antibodies were excluded from further RPPA experiments.

In summary, the experiments showed that most antibodies tested by Western blot analysis worked well on RPPAs. Several phosphospecific ERBB receptor antibodies had to be validated carefully for each single experiment but only the MET specific antibodies failed. However, the quality of each antibody was assessed for each RPPA experiment as explained in the following sections.

3.2.2 Quality control of RPPA data

Three antibodies, anti-pERK1/2 CST4370, anti-pAKT (S473) CST9271, and anti-pp70S6K (T421/S424) 1135-1, were chosen to exemplify the antibody quality control (Fig. 3.4).

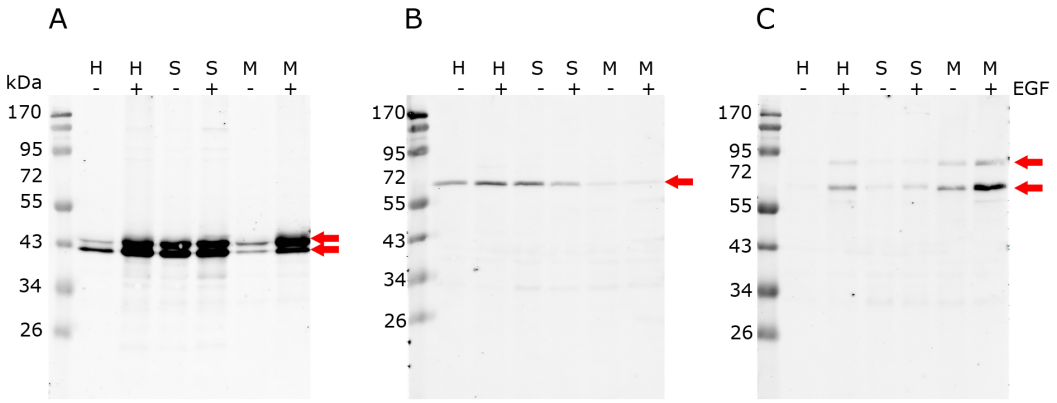

Figure 3.4: Determination of antibody specificity by Western blot
Lysates from starved and EGF-stimulated HCC1954 (H), SKBR3 (S), and MCF7 (M) cells were probed with antibodies against pERK1/2 (A), pAKT (S473) (B), and pp70S6K (T421/S424) (C). Red arrows indicate the specific signals (C: p70S6K and p85S6K).

Each slide contained dilution series of the corresponding cell lines in addition to the measurement samples to serve as basis for antibody quality control. Only antibodies showing a linear correlation between signal intensity and protein concentration were considered for further data analysis. Figure 3.5 shows the dilution curve of the antibodies specific for pERK1/2 (A), pAKT (S473) (B), and pp70S6K (T421/S424) (C). The corresponding Fast Green FCF protein stain of the serial dilution of the protein lysate is shown in figure D. The analysis of the dilution series was performed as described in section 2.2.7. In case of pERK1/2 and pAKT (S473), no point was excluded from the linear fit, indicating a perfect

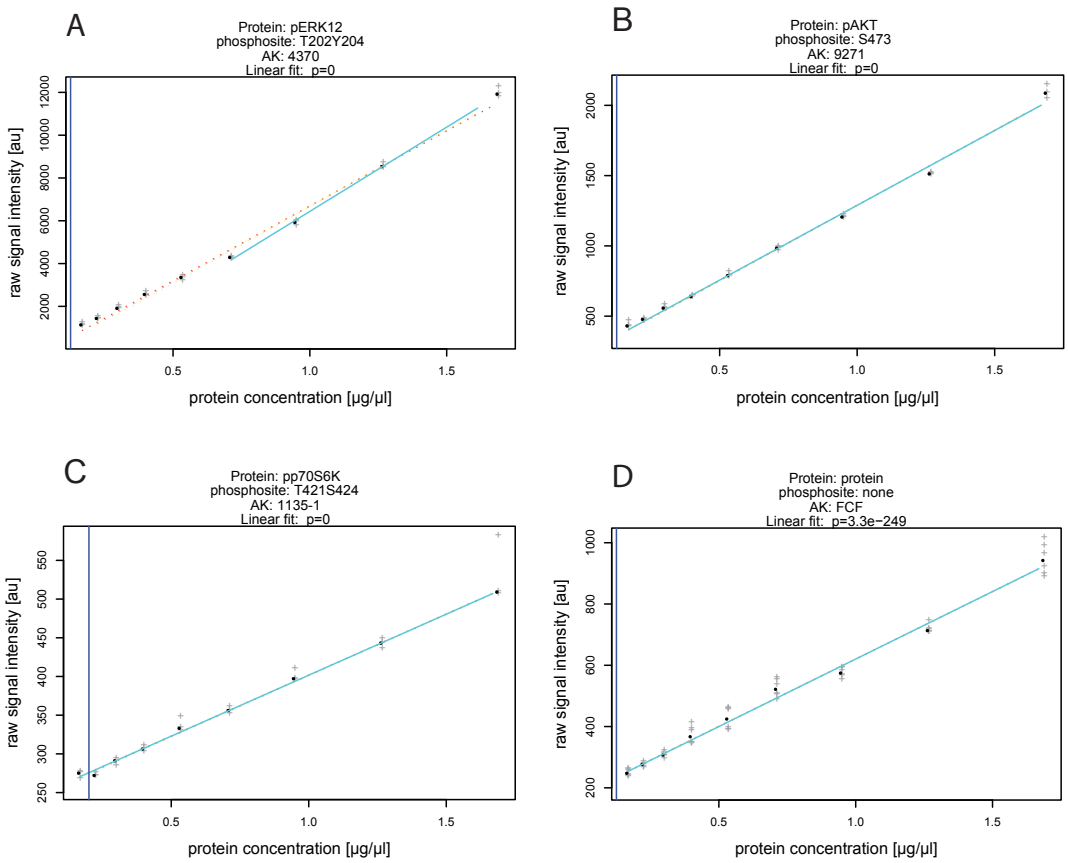

Figure 3.5: Serial dilution curve

The diagrams show the dilution curve of an EGF stimulated lysate immobilised on RPPA and incubated with the pERK1/2 antibody CST4370 (A), the pAKT (S473) antibody CST9271 (B), the pp70S6K (T421/S424) antibody 1135-1 (C) and the protein dye Fast Green FCF (D). The grey crosses represent the single technical replicates, the black circle the median of the replicates. The light blue line represents the linear fit of the dilution series with the lowest p-value. The light dashed lines represent the fits with higher p-values. The vertical blue line shows the cutoff of the 75% CI.

fit of the antibody. Regarding the detection of pp70S6K (T421/S424), only the lowest protein concentration was excluded from the linear correlation, where the antibody signal was not above the background signal.

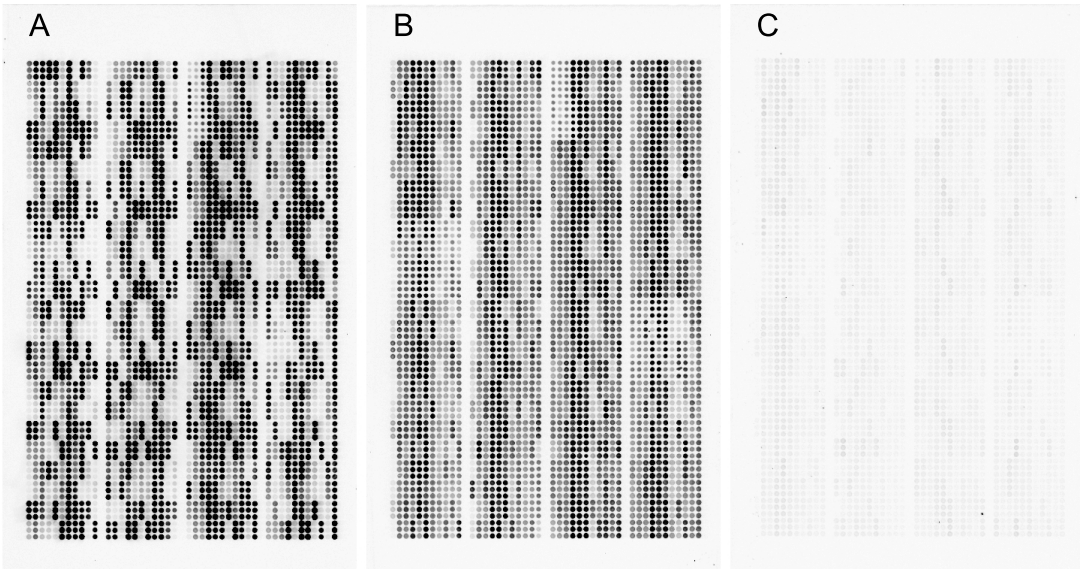

Figure 3.6: Exemplary RPPA slide images
Images of slides from the HCC1954 data set incubated with pERK1/2 antibody (A) pAKT (S473) (B) and pp70S6K (T421/S424) (C) scanned with the same intensity setting of the Odyssey scanner.

RPPA experiments normally comprised a number between 400 and up to more than 1000 samples. Antibody quality was therefore not only evaluated for the control dilution series, printed with every sample set, but for all immobilised samples. The visual inspection of RPPA slide images gave a first impression of the quality and consistency of the antibody incubation (Fig. 3.6). The pERK1/2 and the pAKT (S473) antibody resulted in images with very strong signals while the image of the pp70S6K (T421/S424) antibody showed much weaker signal intensities. For all three phosphospecific antibodies, differences in the signal intensities between the samples were observed indicating a different concentration of the phosphoproteins. Furthermore, the images of all three antibodies revealed an uniform background indicating an even antibody incubation process. To evaluate the quality of the antibody signal, the signal intensity of each antibody was compared with the corresponding blank signal of the secondary antibody.

In order to do this, the measurement signal of each spot was plotted against the corresponding blank signal (Fig. 3.7). In all cases, the specific signal of the antibody was stronger than the blank signal, although the pERK1/2 and the pAKT antibodies revealed much stronger signals than the pp70S6K (T421/S424) antibody, suggesting a careful evaluation of the pp70S6K (T421/S424) time series data.

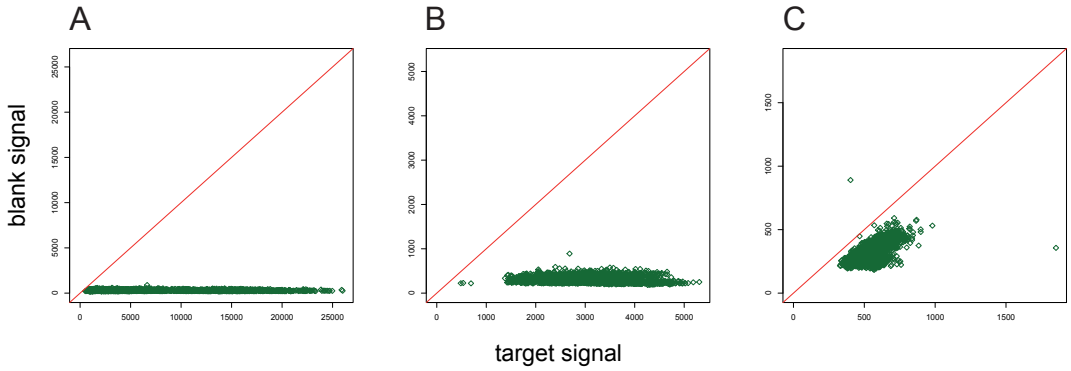

Figure 3.7: Signal *versus* blank
The figure shows all measurement signals plotted against the corresponding blank signal of HCC1954 cells. (A) pERK1/2 antibody plot, (B) pAKT (S473) antibody plot, and (C) pp70S6K (T421/S424) antibody plot.

3.2.3 Data analysis of time-resolved measurements

After quality control, the first step in RPPA data analysis was the normalisation of the raw signal intensities of each antibody using the signal intensities of the total protein stain FCF as described in section 2.2.7. Figure 3.8 shows the effect of normalisation of the pERK1/2 signal for dynamic measurements performed in HCC1954 cells. The five biological replicates are represented by lines of different colours. The antibody signal intensities of the light and the dark blue lines were weaker compared to the others (A). The same was true for the FCF signals of the corresponding lysates indicating a lower amount of protein in these two time series (B). After FCF-based normalisation of the antibody signals, the five biological replicates approximated (C).

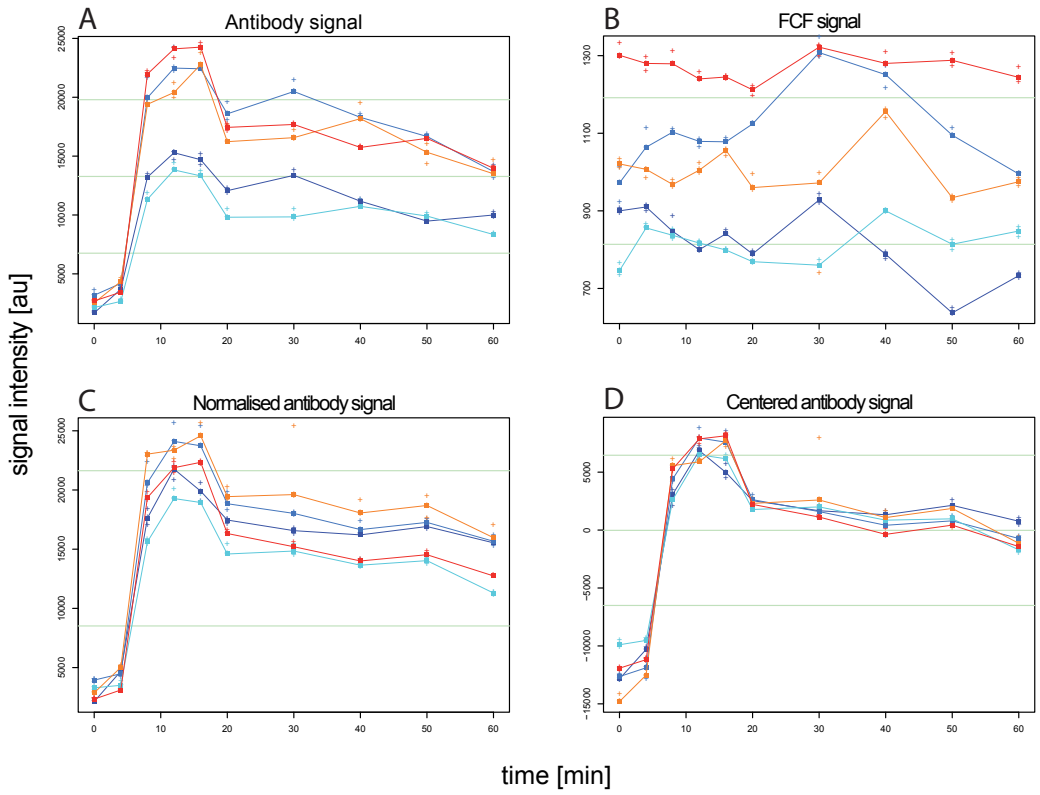

Figure 3.8: Signal normalisation using FCF and centering of the data. Raw signal intensity of pERK1/2 antibody (A), FCF signal (B), normalised antibody signal intensities (C), and centered signal intensities (D). The coloured line represent the five biological replicates.

To facilitate comparability of biological replicates, a centering around zero was tested (D). The centering was performed on the level of technical replicates:

$$\hat{x}_i = x_i - \overline{x} \qquad 1 \leq i \leq 10$$

where x_i is the signal of a technical replicate at a given time point i and $\overline{x}$ the mean of this replicate over all time points. This approach was used for the analysis of the BT474 cells described by Szabó (2009). Yet, this method resulted in masking inhibitory effects. Figure 3.9 shows the comparison of the same biological conditions centered around zero (A) and uncentered (B). In the centered data, effects were displayed according to the time dependent dynamics, but information on the absolute signal intensity was lost. Additionally, different time-dependent model fits were calculated for centered and uncentered data (Fig. 3.9: blue line). The differences were explained with the high distance between the signal intensities of the biological replicates at single time points. The comparison between the two methods pointed out that centering signal intensities did not reflect the biology behind the data. Therefore, dynamic signalling data were analysed uncentered.

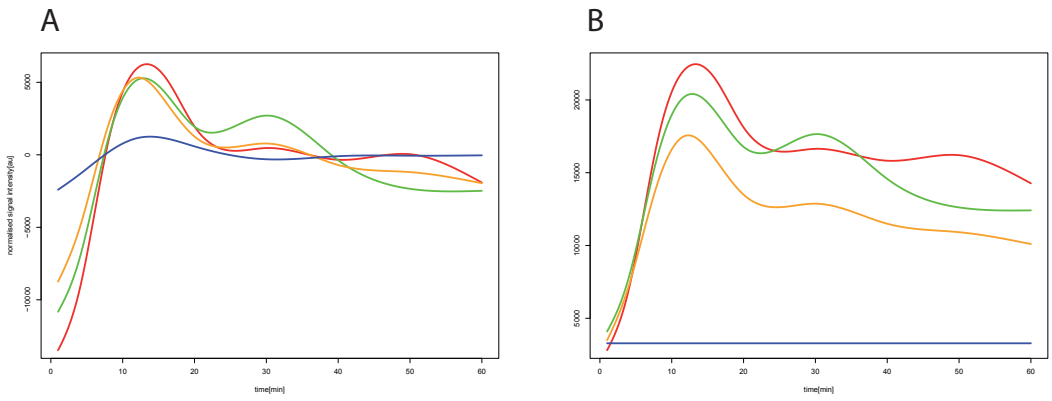

Figure 3.9: Centered and uncentered data
pERK1/2 signal after stimulation with EGF without inhibition (red) and prior inhibition with trastuzumab (green), pertuzumab (orange) and erlotinib (blue). A: Data centered around zero. B: Uncentered data.

To cope with the given variability of biological data, a novel strategy of fitting the smoothing splines was applied to determine time-dependent effects. In figure 3.10, two strategies were compared showing one of the most drastic examples to illustrate the differences in the outcome of the two methods. The biological replicate represented by the blue line did not result in a comparable activation of pERK1/2 as the other two replicate measurements shown in red and light blue. In the first approach, the technical replicates were combined for each time point using the median as a robust estimator. Fitting a spline on the median of each biological replicate resulted in artifactual data due to experimental outliers represented by the blue line (Fig. 3.10 A). In order to account for biological variability and experimental outliers, an algorithm was developed to differently weight biological replicates by fitting the spline over the median of the biological replicates. This resulted in a more robust fit and thus was more suitable to reveal time-dependent effects (Fig. 3.10 B). For experiments without biological outliers, the two methods revealed no difference (data not shown). Therefore, the strategy of fitting the smoothing splines on the median of the biological replicates was chosen for the analysis of time series data.

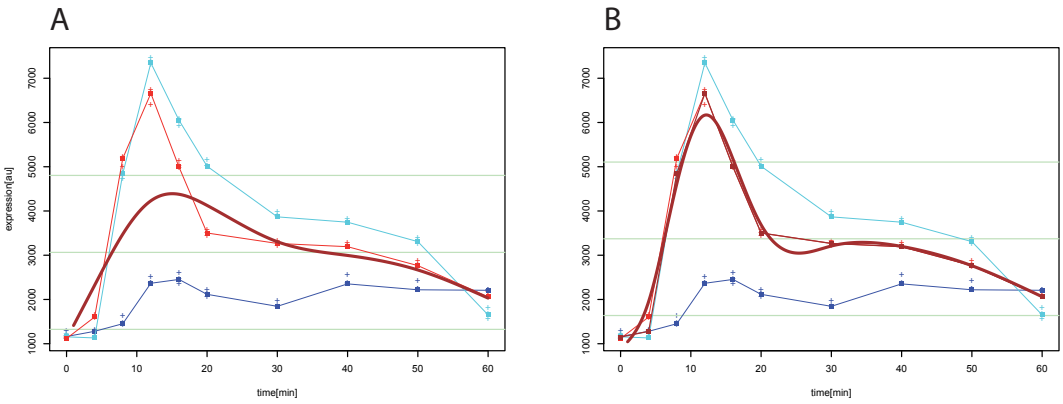

Figure 3.10: Comparison of two different spline fit models
The diagram shows the pERK1/2 signal of simultaneous stimulation with EGF and HRG after erlotinib inhibition. The coloured lines represent three biological replicates. The splines are shown in dark red. The spline fit over the median of the technical replicates is shown in figure A, the spline fit over the median of all technical and biological replicates is shown in figure B.

3.3 Characterisation of breast cancer cell lines

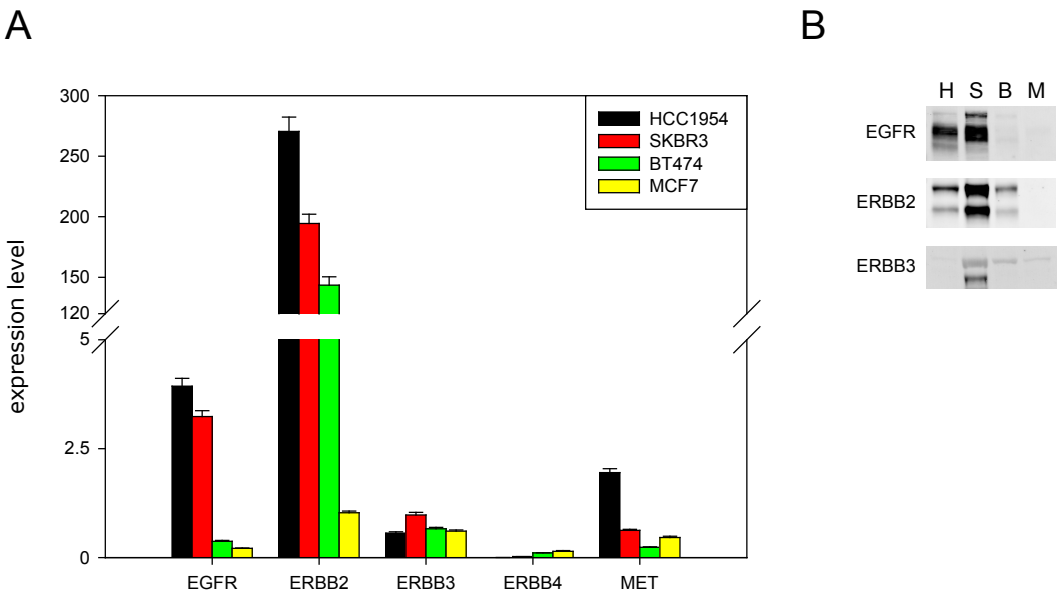

Figure 3.11: Receptor expression in breast cancer cell lines
Expression of the four ERBB receptors and the MET receptor in HCC1954 (black), SKBR3 (red), BT474 (green), and MCF7 (yellow) cells via qRT-PCR (A) and Western blot analysis (B). The expression level of the qRT-PCR results are normalised to the mean expression of EGFR.

For the analysis of the ERBB receptor signalling network in breast cancer, four well established breast cell lines were selected, BT474, HCC1954, MCF7, and SKBR3. First, the expression of the receptors in the different cell lines was characterised on the mRNA level via qRT-PCR and on the protein level by Western blot analysis (Fig. 3.11). ERBB2 was highly expressed in HCC1954, SKBR3, and BT474 but low in MCF7 cells. Additionally, EGFR was highly expressed in HCC1954 and SKBR3 cells. This was detected on the mRNA as well as on the protein level. Transcripts for ERBB3 were of slightly higher abundance in SKBR3 cells and expressed in nearly equal amounts in the other three cell lines. On the protein level, ERBB3 was only detected in SKBR3 cells. According to the transcript data, the ERBB4 receptor was expressed at a very low level in BT474 and MCF7 cells, and not expressed in HCC1954 and SKBR3 cells. However, ERBB4 was not detectable on protein level in any of the cell lines. The MET receptor was mainly expressed in HCC1954 cells in comparison

to the other three cell lines when assessed by qRT-PCR, but was not detectable by Western blot.

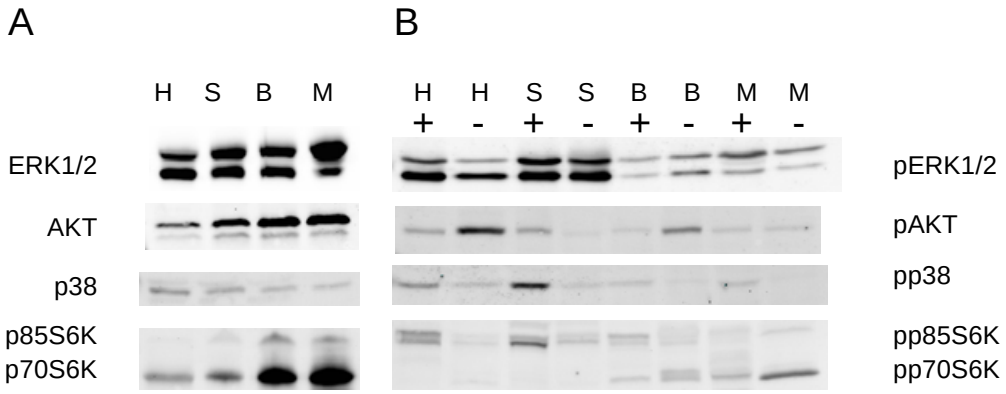

Figure 3.12: Kinase expression and activation in breast cancer cell lines The Western blots show the expression (A) and the phosphorylation status (B) of ERK1/2, AKT, p38 and p70S6K in steady-state (+) and 24 h serum-starved (-) HCC1954 (H), SKBR3 (S), BT474 (B) and MCF7 (M) cells.

The abundance and the phosphorylation status of ERK1/2, AKT, p38, and p70S6K in steady-state and in cells serum-starved for 24 h was determined by Western blot (Fig. 3.12). ERK1 and ERK2 were equally expressed in HCC1954, SKBR3, and BT474 cells, while ERK1 was higher expressed than ERK2 in MCF7 cells. AKT expression was low in HCC1954 and higher in BT474 and MCF7 cells compared to SKBR3 cells. HCC1954 cells revealed higher p38 expression compared to the other three cell lines. Overall, differences in protein expression were not so strong for ERK1/2, AKT, and p38 as those observed for p70S6K which was highly expressed in BT474 and in MCF7 cells. p70S6K and p85S6K are two isoforms of the same kinase. p85S6K is identical to p70S6K except for additional 23 amino acids at the N-terminus which encode a nuclear translocation motif. Antibodies specific for p70S6K also detect p85S6K which is also true for phosphospecific antibodies, as the phosphosites are identical. Therefore, it was not possible to distinguish between these two kinases using RPPA. Both isoform were reported to be equally regulated and are therefore referred to as p70S6K. In Western blot analysis, separation of the proteins depending on the size allowed the differentiation of the isoforms.

Regarding the phosphorylation status of these proteins, differences between the cell lines were revealed. For example, HCC1954 and SKBR3 cells showed a high baseline level of ERK1/2 phosphorylation, which was reduced after starvation in HCC1954 cells but not in SKBR3 cells. In contrast, starvation resulted in an increase of AKT phosphorylation in HCC1954 and BT474 cells. Phosphorylation of p38 was reduced by starvation in all four cell lines while p70S6K phosphorylation was increased after starvation in MCF7 cells. Notably, HCC1954 and SKBR3 cells revealed a higher phosphorylation of p85S6K compared to the p70S6K isoform, although total protein expression indicated a higher abundance of the p70S6K isoform.

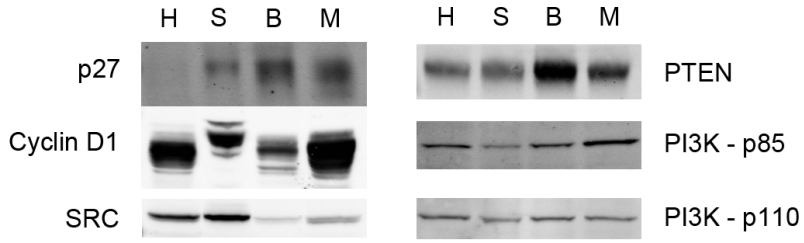

Figure 3.13: Protein expression in breast cancer cell lines
Western blot analysis of expression of p27, cyclinD1, SRC, PTEN, and the PI3K subunits in HCC1954 (H), SKBR3 (S), BT474 (B), and MCF7 (M) cells.

Further analysis of the cell lines revealed that there was almost no p27 expression in HCC1954 and only weak in SKBR3 cells whereas cyclin D1 was mainly expressed in HCC1954 and MCF7 cells (Fig. 3.13). PTEN was most strongly expressed in BT474 cells while SRC had a high abundance in HCC1954 and SKBR3 cells. The p110 subunit of the PI3K was expressed equally in the four cell lines while p85 was slightly stronger expressed in HCC1954 and MCF7 cells.

As HCC1954 cells were reported to be trastuzumab resistant and sensitivity was correlated with an increase of p27 expression (Sahin et al., 2009), the induction of p27 after treatment with trastuzumab was analysed in the three ERBB2 overexpressing cell lines. Indeed, no increase in p27 expression after addition of trastuzumab was observed in HCC1954 cells while an induction of p27 was detected in BT474 and SKBR3 cells as shown in figure 3.14.

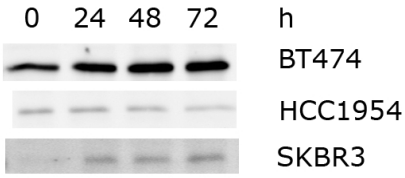

Figure 3.14: Trastuzumab induced p27 expression
Western blot analysis of p27 expression after trastuzumab treatment for 24, 28, and 72 h in HCC1954, BT474, and SKBR3 cells.

To complete the information about the cell lines, breast cancer literature as well as the Catalogue Of Somatic Mutations In Cancer (http://www.sanger.ac.uk/genetics/CGP/cosmic/) was screened for known amplifications of ERBB2 (Kauraniemi et al., 2001), p70S6K (Barlund et al., 2000, Couch et al., 1999), and PI3K mutations (Saal et al., 2005). A summary of the expression and mutation status of key proteins is given in table 3.4.

Table 3.4: Expression and mutation of proteins

protein	**HCC1954**	**SKBR3**	**BT474**	**MCF7**	
EGFR	high	high	low	low	own data
ERBB2	amplified	amplified	amplified	*wt*	literature
PI3K	H1047R	*wt*	K111N	E545K	literature
p27	low	high	high	high	own data
p70S6K	*wt*	*wt*	amplified	amplified	literature
PTEN	low	low	high	low	own data

3.4 Quantitative analysis of ligand-induced ERBB signalling in MCF7 cells

The breast cancer cell line MCF7 was chosen as model system for the analysis of ligand-induced ERBB signalling. In this cell line, the four ERBB receptors were expressed at a low level and in comparable amounts (Fig. 3.11). Therefore, the unperturbed ERBB signalling was measured without the impact of alterations due to overexpression of one or several receptors. Three ligands (epidermal growth factor (EGF), heregulin-β1 (HRG), and betacellulin (BTC)), representing three different receptor specificity groups (Fig. 1.4), were chosen for analysis.

3.4.1 Quantitative measurements of ligand-induced signalling

First, the dose-dependent, ligand-induced phosphorylation of downstream targets within the ERBB receptor signalling network, namely pERK1/2 (T202/Y204), pSTAT3 (S727), pAKT (S473), and pAKT (T308), was studied applying the MIA approach. Each ligand was applied in a series of different concentrations ranging between 0.1 and 20 nM.

Cell stimulation with HRG resulted in a strong increase in phosphorylation of all four phosphoproteins. The time courses for pERK1/2, pAKT, and pSTAT3 of one biological replicate are shown in figure 3.15. The amount of phosphorylated ERK1/2 ranged from 235 ng/µg (0.1 nM) over 1880 ng/µg (1 nM) to 4200 ng/µg (3 nM). The phosphorylation of AKT (S473) increased after addition of HRG from 10 (0.1 nM) over 200 (1 nM) to 800 ng/µg (3 nM) and of AKT (T308) from almost zero (0.1 nM) over 100 (1 nM) to 300 ng/µg (3 nM). For STAT3 phosphorylation, a further effect was observed. In addition to the quantitative disparity between stimulation with 1 nM and 3 nM HRG, phosphorylation dynamics shifted. In detail, for concentrations higher than 3 nM, the phosphorylation immediately increased after stimulation while the baseline phosphorylation level remained unaffected for 4 min at lower concentrations. The phosphorylation was sustained for all phosphoproteins at a high level. The activation of AKT and STAT3 remained on the highest activation level for more than 60 min while pERK1/2 level started to decline 30 min after treatment.

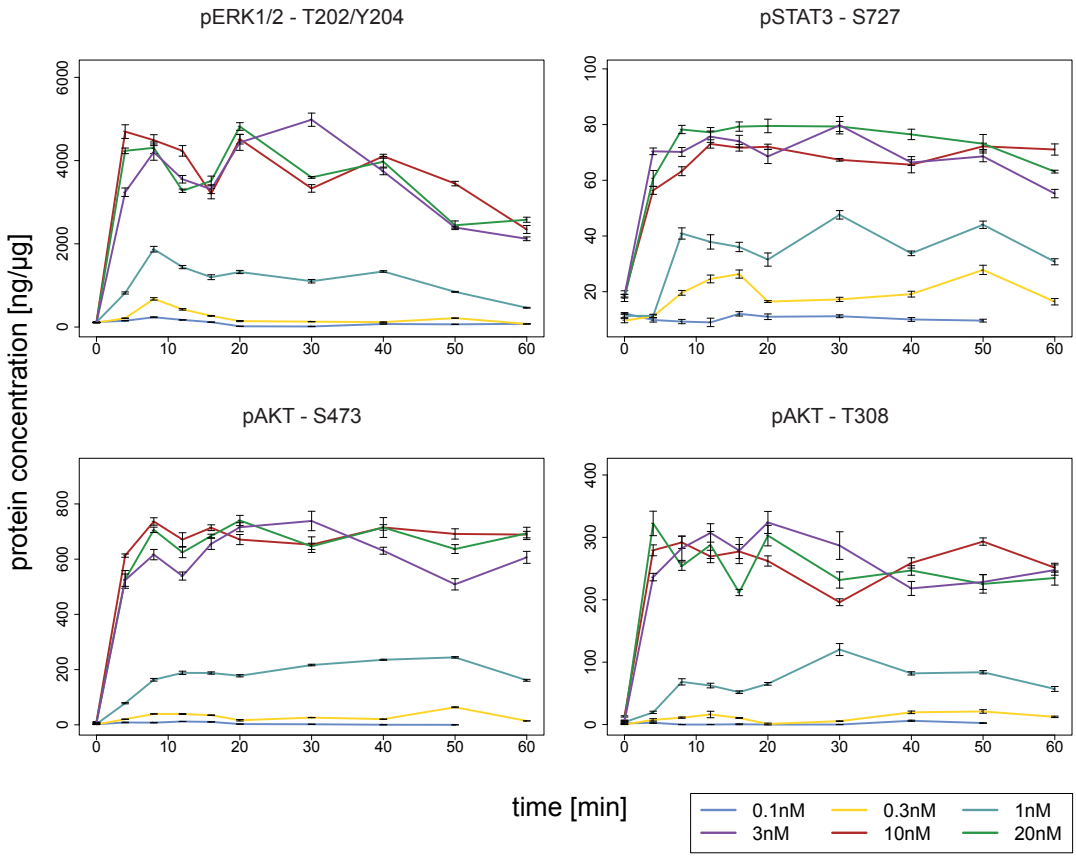

Figure 3.15: Dose-dependent stimulation of MCF7 cells with HRG
MCF7 cells were stimulated with HRG in concentrations ranging from 0.1 nM to 20 nM. Phosphorylation of ERK1/2, STAT3 (S727), AKT (S473), and AKT (T308) was quantified.

The activation of ERK1/2 and AKT was dose-dependent in response to EGF. The phosphorylation of ERK1/2 peaked between 12 and 16 min for concentrations below 1 nM and shifted to a 4 min peak for concentrations above 3 nM (Fig. 3.16). No difference in ERK1/2 activation between 10 and 20 nM EGF was observed. In contrast to HRG, stimulation with EGF resulted in a sharp peak. The activation rapidly declined, returned to a low level after 20 min and continued to fade slowly. The phosphorylation of AKT (S473) was very weak after stimulation with EGF although dose-dependent and reaching a concentration of 100 ng/µg pAKT (S473) after addition of 20 nM EGF. AKT phosphorylation dynamics were similar to the pattern described for ERK1/2 phosphorylation. The peak of activation was reached after 16 min for the low and after 4 min for the higher EGF concentrations, and a steady state was reached again 20 min

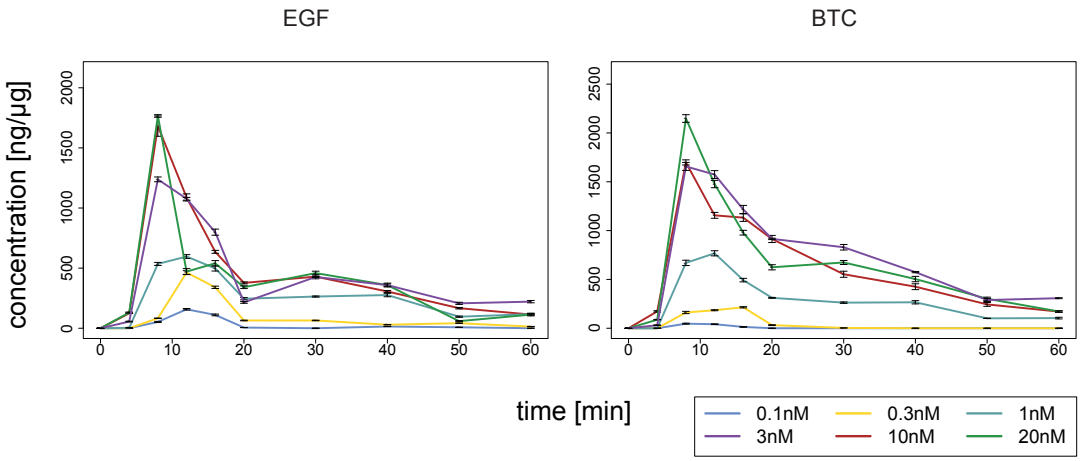

Figure 3.16: Ligand-induced ERK1/2 phosphorylation in MCF7 cells
MCF7 cells were stimulated with EGF and BTC in concentrations ranging from 1 nM to 20 nM and concentration of pERK1/2 was measured over time.

after stimulation. No pronounced phosphorylation of pAKT (T308) was measured after EGF stimulation and also STAT3 was phosphorylated only to a minor extent (Fig. A.1).

Finally, the activating potential of BTC was analysed. In addition to EGFR, BTC also binds to ERBB4. The activation was dose-dependent for all four phosphoproteins. The ERK1/2 and AKT activation kinetics were very similar compared to EGF (Fig. 3.16). The highest amount of phosphorylated ERK1/2 was measured after 12 min for the low concentrations, shifting to 8 min for 10 and 20 nM BTC. The activation rapidly declined until 20 min after stimulation. The concentration of pERK1/2 ranged from 40 ng/µg (0.1 nM) to 2150 ng/µg (20 nM). The phosphorylation of AKT (S473) also showed the same dynamics as observed for ERK1/2 ranging from 10 to 200 ng/µg (Fig. A.2). AKT (T308) was weakly phosphorylated with the highest concentration of 60 ng/µg after addition of 20 nM BTC. The kinetics of STAT3 phosphorylation differed from the pattern described for pERK1/2 and pAKT as it continously increased for 30 min reaching a concentration of 80 ng/µg for 20 nM BTC.

Although the activation of all phosphoproteins was dose-dependent for all biological replicates and the relative correlation of the stimulation curves was highly comparable for the different biological replicates, the absolute amount of phosphoprotein varied. The median of phosphoprotein formation 8 min after addition of a certain ligand was calculated from three biological replicates and is listed for

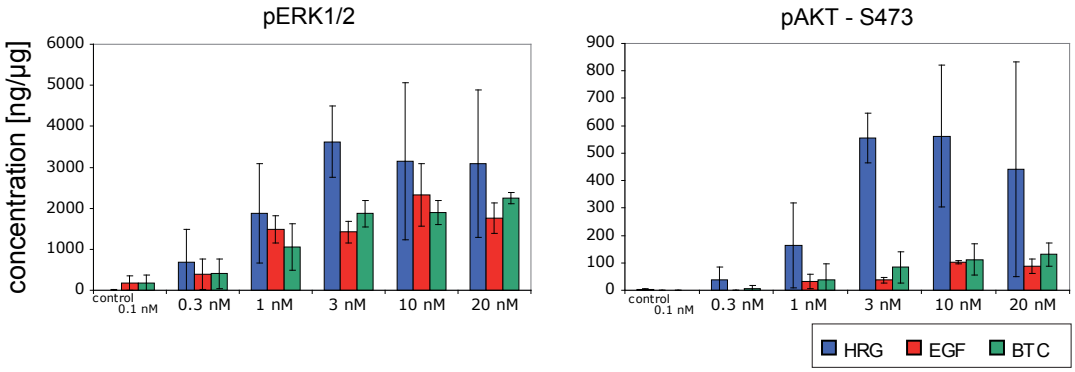

Figure 3.17: Dose-dependency of ERK1/2 and AKT phosphorylation
MCF7 cells were stimulated with HRG, EGF, and BTC at concentrations ranging between 0.1 and 20 nM. Bar plots show the amount of phosphoprotein 8 min after stimulation.

the four phosphoproteins in table 3.5. To make the biological replicates more comparable, the data was scaled for each biological replicate separately. For each experiment comprising six time series, the maximum value of phosphoprotein was set to one, and the data was scaled in relation to this data point. The correlation between the time series of the scaled data resembled the data of the single biological measurements (Fig. A.3).

To sum up, the phosphorylation of ERK1/2 and AKT was clearly dose-dependent for the three ligands but saturation was reached at different concentrations (Fig. 3.17). HRG resulted in the strongest increase in phosphorylation, reaching saturation at a concentration of 3 nM. EGF mediated activation was saturated at 10 nM for most phosphoproteins while addition of BTC was still increasing at the highest measured concentration. STAT3 was phosphorylated only after stimulation with HRG and BTC while addition of EGF resulted in very weak phosphorylation. For further analysis of ligand-dependent ERBB signalling in MCF7 cells, a concentration of 1 nM for each ligand was chosen. This ligand concentration induced strong activation of the target proteins but the phosphorylation rate was not saturated. This was important for the analysis of possible additive effects of the ligands.

3.4.2 Quantitative analysis of signalling in response to ligand combinations

After analysing the dose-dependency of ligand-mediated signalling in MCF7 cells, combinatorial ligand treatment was studied. The quantitative analysis of the combinations revealed significant differences between the three biological replicates. Not only the absolute readout but also the relation between the ligands differed. To gain a better understanding of the signalling features of the ligands and the combinations, the data was scaled in relation to the highest value of each biological replicate which was set to one as already explained before.

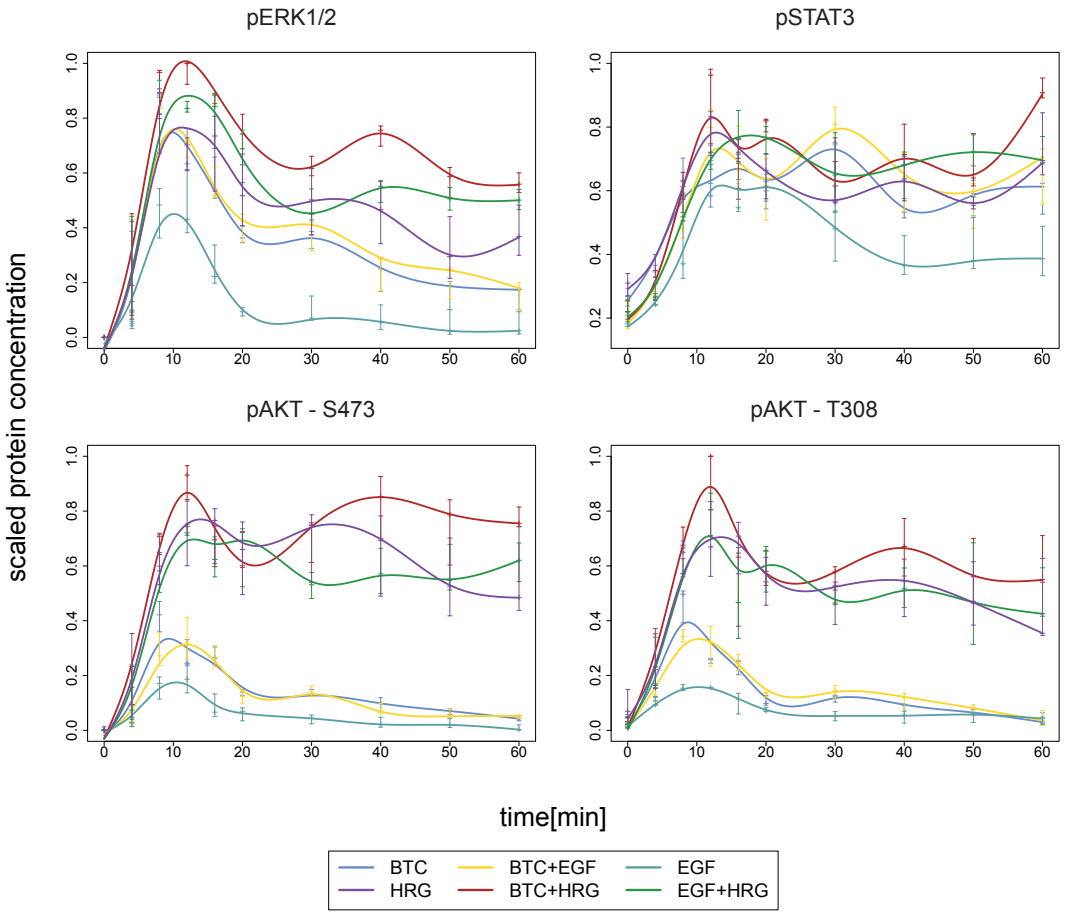

Figure 3.18: Ligand-dependent signalling in MCF7 cells.
Cells were serum-starved for 24 h and subsequently stimulated with 1 nM of each ligand, alone and in combination. Each biological replicate was scaled to its maximal value. Phosphorylation of ERK1/2, AKT, and STAT3 is shown.

Figure 3.18 shows the phosphorylation dynamics of the four phosphoproteins. The median values are listed in table 3.5.

EGF had the weakest capacity to activate ERK1/2 and AKT, while stimulation with BTC resulted in a slightly stronger activation of both proteins. The combination of BTC and EGF compared to BTC alone did not result in an increase of pERK1/2 and was even weaker regarding the AKT activation. BTC+EGF reached 35% of the maximal phosphorylation of AKT and 80% of maximal ERK1/2 phosphorylation. HRG stimulation resulted in a more sustained phosphorylation of both proteins and contrasted the dynamics observed for the other two ligands. Compared to BTC, HRG led to the phosphorylation of twice the amount of AKT which was slightly increased after simultaneous treatment with EGF or BTC. In contrast, activation of ERK1/2 was slightly stronger upon additional EGF or much stronger by BTC and HRG cotreatment. With exception of EGF, all ligands and combinations resulted in a uniform phosphorylation of STAT3. EGF only led to a transient activation reaching the highest phosphorylation after 20–30 min, which was corresponding to almost 70% of maximal phosphorylation, while the other combination resulted in a sustained phosphorylation.

In summary, HRG was the most potent ligand in MCF7 cells and strongly activated the key signalling pathway proteins downstream of ERBB family receptors. With regard to activation of ERK1/2, EGF and BTC slightly increased this pathway due to the simultaneous activation of EGFR and ERBB4. However, this effect did not result in increasing AKT phosphorylation. This data will provide a basis to calculate a quantitative model of fast ligand-induced and dose-dependent signalling via ERBB receptors in a systems biology approach.

Table 3.5: Median amount of phosphoproteins 8 min after stimulation [ng/µg]

HRG	pERK1/2	pAKT S473	pAKT T308	pSTAT3 S727
control	6	2	8	20
0.3 nM	676	39	13	19
1 nM	1871	163	68	40
3 nM	3617	555	200	70
10 nM	3150	562	202	63
20 nM	3093	441	173	64
EGF	pERK1/2	pAKT S473	pAKT T308	pSTAT3 S727
0.1 nM	174	0	4	31
0.3 nM	389	0	7	24
1 nM	1482	31	13	39
3 nM	1419	37	18	39
10 nM	2318	102	33	55
20 nM	1765	88	34	52
BTC	pERK1/2	pAKT S473	pAKT T308	pSTAT3 S727
0.1 nM	179	0	0	20
0.3 nM	406	7	2	20
1 nM	1051	39	16	39
3 nM	1871	84	41	65
10 nM	1897	112	48	61
20 nM	2243	131	58	55
1 nM each	pERK1/2	pAKT S473	pAKT T308	pSTAT3 S727
BTC	1986	169	74	50
EGF	1355	88	29	42
HRG	1831	263	140	42
BTC+EGF	1875	154	78	48
BTC+HRG	2171	287	145	48
EGF+HRG	1968	236	117	43

3.4.3 Ligand-induced ERBB signalling

Having analysed the dose-dependent measurements in a quantitative manner using the MIA technique, the ligand-induced signalling was examined applying the RPPA approach. This allowed studying the phosphorylation status of further pathway proteins in addition to ERK1/2, AKT, and STAT3. Figure 3.19 shows the phosphorylation of ERK1/2, cRAF, AKT, p70S6K, STAT3, PLCγ, mTOR, EGFR, ERBB2, and ERBB3 after stimulation with 1 nM EGF, HRG, or BTC for four biological replicates. The effects of the three ligands were ranked as weak, moderate, and strong (table 3.6). Proteins, which showed no effect for any of the ligands were not listed.

Table 3.6: Effects in MCF7 cells after stimulation with ligands

protein	phosphosite	BTC	EGF	HRG
AKT	S473	weak	weak	strong
AKT	T308	weak	no	strong
cRAF	S289/296/301	moderate	weak	strong
EGFR	Y845	moderate	no	strong
EGFR	Y992	weak	no	moderate
EGFR	Y1173	moderate	no	strong
ERBB2	Y1139	no	no	weak
ERBB2	Y1248	no	no	weak
ERBB3	Y1197	no	no	strong
ERBB3	Y1289	no	no	strong
ERK1/2	T202/Y204	moderate	weak	strong
MEK1/2	S217/221	moderate	weak	strong
mTOR	S2481	no	no	weak
p38	T180/Y182	no	no	no
p70S6K	T389	weak	no	strong
p70S6K	T421/S424	strong	moderate	strong
PLCγ	S1248	no	no	weak
SRC	Y416	no	no	weak
STAT3	S727	weak	no	weak

HRG had by far the strongest impact on the activation of several downstream pathways. ERBB3 was phosphorylated at Y1197 and Y1289, and the phosphorylation of EGFR and ERBB2 was induced by transphosphorylation as HRG

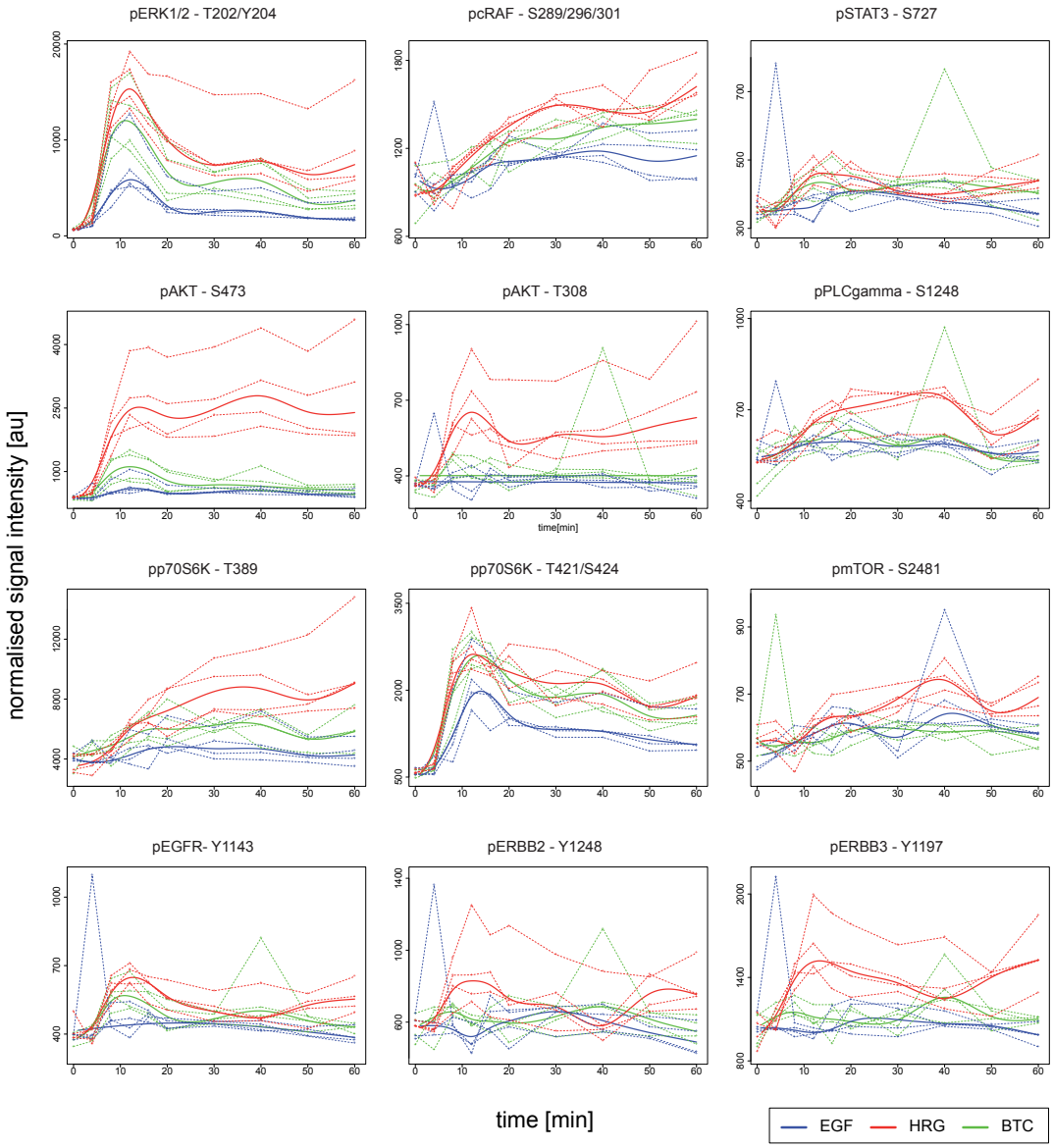

Figure 3.19: RPPA measurements of ligand-dependent responses in MCF7 cells.

MCF7 cells were stimulated with 1 nM EGF (blue), HRG (red) or BTC (green). The plots show the phosphorylation of ERK1/2, cRAF (S289/296/301), STAT3 (S727), AKT (S473, T308), PLCγ (S1248), p70S6K (T389, T421/S424), mTOR (S2481), EGFR (Y1173), ERBB2 (Y1248), and ERBB3 (Y1197). The thick lines are the smoothing splines, the dashed lines represent the biological replicates.

only binds to ERBB3 and induces activation by dimerisation with ERBB2. Upon receptor phosphorylation, a maximum peak of ERK1/2 phosphorylation was observed after 12 min. The curve declined until 30 min after stimulation but did not return to the baseline level of the starved conditions within 60 min. AKT was also phosphorylated at both phosphorylation sites S473 and T308. This activation reached its highest level after 12 min and was sustained over a time period of 60 min except a weak drop after 20 min which was noted for both phosphorylation sites. A significant activation was observed for p70S6K also for both phosphorylation sites T389 and T421/S424. However, the dynamics of the phosphorylation were different: Addition of HRG resulted in a continuous increase in phosphorylation of p70S6K (T389) which was comparable to the activation of cRAF and mTOR. In contrast, the phosphorylation of p70S6K (T421/S424) resembled the dynamics of ERK1/2 activation with a peak after 12 min, although the decline of activation was weaker for p70S6K than for ERK1/2. PLCγ, SRC, and STAT3 showed a weak increase after addition of HRG reaching the highest level 12 min after stimulation. The pmTOR signal slowly increased within the 60 min. The same behaviour was observed for cRAF, but to a higher extent. No activation of p38 and PKCα by any of the ligands was seen in MCF7 cells.

After addition of EGF, no phosphorylation of EGFR, ERBB2, and ERBB3 was detectable. However, the activation of the MAPK pathway including cRAF, MEK1/2 and ERK1/2, and p70S6K (T421/S424) points to an activation of EGFR. AKT phosphorylation after addition of EGF was not detected by RPPA.

For almost all phosphoproteins measured by RPPA, the activating potential of BTC ranked between that of the other two ligands, EGF and HRG. In contrast to EGF, BTC was able to induce a weak AKT activation. Phosphorylation of the EGFR was also stronger after addition of BTC when compared to the EGF stimulation. However, the time-dependent dynamics of the phosphoprotein formation were similar between the three ligands.

The results obtained from RPPA analysis confirmed the MIA result that HRG was the most potent ligand in MCF7 cells. Therefore, further analysis of ERBB signalling in MCF7 cells was performed using HRG as ligand.

3.4.4 Ligand-induced ERBB signalling after kinase inhibition

To analyse the pathways in more detail, several kinase inhibitors were applied and the activation of the proteins described before was studied. Although the inhibitor experiments were only performed once, they allowed to describe the interplay of the various proteins and the impact of the inhibitors on signal transduction. The results are shown in figure 3.20. For this study, the specific pathway inhibitors PD98059 (inhibiting MEK1/2), LY294002 (inhibiting PI3K), rapamycin (inhibiting mTORC1) and gefitinib (inhibiting EGFR) were applied. Inhibitors were added at a concentration of 10 µM (PD98059, LY294002, gefitinib) or 10 nM (rapamycin) corresponding to concentrations used in the literature.

The preincubation with gefitinib for 1 h resulted in the prevention of ligand-induced phosphorylation, not only of EGFR, but also of the other ERBB receptors. Thus, HRG did not induce phosphorylation of ERBB2 or ERBB3 after gefitinib treatment. The inactivation of all ERBB receptors was also reflected in the inhibition of all downstream pathways. MAPK, PI3K, p70S6K, and mTOR activation was entirely inhibited by gefitinib. Although the activation of PLCγ, STAT3, and SRC was very weak in response to HRG, gefitinib prevented PLCγ and STAT3 activation and delayed and reduced the phosphorylation of SRC.

To analyse which downstream targets were activated through the MAPK pathway or the PI3K pathway, selective inhibitors against MEK1/2, PD98059, and PI3K, LY294002, were applied. As expected, PD98059 did not affect the phosphorylation of the receptors or of cRAF, which is upstream of MEK1/2, and inhibited only the phosphorylation of MEK1/2 and the downstream kinase ERK1/2. However, the inhibition of both kinases was not complete. This might be due an insufficient inhibition caused by a too low concentration of the inhibitor PD98059. Furthermore, the phosphorylation of p70S6K (T421/S424) was slightly delayed after preincubation with PD98059, but no inhibition was observed. No change was observed for p70S6K (T389) activation. Although the phosphorylation of mTOR after addition of HRG was very weak, PD98059 treatment led to a slight but not significant increase in mTOR phosphorylation. In contrast, LY294002 had strong effects on HRG signalling. Similar to the inhibition with PD98059, LY294002 was not able to inhibit or block the activation and phosphorylation of the receptors, but inhibited the phosphorylation

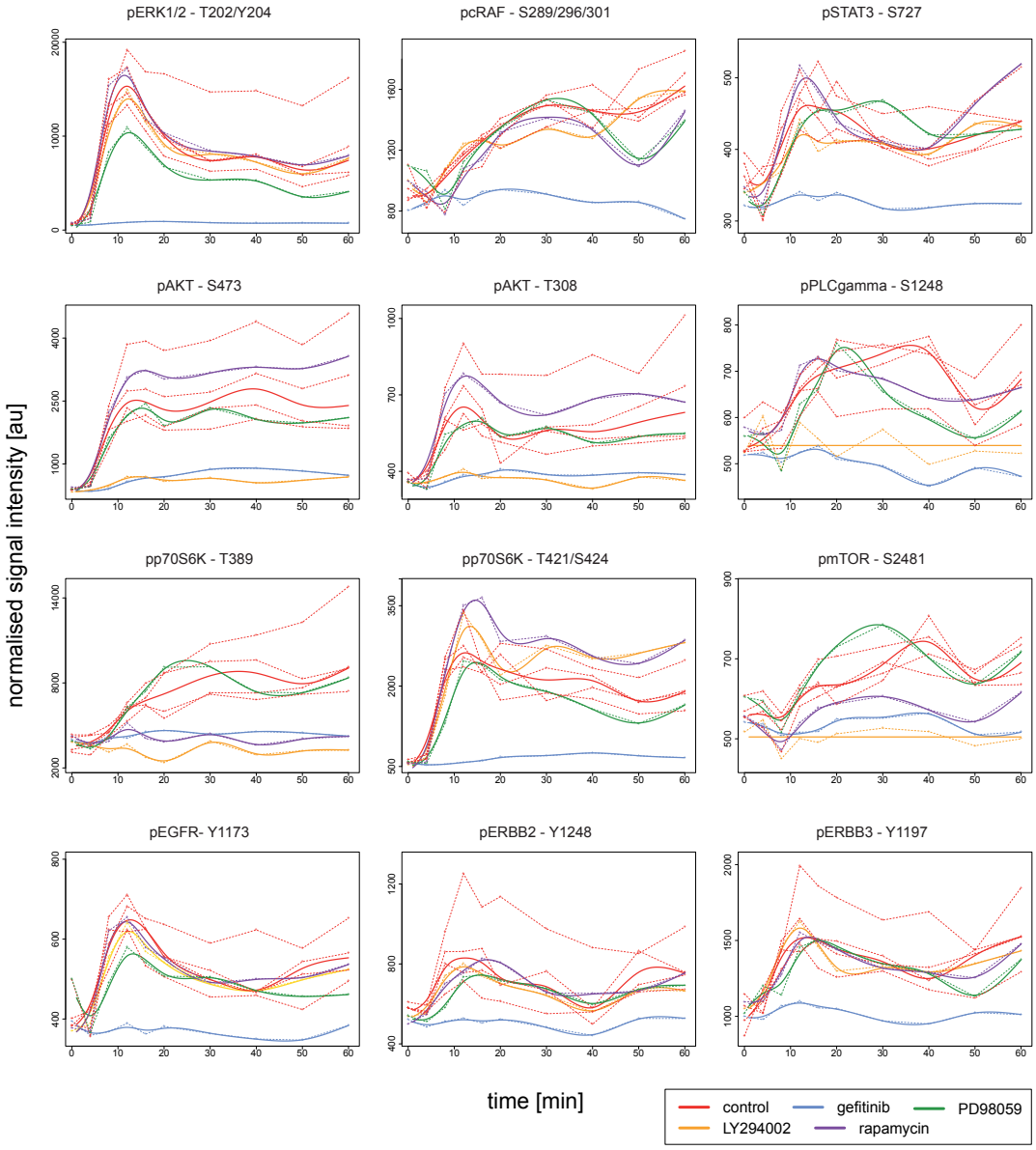

Figure 3.20: Inhibitory effects on HRG-mediated signalling in MCF7 cells.

The plots show the effects of gefitinib (blue), PD98059 (green), LY294002 (orange), and rapamycin (violet) on HRG-mediated signalling in comparison to the uninhibited control (red) in MCF7 cells. The thick lines are the smoothing splines, the dashed lines represent the biological replicates.

of AKT at both phosphorylation sites as well as of p70S6K (T389). Additionally, the phosphorylation of mTOR and PLCγ was prevented by LY294002, but MEK1/2, ERK1/2, and p70S6K (T421/S424) were not affected.

Finally, the mTORC1 inhibitor rapamycin was analysed. As expected, rapamycin inhibited mTOR phosphorylation and displayed the same inhibitory potential on p70S6K (T389) phosphorylation as gefitinib and LY294002, whereas it slightly increased the phosphorylation of p70S6K (T421/S424). Additionally, the phosphorylation of ERK1/2 and AKT was also slightly increased. Table 3.7 summarises the effects of the different inhibitors on HRG signalling. As expected, gefitinib inhibited all downstream pathways and its impact on signalling proteins is therefore not listed in the table.

Table 3.7: Effects of inhibitors in MCF7 cells on HRG mediated signalling

protein	phosphosite	PD	LY	rapamycin
AKT	S473	no	strong	induction
AKT	T308	no	strong	induction
cRAF	S289/296/301	no	no	no
ERK	T202/Y204	weak	no	induction
MEK	S217/221	strong	no	weak
mTOR	S2481	induction	strong	weak
p70S6K	T389	no	strong	strong
p70S6K	T421/S424	no	no	induction
PLCy	Y1248	no	strong	no
SRC	Y416	weak	no	no
STAT3	S727	no	no	induction

The impact of the different inhibitors was similar after EGF or BTC stimulation as the described for HRG (data not shown) with a few exceptions. For example, stimulation with EGF after preincubation with rapamycin resulted in a doubling of ERK1/2 phosphorylation from 850 ng/µg to 1665 ng/µg, as measured by MIA (Fig. A.4).

Two signalling modules were identified as major effectors of ERBB signalling and the key effects are summarised in figure 3.21. First, HRG induced AKT signalling via ERBB3/ERBB2 and PI3K. This led to the downstream activation of mTOR and p70S6K (T389) which both revealed a steadily increasing phosphorylation. This HRG/PI3K signalling module was LY294002 sensitive. The

second cascade started with the activation of cRAF, MEK1/2, and ERK1/2 and resulted in the phosphorylation of p70S6K (T421/S424). Except for cRAF, all other proteins from this PD98059 sensitive pathway revealed a transient phosphorylation. A crosstalk between both pathways was observed as inhibition of PI3K led so a slight upregulation of the pERK1/2 (Fig. A.4). Additionally, inhibition with rapamycin resulted in an upregulation of the PD98059 sensitive pathway. To analyse this crosstalk in more detail, other selective inhibitors against all kinases of both pathways would have to be analysed. As the kinase domains of the receptors are very similar, gefitinib might inhibit other ERBB receptors in addition to EGFR. Therefore, it is difficult to attribute inhibitory effects mediated by gefitinib solely to EGFR inhibition.

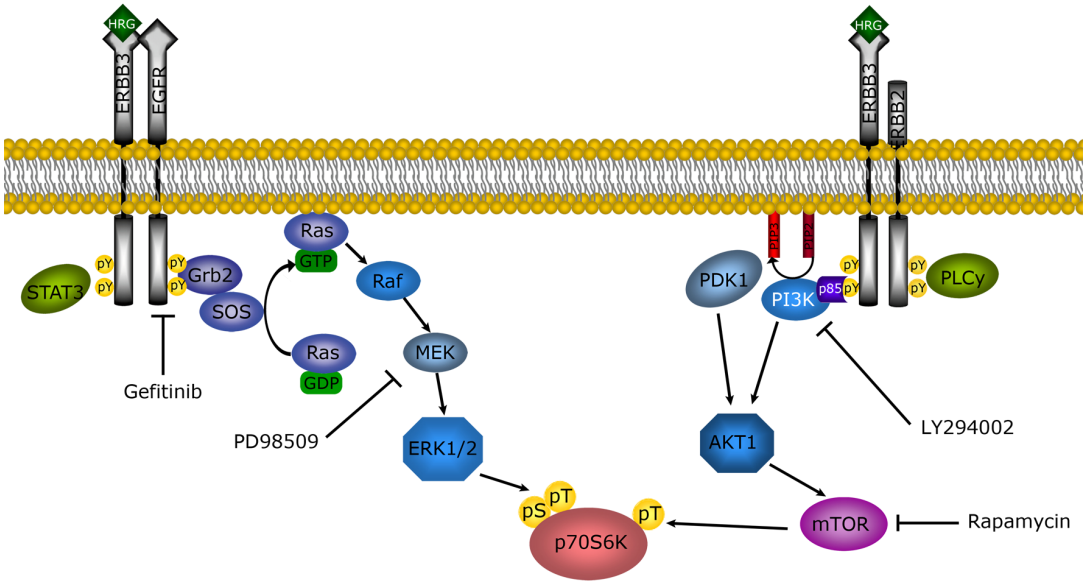

Figure 3.21: ERBB signalling in MCF7 cells.
Schematic overview of inhibitory effects on HRG mediated signalling in MCF7 cells. Phosphorylation of p70S6K is depicted for T421/S421 (pSpT) and T389 (pT).

3.4.5 Ligand-induced signalling after siRNA-mediated knockdown of ERBB receptors

To further analyse the impact of ERBB1–4, ligand-induced signalling was analysed after siRNA-mediated knockdown. MCF7 cells were transfected with siRNA

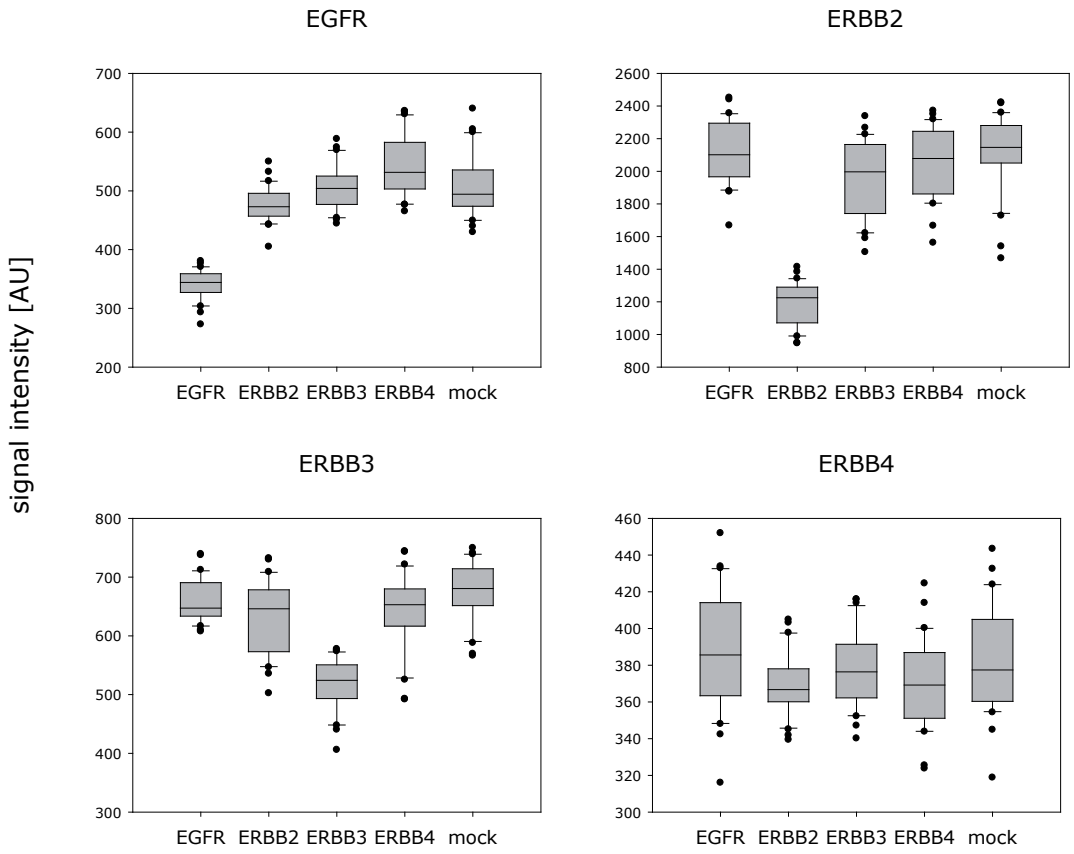

Figure 3.22: siRNA-mediated knockdown of the four ERBB receptors in MCF7 cells.
MCF7 cells were transfected with siRNA targeting each of the four ERBB receptors for 48 h and serum-starved for additional 24 h. The plots show the knockdown of the four ERBB receptors and the mock control detected with antibodies against EGFR, ERBB2, ERBB3, and ERBB4.

for 48 h and serum-starved for an additional 24 h period prior to stimulation with 1 nM HRG, EGF, or BTC, respectively. First, antibody quality was analysed as already described in section 3.2.2. The phosphospecific ERBB receptor antibodies did not perform well in this experiment as signals were below the blank signal and thus were not further analysed. However, antibodies recognising ERBB receptors and several downstream signalling proteins showed good results and were analysed.

Figure 3.22 shows the validation of the knockdown on the protein level. Applying total protein antibodies against the receptors, the specific knockdown of EGFR, ERBB2 and ERBB3 was confirmed. Knockdown was ignificant as

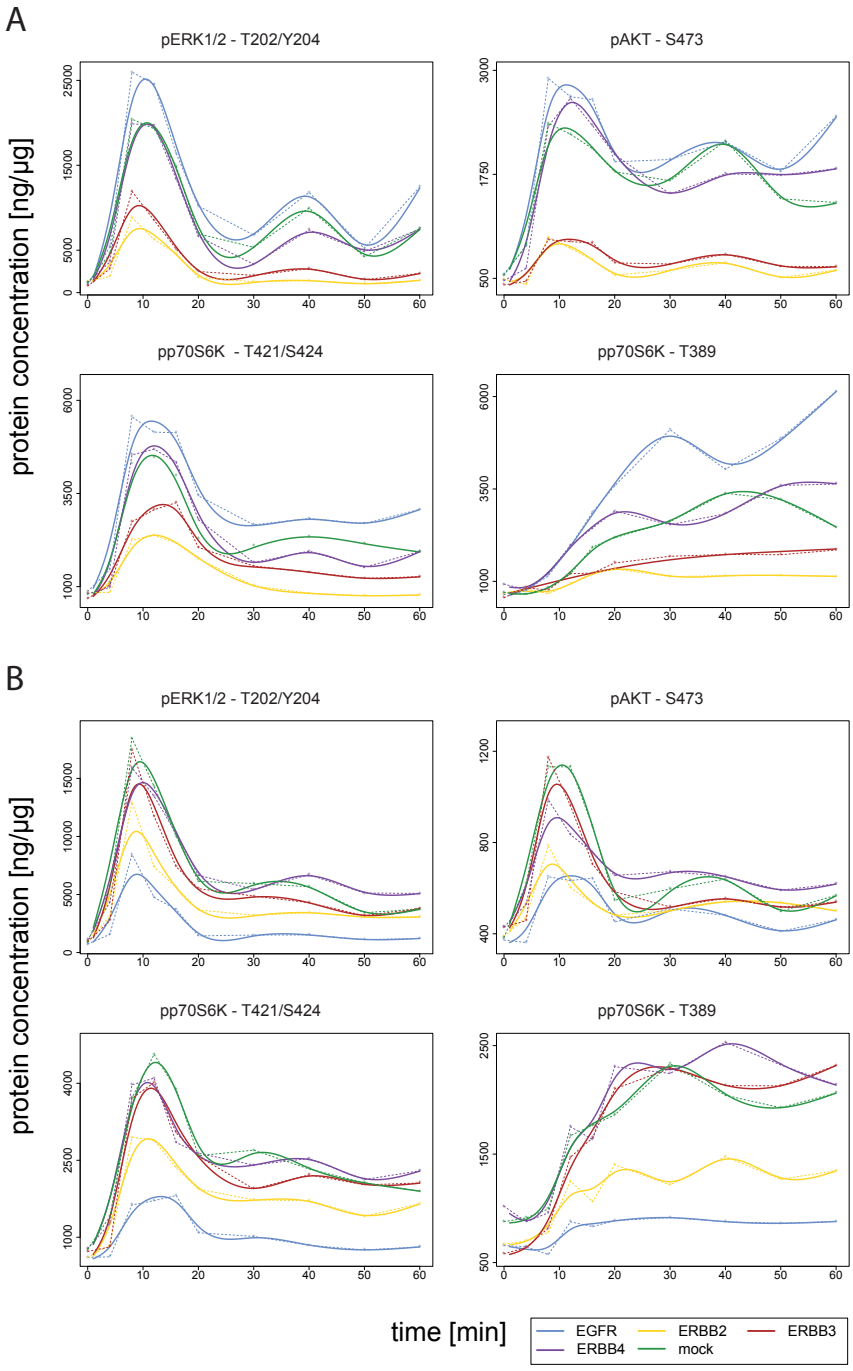

Figure 3.23: Ligand-induced signalling in MCF7 cells after siRNA-mediated knockdown of ERBB receptors

MCF7 cells were transfected with siRNA targeting the four ERBB receptors and subsequently stimulated with 1 nM HRG (A) or EGF (B). The diagrams show the phosphorylation of ERK1/2, AKT, p70S6K (T421/S424), and p70S6K (T389).

Table 3.8: Estimated receptor knockdown efficiency [%]

	EGFR	ERBB2	ERBB3	ERBB4
HRG	52	63	61	10
EGF	78	50	42	19

calculated using Wilcoxon test ($p<0.01$). Probably due to low protein expression and insufficient antibody quality, an ERBB4 knockdown was not observed. Knockdown efficiency for the EGF- and HRG-induced time series was calculated using the R-package "RPPanalyzer" (table 3.8).

Knockdown of ERBB2 and ERBB3 had the highest impact on HRG induced signalling (Fig. 3.23 A), and AKT activation was more affected than ERK1/2 signalling. Quantitative analysis applying MIA revealed that ERK1/2 phosphorylation was reduced by 50% from 2200 ng/µg to 1370 ng/µg for ERBB3 knockdown and 1090 ng/µg for ERBB2 knockdown, while AKT phosphorylation was reduced by 80% from 160 ng/µg to 30 ng/µg (Fig. A.5 A). In contrast to AKT activation, which was equally dependent on both receptors, ERK1/2 and p70S6K activation was stronger affected by ERBB2 than by ERBB3 downregulation.

EGFR knockdown had the highest impact on EGF mediated signalling (Fig. 3.23 B). It strongly reduced the phosphorylation of all measured signalling proteins. Applying MIA, a reduction of ERK1/2 phosphorylation from 1990 ng/µg by 54% down to 930 ng/µg for EGFR knockdown and by 33% down to 1340 ng/µg for ERBB2 knockdown was measured. AKT phosphorylation was reduced from 62 ng/µg by 63% for EGFR and ERBB2 knockdown (Fig. A.5 B). As seen for ERK1/2, p70S6K activation was more affected by EGFR than by ERBB2 knockdown. This might be due to the different knockdown efficiency of EGFR and ERBB2 (table 3.8). However, the impact on AKT signalling was similar despite the difference. Knockdown of ERBB3 and ERBB4 did not show any difference compared to the mock control.

In summary, ERBB3 knockdown reduced HRG induced signalling while EGFR knockdown decreased EGF mediated signalling (Fig. 3.24). Knockdown of ERBB2 had a strong impact on both signalling cascades, HRG- and EGF-induced, but AKT signalling was stronger impaired than ERK1/2 signalling. Additionally, the ERBB2 knockdown had a stronger impact on HRG than on EGF signalling.

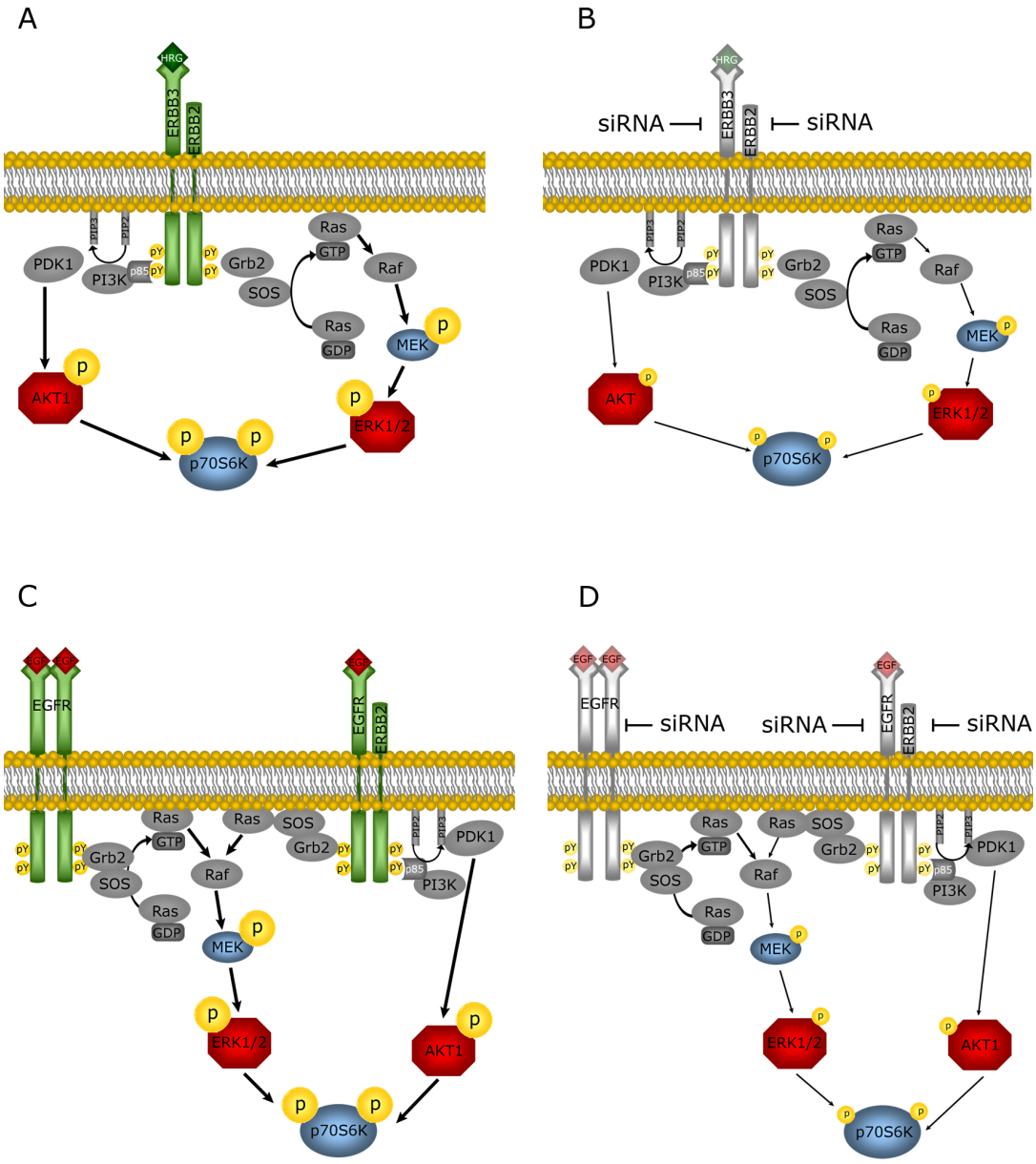

Figure 3.24: Effects of ERBB knockdown on ligand-induced signalling
Schematic overview of HRG- (A) and EGF-induced (C) signalling and effects of siRNA-mediated ERBB knockdown (B, D). Green receptors illustrate activation, faint colour shows receptor reduction. Thick arrows indicate a strong, thin arrows a weak activation. Strong phosphorylation is depicted by large phospho-symbols, weak phosphorylation by small phospho-symbols. Only coloured proteins were analysed.

3.5 Impact of targeted therapeutics on ERBB-mediated signal transduction

The aim of the study was to analyse the impact of single and combinatorial drug administration of ERBB receptor targeting therapeutics on ligand-induced pathway activation and to determine the most potent drug combination for treatment of ERBB2 overexpressing breast cancer. To analyse the impact on the network level as well as for the reconstruction of dynamic protein networks in ERBB2 overexpressing breast cancer, a time-resolved data set was generated. Three ERBB2 overexpressing breast cancer cell lines HCC1954, SKBR3, and BT474 representing different molecular characteristics were chosen. HCC1954 and SKBR3 cells highly express EGFR while BT474 have a low EGFR expression level, and HCC1954 and BT474 cells additionally harbour different oncogenic PI3K mutations (section 3.3). The three different therapeutics trastuzumab (10 ng/µl), pertuzumab (10 ng/µl), and erlotinib (1 µM) and the two ligands EGF and HRG (5 nM) were applied in all possible combinations in triplicate measurements. The results of BT474 cells were already published as master thesis by Szabó (2009). Each dynamic measurement consisted of 10 time points and resulted in 1010 data points per cell line. Finally, the phosphorylation status of 16 cytoplasmic signalling proteins was measured. These proteins did not cover only the ERBB signalling network but did also include proteins from other pathways to analyse the potential crosstalk. Additionally, the phosphorylation status of the ERBB receptors was measured. To generate such a large data set, proteins arrays were used.

3.5.1 Ligand-dependent ERBB signalling in HCC1954 and SKBR3 cells

The first step of ligand-induced signalling was the receptor phosphorylation, subsequently leading to receptor activation. Unfortunately, a ligand-dependent phosphorylation of the EGFR was not detectable by RPPA and was only seen after addition of the antibody therapeutics (see section 3.5.2). For this reason, the activation of EGFR after stimulation with EGF was analysed by Western blot in HCC1954 and SKBR3 cells including several EGFR phosphotyrosine residues (Fig. 3.25). EGFR was phosphorylated at Y1068, Y1086, and Y1173

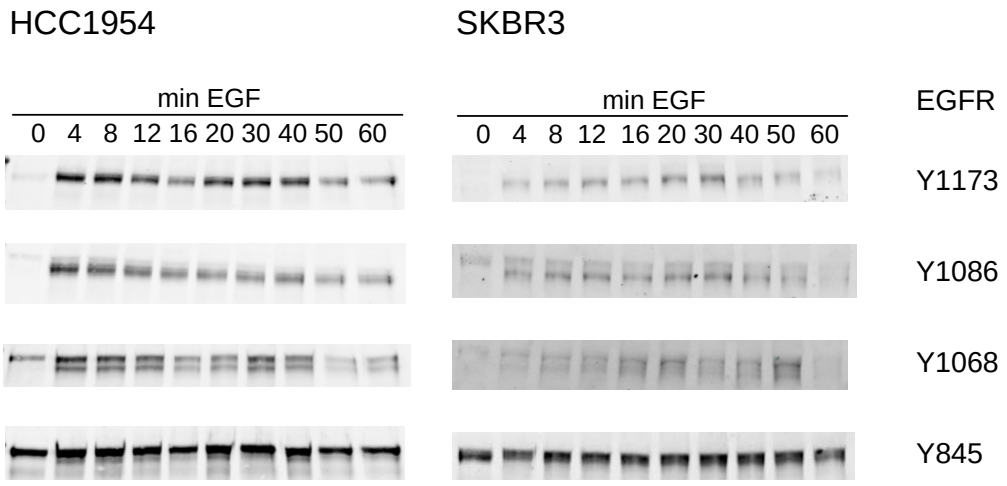

Figure 3.25: Western blot analysis of EGFR phosphorylation in HCC1954 and SKBR3 cells after stimulation with EGF.
Western blot results for EGFR phosphorylation at residues Y1173, Y1086, Y1068, and Y845 after stimulation with EGF for the indicated time points are shown.

within 4 min after stimulation with EGF but not phosphorylated at Y1148 and Y992. Furthermore, Y845 was already phosphorylated before addition of EGF and stimulation produced only a slight increase. In summary, the phosphorylation of the EGFR after addition of EGF was similar in HCC1954 and SKBR3 cells.

As the next step, the activation of the downstream pathways in response to the ligands EGF, HRG, and the combination of EGF and HRG was analysed without adding inhibitors. As both cell lines expressed different levels of ERBB receptors, the responses to the ligands was expected to be different.

ERBB signalling in HCC1954 cells

To gain insight into ERBB signalling in HCC1954 cells, the influence of the two ligands EGF, HRG, and the combination of both ligands on downstream pathways was studied without perturbation of inhibitors. Figure 3.26 shows the phosphorylation of ERK1/2, MEK1/2, p38, AKT, SRC, p70S6K, S6, PLCγ, STAT3, and STAT5 including different phosphorylation sites of AKT and p70S6K after stimulation with EGF, HRG, and both ligands in combination in HCC1954 cells.

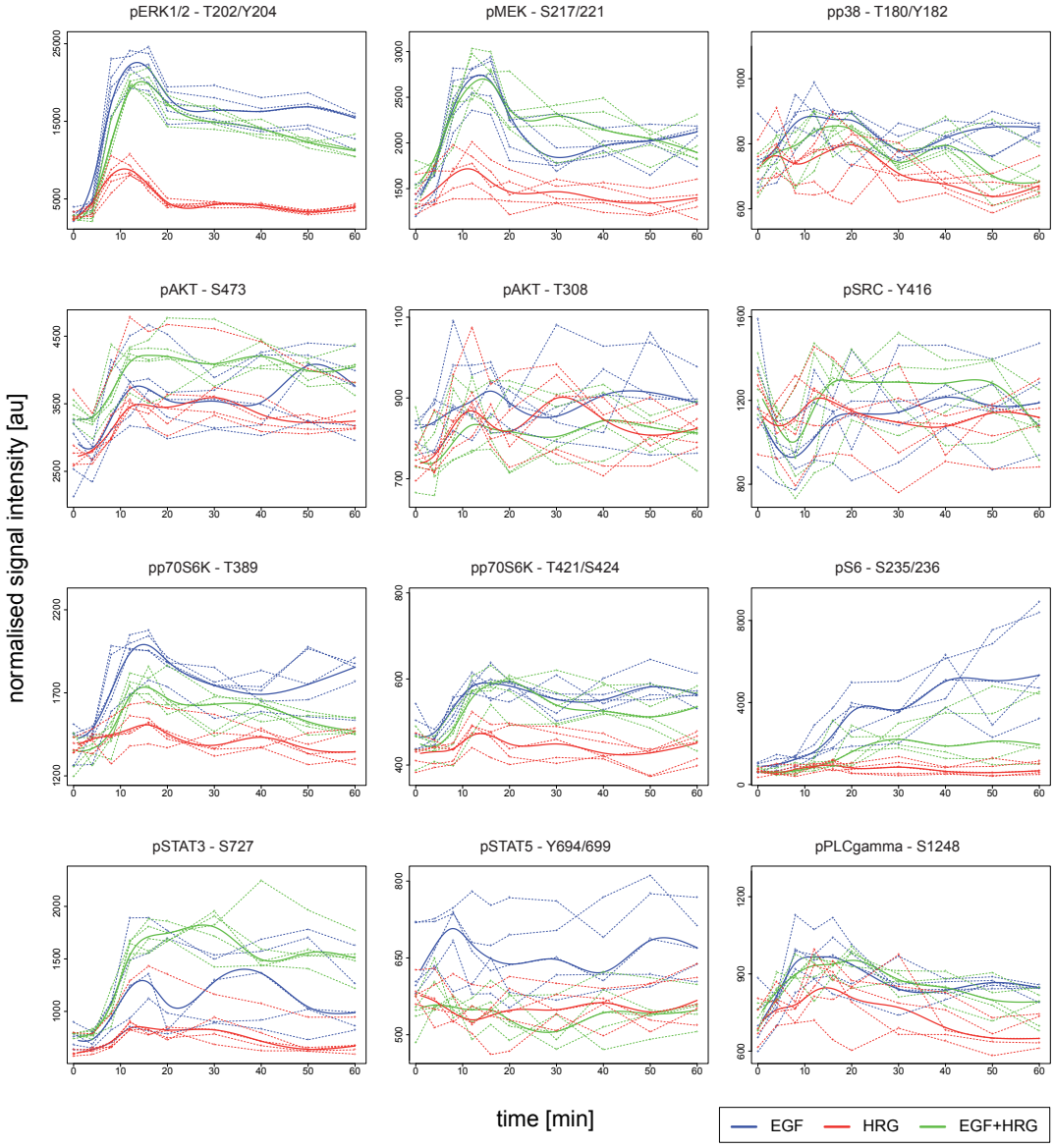

Figure 3.26: Ligand-specific responses in HCC1954 cells
Phosphorylation of ERK1/2, MEK1/2, p38, AKT, SRC, p70S6K, S6, PLCγ, STAT3, and STAT5 after stimulation with EGF (blue), HRG (red), and the combination of both ligands (green). The dashed lines represent the biological replicates, the thick lines show the fit of the smoothing splines.

First, the impact of EGF on different downstream targets in HCC1954 cells was analysed (Fig. 3.26, blue lines). EGF strongly activated the MAPK pathway as indicated by a strong phosphorylation of MEK1/2 and ERK1/2. The activation reached a peak 12 min after stimulation and slightly decreased afterwards. The basal phosphorylation level was not reached again during the 60 min measurement. Another protein which was phosphorylated with comparable kinetics as the MAPK pathway was p70S6K at T389. The activation reached its peak after 12 min and declined afterwards. The activation of a second phosphorylation site of p70S6K, T421/S424, was weaker compared to T389 but more sustained. The ribosomal protein S6, a downstream target of p70S6K, showed a continuous increase in phosphorylation and a dynamic behaviour which was different from all other analysed phosphoproteins. The PI3K pathway was only weakly activated by EGF. Both phosphorylation sites of AKT, S473 and T308, were determined and only AKT (S473) showed a weak response to EGF stimulation. In addition, p38 showed almost no activation after addition of EGF. Four proteins, which directly bind to the phosphorylated ERBB receptors, SRC, PLCγ, and the two STAT proteins STAT3 and STAT5, were analysed additionally. SRC showed a decrease of phosphorylation within the first 10 min after EGF stimulation with a subsequent increase for the next 10 min. Afterwards, SRC phosphorylation remained on the same level. PLCγ showed a weak increase of phosphorylation with a peak after 10 min. STAT3 responded with phosphorylation of S727 to the addition of EGF, while STAT5 was poorly phosphorylated at Y694/699.

In comparison to EGF, the effect of the ERBB3 ligand HRG resulted in only weak or no activation of the proteins described before (Fig. 3.26, red lines). Thus, the MAPK pathway was activated to a minor extent. Regarding the activation of AKT and SRC, there was no difference between the ligands. Furthermore, the STAT proteins, p70S6K, S6 and PLCγ also showed no response to a stimulation with HRG. None of the proteins assessed revealed strong HRG-mediated activation in HCC1954 cells.

Finally, the combination of both ligands, EGF and HRG, was analysed (Fig. 3.26, green lines). The simultaneous stimulation with EGF and HRG led to different effects, depending on the downstream protein. For ERK1/2, p70S6K (T389), and S6, the response was slightly weaker than for EGF alone. Although MEK1/2 is upstream of ERK1/2 and the effects should be similar, the differentiation between EGF and the combination was not so clear in case of MEK1/2.

Table 3.9: Alteration of protein phosphorylation status in HCC1954 cells after stimulation with ligands

protein	phosphosite	EGF	HRG	EGF+HRG
AKT	S473	weak	weak	weak
AKT	T308	no	weak	weak
β-catenin		no	no	no
ERK	T202/Y204	strong	weak	strong
GSK3$\alpha\beta$	Y279/216	no	no	no
MEK	S217/221	strong	weak	strong
mTOR	S2448	no	no	no
mTOR	S2481	no	no	no
NFκB	S536	no	no	no
p38	T180/Y182	no	no	no
p70S6K	T389	strong	no	moderate
p70S6K	T421/S424	moderate	no	moderate
PDK1	S241	no	no	no
PKCα	S657Y658	no	no	no
PLCγ	S1248	weak	no	weak
PRAS	T246	no	no	no
S6	S235/236	strong	no	moderate
SRC	Y416	weak	no	weak
STAT1	Y701	no	no	no
STAT3	Y705	no	no	no
STAT3	S727	moderate	no	strong
STAT5	Y694/699	weak	no	no

This is possibly due to the higher dynamic range of the pERK1/2 antibody which permitted the detection of only small changes of phosphoprotein. For p70S6K (T421/S424) and PLCγ, no difference between EGF and the combination of EGF and HRG was detected. However, STAT3 (S727) responded with an additive effect and the phosphorylation was significantly higher for the combination compared to the single ligands.

In summary, addition of EGF resulted in the strongest increase of phosphorylation of signalling proteins while HRG only led to a small increase of signalling activities in HCC1954 cells. The impact of the combination was slightly weaker

than for EGF alone except for STAT3 (S727). In this instance, the combination of both ligands induced the strongest phosphorylation. The signalling dynamics for each protein were similar for the single ligands and the combination. AKT, PLCγ, and SRC showed no distinct differences between the different conditions. Table 3.9 shows the summary of ligand-dependent effects in HCC1954 cells.

ERBB signalling in SKBR3 cells

The same analysis described before was performed in SKBR3 cells. Figure 3.27 shows the phosphorylation of the same proteins ERK1/2, MEK1/2, p38, AKT, SRC, p70S6K, S6, PLCγ, STAT3, and STAT5 after stimulation with EGF, HRG, and the combination of both ligands in SKBR3 cells.

EGF led to a strong and sustained activation of ERK1/2 as well as of MEK1/2 (Fig. 3.27, blue lines). The highest phosphorylation level was reached after 12 min and remained on this high level for at least 60 min. p38 reached the strongest phosphorylation after 16 min and declined to the basal level after 40 min. AKT showed a weak activation after addition of EGF at its phosphosite S473 and an even fainter phosphorylation at T308. STAT5 responded weakly to the addition of EGF. The phosphorylation level of PLCγ even seemed to decline after addition of the ligand. EGF induced a strong S6 phosphorylation which reached a plateau 16 min after stimulation. SRC, p70S6K, and STAT3 showed no distinct activation.

Stimulation with HRG resulted in a different outcome in comparison to EGF (Fig. 3.27, red lines). ERK1/2 and MEK1/2 showed the same activation dynamics as well as amplitude after stimulation with both ligands alone. AKT was phosphorylated strongly after stimulation with HRG and remained on a high level for at least 60 min. p38 showed only a weak response to HRG compared to EGF but the dynamics were the same. STAT5 was not phosphorylated at all, and S6 was activated weakly compared to the stimulation with EGF.

Analysing the impact of the combination of the ligands on cellular signalling, different responses were observed (Fig. 3.27, green lines). Again, the activation of ERK1/2 and MEK1/2 after stimulation with the combination showed no difference compared to the single agents. AKT and S6 activation was the same as for HRG alone. On the other hand, STAT5 responded stronger to the combination of EGF and HRG than to both ligands alone. SRC showed a weak

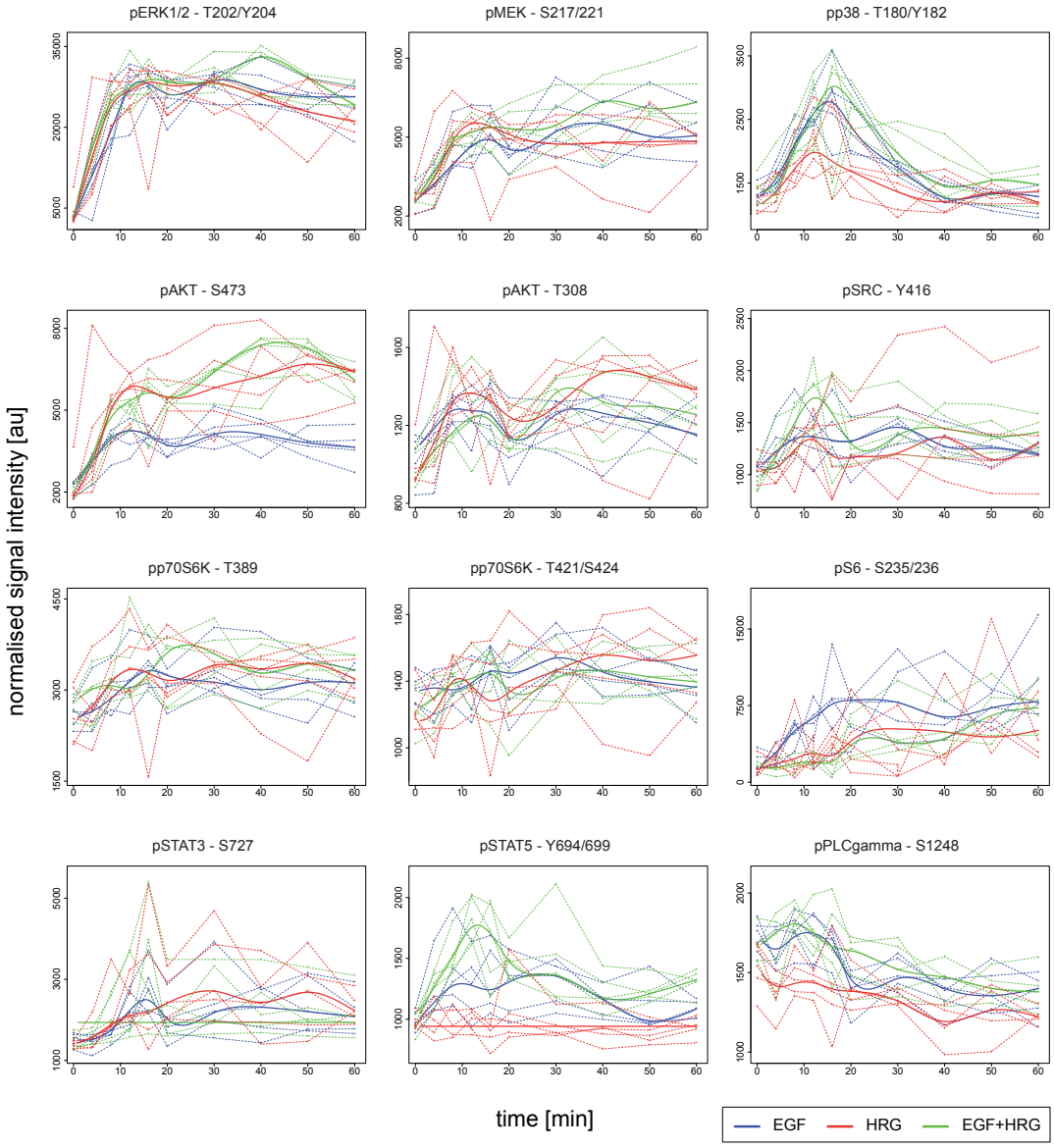

Figure 3.27: Ligand-specific responses in SKBR3 cells
Phosphorylation of ERK1/2, MEK1/2, p38, AKT, SRC, p70S6K, S6, PLCγ, STAT3, and STAT5 after stimulation with EGF (blue), HRG (red), and the combination of both ligands (green).

activation 12 min after addition of the combination whereas both ligands alone were not able to induce SRC phosphorylation.

Table 3.10: Alteration of protein phosphorylation status in SKBR3 cells after stimulation with ligands

protein	phosphosite	EGF	HRG	EGF+HRG
AKT	S473	moderate	strong	strong
AKT	T308	moderate	moderate	moderate
β-catenin		no	no	no
ERK	T202/Y204	strong	strong	strong
GSK3$\alpha\beta$	Y279/216	no	no	no
MEK	S217/221	strong	strong	strong
mTOR	S2448	no	no	no
mTOR	S2481	no	no	no
NFκB	S536	no	no	no
p38	T180/Y182	strong	moderate	strong
p70S6K	T389	weak	weak	weak
p70S6K	T421/S424	no	no	no
PDK1	S241	no	no	no
PKCα	S657/Y658	no	no	no
PLCγ	S1248	weak	weak	weak
PRAS	T246	no	no	no
S6	S235/236	strong	weak	weak
SRC	Y416	weak	weak	moderate
STAT1	Y701	no	no	weak
STAT3	Y705	no	no	weak
STAT3	S727			
STAT5	Y694/699	moderate	weak	strong

To recapitulate, EGF, HRG, and the combination had a similar potential with respect to activating signalling in SKBR3 cells. AKT was stronger activated by HRG and the combination than by EGF, while EGF and the combination had a stronger impact on p38 activation than HRG. For STAT5, the simultaneous stimulation with both ligands resulted in the strongest increase in phosphorylation. Table 3.10 summarises the effects of the ligands in SKBR3 cells.

In conclusion, the response of downstream pathways differed between the cell lines. Only ERK1/2 and MEK1/2 were strongly activated in both cell lines. However, the activation in SKBR3 cells was more sustained. While p70S6K, S6, and STAT3 were mainly activated in HCC1954 cells, the most distinct effects were observed for p38 and STAT5 in SKBR3 cells. In both cell lines, activation kinetics were comparable for the single ligands and the combination. In contrast, the differences between EGF and HRG were much stronger in HCC1954 than in SKBR3 cells. Furthermore, the biological replicates revealed that the signalling in SKBR3 cells was of higher biological variability compared to HCC1954 cells.

3.5.2 Immediate effects of targeted therapeutics

First of all, the immediate effect of the therapeutics within the first hour of preincubation was analysed. This was additionally measured for BT474 cells, as this experiment was not included by Szabó (2009). Adding the antibody therapeutics trastuzumab and pertuzumab had already activating potential and resulted in the phosphorylation of receptors, not only of ERBB2, but also of EGFR and ERBB3. Table 3.11 summarises if a specific phosphosite of a receptor was phosphorylated (yes) or not (no). If a phosphorylation site was activated in a particular cell line, it responded comparably to both antibody therapeutics.

Table 3.11: Phosphorylation status of ERBB receptors after addition of trastuzumab or pertuzumab

target	phosphosite	HCC1954	SKBR3	BT474
EGFR	Y992	yes	no	yes
EGFR	Y1068	yes	yes	yes
EGFR	Y1086	yes	no	yes
EGFR	Y1173	no	yes	no
ERBB2	Y877	NA	yes	yes
ERBB2	Y1112	yes	NA	no
ERBB2	Y1139	yes	yes	yes
ERBB2	Y1221/2	yes	yes	yes
ERBB2	Y1248	yes	yes	yes
ERBB3	Y1197	no	yes	no
ERBB3	Y1289	yes	no	yes

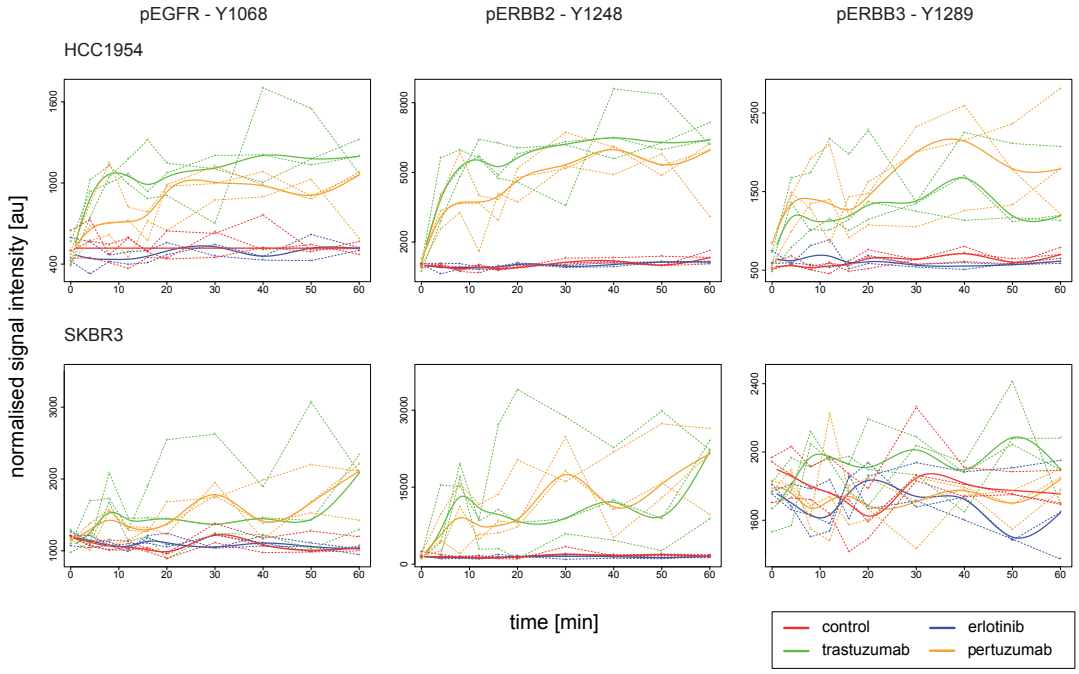

Figure 3.28: Receptor phosphorylation after drug treatment
The phosphorylation of EGFR (Y1068), ERBB2 (Y1248), and ERBB3 (Y1289) after treatment with pertuzumab (orange), trastuzumab (green), erlotinib (blue) and the control (red) is shown for HCC1954 (A) and SKBR3 cells (B) within 60 min. The dashed lines represent the biological replicates while the thick lines show the fit of the smoothing splines.

The phosphorylation dynamics were nearly identical for all phosphorylation sites. Figure 3.28 shows as example phosphorylation sites of the three receptors, EGFR (Y1068), ERBB2 (Y1248) and ERBB3 (Y1289). Strikingly, cell line dependent and specific phosphorylation sites were detected for all receptors. For ERBB3, the phosphorylation of the two tyrosines Y1197 and Y1289 was cell line specific, position Y1289 was phosphorylated in HCC1954 and BT474 cells, phosphorylation of Y1197 was exclusively detected in SKBR3 cells. Erlotinib showed no effect on receptor phosphorylation.

Additionally, cell line specific effects on downstream targets were observed (Fig. 3.29). In HCC1954 cells, the incubation with trastuzumab and pertuzumab resulted in phosphorylation of SRC, STAT5, and STAT3 (Y705). In SKBR3 cells, the incubation with the antibody drugs resulted in activation of SRC, STAT5 and PLCγ. Erlotinib on the other hand resulted in a downregulation of pERK1/2 (Fig. A.6).

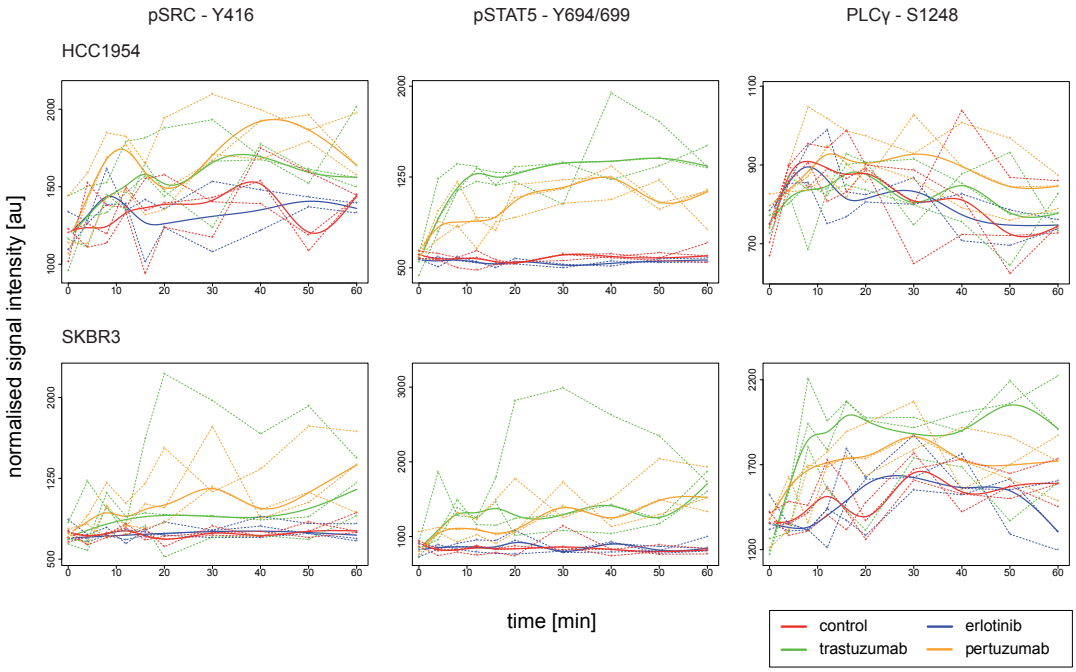

Figure 3.29: Immediate effects of the targeted therapeutics
The diagrams show the phosphorylation of SRC, STAT5, and PLCγ in HCC1954 (A) and SKBR3 cells (B) after addition of pertuzumab (orange), trastuzumab (green), erlotinib (blue) and the control (red). The dashed line represent the biological replicates while the thick lines show the fit of the smoothing splines.

3.5.3 Impact of therapeutics on ligand-induced signalling

After the analysis of the direct effects of trastuzumab, pertuzumab, and erlotinib on receptor and effector protein phosphorylation, the inhibitory potential of the single therapeutics on ligand-induced pathway activation was measured.

Impact of therapeutics on ligand-dependent signalling in HCC1954 cells

In HCC1954 cells, mainly the impact of the inhibitors on EGF signalling was analysed, as this ligand resulted in the highest activation of downstream pathways compared to HRG and to both ligands in combination. Figure 3.30 shows the impact of the three inhibitors after addition of EGF on the proteins ERK1/2, AKT, p70S6K, S6, STAT3, PLCγ, and SRC. The inhibitors led to similar effects on the MAPK pathway, p70S6K, S6, PLCγ, and STAT3. Trastuzumab and pertuzumab had almost no inhibitory effect on these proteins. However,

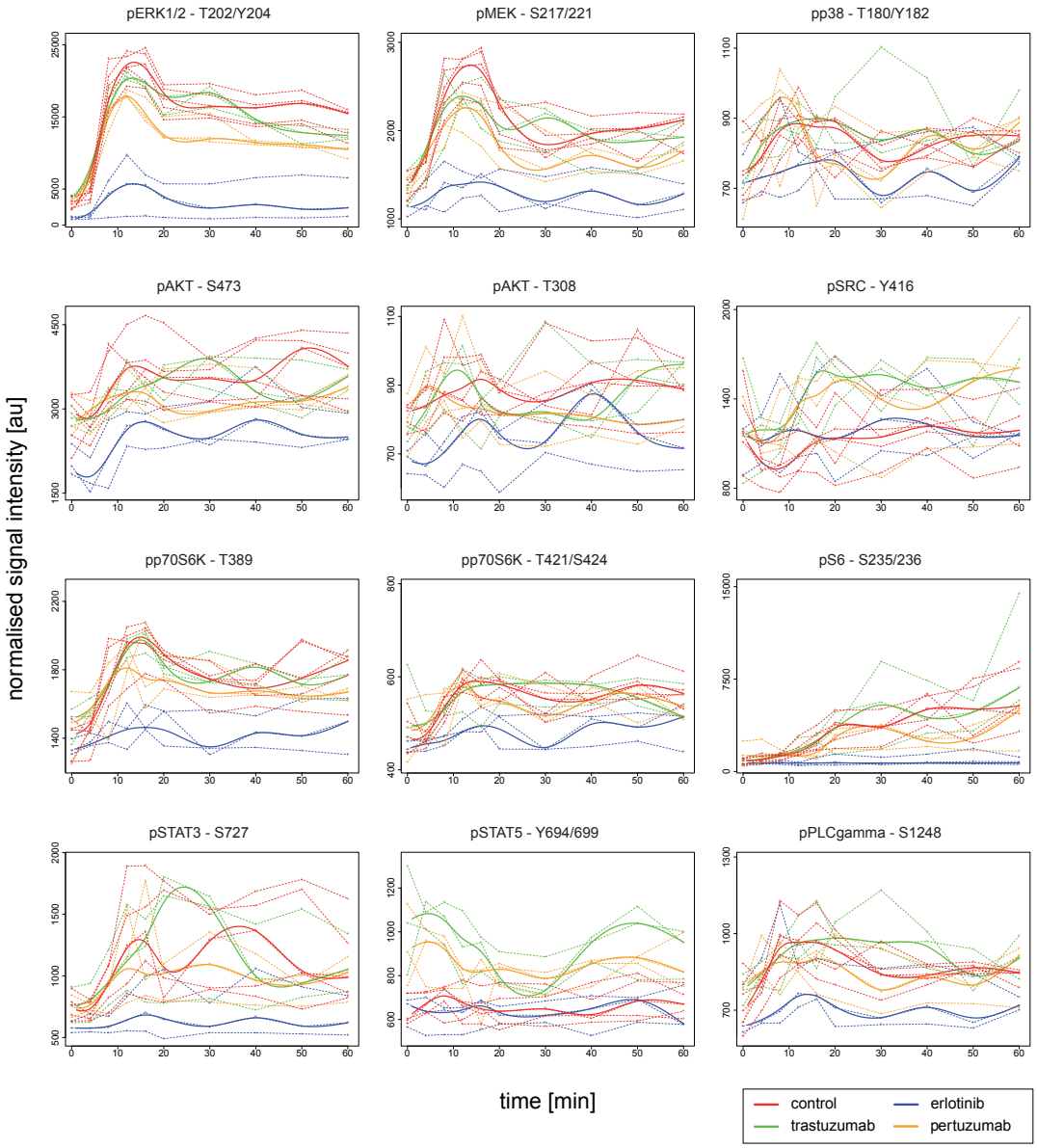

Figure 3.30: Impact of inhibitors after stimulation with EGF in HCC1954 cells.

The diagrams show the phosphorylation of ERK1/2, AKT, p70S6K, S6, STAT3, PLCγ, and SRC after preincubation with the control (red), erlotinib (blue), trastuzumab (green), pertuzumab (orange) and subsequent stimulation with EGF. The dashed line represent the biological replicates while the thick lines show the fit of the smoothing splines.

the inhibitory effect of pertuzumab was slightly stronger. In contrast, erlotinib clearly inhibited the phosphorylation of all these proteins. The addition of EGF resulted in a further increase of SRC phosphorylation, which was already induced by the antibody therapeutics alone (Fig. 3.29). The phosphorylation of STAT5 was decreased within 30 min after addition of EGF. The response of AKT was complex. While the antibody drugs had no effect on AKT phosphorylation, erlotinib reduced the basal phosphorylation of AKT, but it was not able to inhibit the increase of phosphorylation after addition of EGF. Thus, erlotinib did not inhibit the slope of AKT activation but shifted the activation to a lower level.

HRG had only very weak activating potential in HCC1954 cells compared to EGF. However, trastuzumab and pertuzumab did not reduce ERK1/2 phosphorylation after HRG stimulation. Erlotinib, in contrast, inhibited the activation of ERK1/2. The same was true for MEK1/2, p70S6K, S6, and STAT3 (S727) (Fig. A.7). Regarding the combination of EGF and HRG, the inhibitors had the same effect as observed for the ligands alone.

In summary, trastuzumab and pertuzumab slightly decreased the activation of the proteins mainly activated by the ligands but the effects were not significant. Erlotinib instead was able to inhibit the activation of all proteins.

Impact of therapeutics on ligand-dependent signalling in SKBR3 cells

In SKBR3 cells, the impact of the three inhibitors was similar to HCC1954 cells. Figure 3.31 shows the phosphorylation of 10 proteins after preincubation with erlotinib, trastuzumab, and pertuzumab and subsequent stimulation with EGF. While trastuzumab and pertuzumab showed almost no inhibitory effect, erlotinib inhibited the phosphorylation of all 10 proteins. The preincubation with pertuzumab and trastuzumab led to an increase in the phosphorylation of PLCγ, SRC, and STAT5. This phosphorylation was further increased after addition of EGF. While no inhibitor was able to inhibit AKT signalling in HCC1954 cells, erlotinib and pertuzumab were both able to downregulate and diminish phosphorylation of both phosphorylation sites in SKBR3 cells. In two of three biological replicates, the downregulation of AKT phosphorylation by pertuzumab was significant. Notably, the activation mode of the third biological replicate correlated with the uninhibited control for all measured proteins,

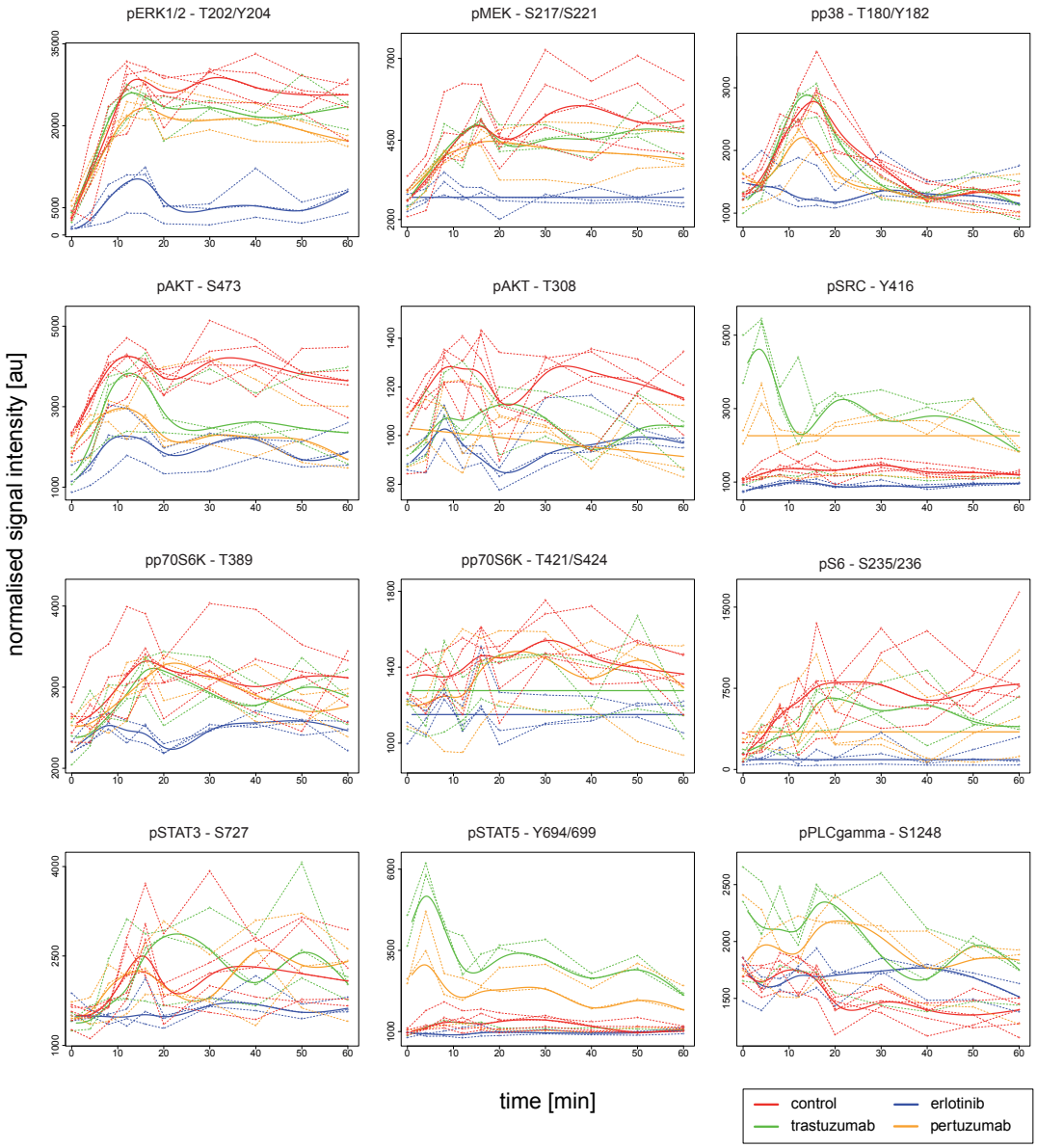

Figure 3.31: Impact of inhibitors after stimulation with EGF in SKBR3 cells

The diagrams show the phosphorylation of ERK1/2, AKT, p70S6K, S6, STAT3, PLCγ, and SRC after preincubation with the control (red), erlotinib (blue), trastuzumab (green), pertuzumab (orange) and subsequent stimulation with EGF. The dashed line represent the biological replicates while the thick lines show the fit of the smoothing splines.

where pertuzumab showed an effect for the other two replicates, indicating an experimental error of this replicate. Although trastuzumab was not able to inhibit activation of AKT, the dynamics were altered and resulted in a decrease of phosphorylation after 20 min. For p38, the effects of the inhibitors were very similar. Trastuzumab had no effect, pertuzumab slightly inhibited p38 activation while erlotinib completely prevented this step.

As observed for HCC1954 cells, trastuzumab and pertuzumab only slightly decreased signalling activation, while erlotinib was able to inhibit phosphorylation of all measured proteins. In contrast, AKT activation was downregulated by trastuzumab and pertuzumab in SKBR3 cells.

The main difference between EGF- and HRG-induced signalling resided in an AKT phosphorylation which was much stronger upon addition of HRG in SKBR3 cells. Activation of AKT was only reduced weakly by erlotinib, while the antibody drugs showed no inhibitory potential against HRG-initiated signalling (Fig. 3.32). Preincubation with trastuzumab even seemed to increase the phosphorylation of AKT after addition of HRG. Stimulation with EGF and HRG resulted in a strong activation of AKT which was not prevented by erlotinib. Regarding the other proteins, the impact of the inhibitors was ligand independent.

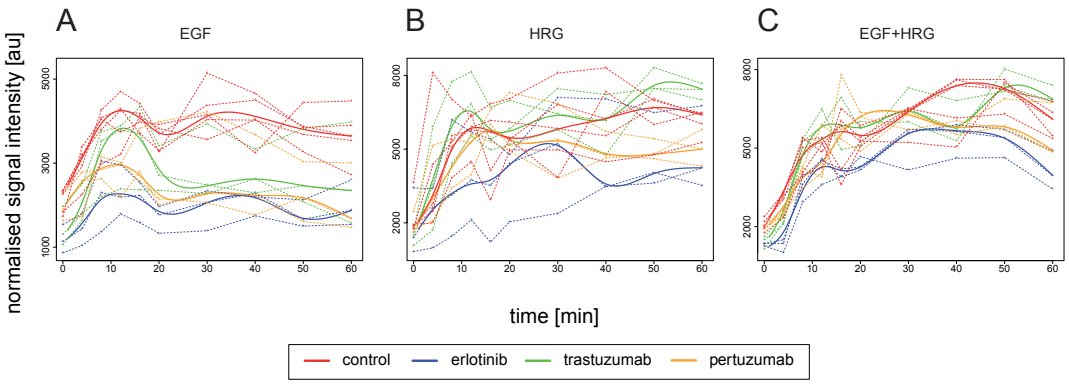

Figure 3.32: Activation of AKT in SKBR3 cells
Cells were preincubated with trastuzumab (green), pertuzumab (orange), erlotinib (blue) and subsequently stimulated with EGF (A), HRG (B), or EGF and HRG (C). The plots show the phosphorylation of AKT (S473). The dashed lines represent the biological replicates, the thick lines show the smoothing splines.

3.5.4 Combinatorial impact of therapeutics on ligand-induced signalling

In contrast to pertuzumab and erlotinib, trastuzumab is already part of the clinical routine in the treatment of ERBB2 positive breast cancer. According to results from single drug treatment, trastuzumab was not able to significantly inhibit fast signalling downstream of ERBB2. Since one aim of the study was to analyse the potential benefit of combinatorial treatments, the three therapeutics were applied in all combinations in HCC1954 and SKBR3 cells to identify additive effects may circumvent *de novo* resistance mechanisms. The impact of the combinations of trastuzumab and pertuzumab, trastuzumab and erlotinib, pertuzumab and erlotinib, and all three inhibitors was analysed after addition of EGF. To cover all major pathways, phosphorylation of ERK1/2 (T202/Y204), AKT (S473), p70S6K (T389), S6 (S235/236), STAT3 (S727), and p38 (T180/Y182) was measured.

Combinatorial treatment of HCC1954 cells

Figure 3.33 shows the time series of these six proteins preincubated with the drug combinations after addition of EGF to HCC1954 cells. The combination of trastuzumab and pertuzumab resulted in a small increase of the inhibitory potential towards MAPK signalling compared to single drug treatments. All erlotinib containing combinations nearly abolished the activation of MEK1/2 and ERK1/2, but no significant differences between the combinations were observed. None of the applied drug combinations was able to inhibit activation of AKT. The downregulation of AKT phosphorylation by the erlotinib containing combinations resulted in a lower activation level, but the absolute change of phosphorylated protein remained similar as observed for erlotinib alone. The inhibitory behaviour of the combinations towards p70S6K was similar to those observed for ERK1/2. An exception was that trastuzumab and pertuzumab in combination slightly increased the phoshorylation of T389 instead of leading to a decrease. Within the first 16 min, the combination of trastuzumab and pertuzumab also caused a stronger increase of S6 phosphorylation in comparison to the control. This correlated with the activation peak of p70S6K (T389). However, after 16 min the phosphorylation remained static while the control steadily increased. All erlotinib containing combinations entirely inhibited S6 phosphorylation in HCC1954 cells.

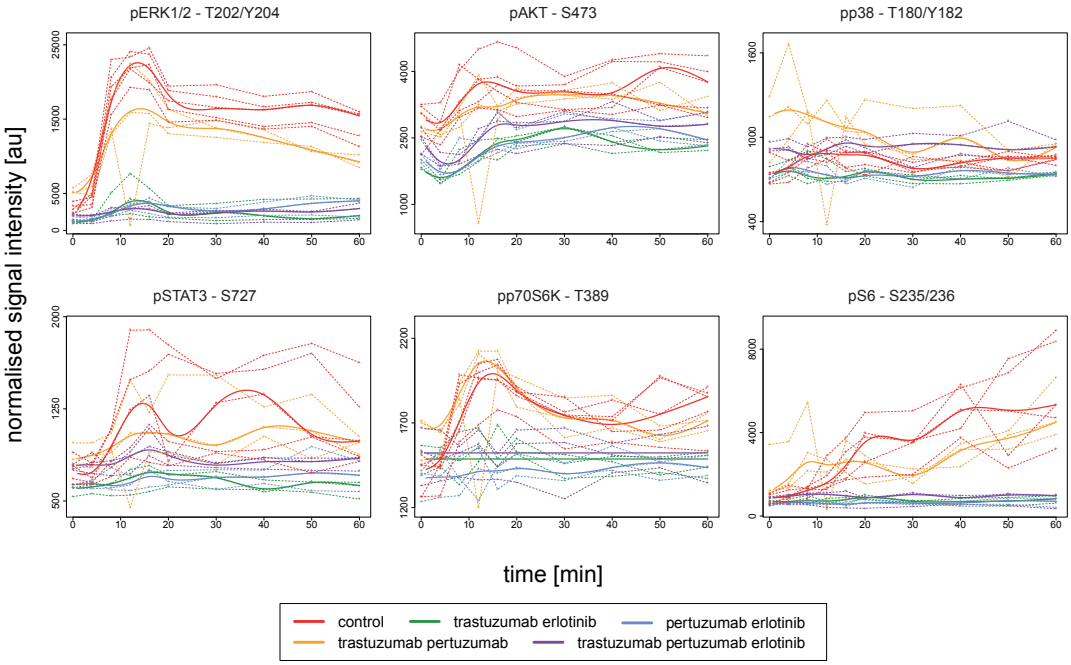

Figure 3.33: Combinatorial drug treatment in HCC1954 cells.
Cells were preincubated with drug combinations for 1 h and subsequently stimulated with EGF for the indicated time points. The dashed lines represent the single biological replicates, the thick shows the fitted smoothing spline.

Combinatorial treatment of SKBR3 cells

Comparable to HCC1954 cells, the erlotinib containing combinations strongly reduced the activation of ERK1/2 allowing just a small peak after 12 min followed by total downregulation after 20 min, as shown in figure 3.34. In contrast, the combination of trastuzumab and pertuzumab showed no combinatorial benefit and the inhibition was indeed weaker than for pertuzumab alone. In terms of AKT inhibition, all combinations resulted in a significant inhibition of the activation peak and subsequent downregulation of the signal to the basal level. But again, trastuzumab and pertuzumab had only a minimal effect. The same was true for the p38 phosphorylation. The phosphorylation of S6 was prevented by all erlotinib containing combinations. In contrast to HCC1954 cells, the combination of trastuzumab and pertuzumab was capable of reducing the activation of S6 in SKBR3 cells.

Since the HRG induced AKT (S473) activation was not inhibited by single drug treatment, the impact of combinatorial treatment was analysed (Fig. 3.35).

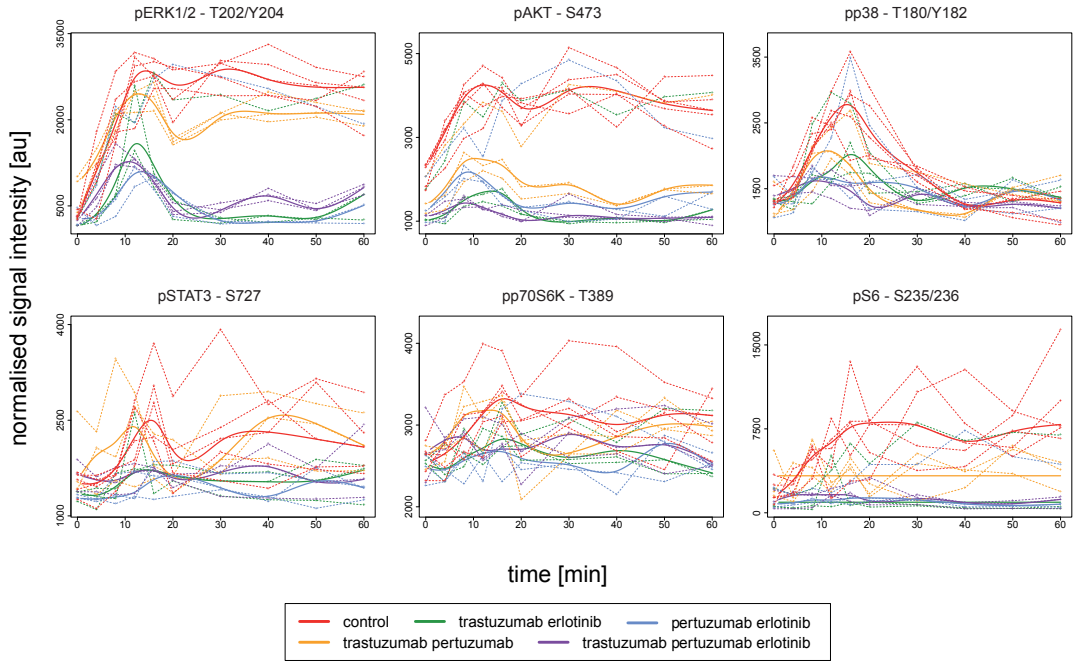

Figure 3.34: Combinatorial drug treatment in SKBR3 cells.
SKBR3 cells were preincubated with all possible drug combinations for 1 h and subsequently stimulated with EGF. The dashed lines represent the single biological replicates, the thick shows the fitted smoothing spline.

The dual combinations containing trastuzumab slightly reduced HRG-induced AKT phosphorylation and to a weaker extent EGF+HRG-induced AKT phosphorylation. However, the combinations containing pertuzumab and erlotinib completely prevented HRG induced AKT activation and significantly inhibited EGF+HRG-induced AKT phosphorylation.

In summary, the application of an antibody drug together with the small molecule erlotinib resulted in improved inhibition of the MAPK and the PI3K pathways represented by ERK1/2 and AKT1. This effect was also observed for p70S6K and, in the case of SKBR3 cells, also for p38. In contrast, the combinatorial treatment of trastuzumab and pertuzumab did not result in an enhanced inhibitory effect in HCC1954 cells. However, in SKBR3 cells this combination was able to reduce the activation of AKT and S6. The combination of pertuzumab and erlotinib effectively inhibited HRG-induced AKT activation in SKBR3 cells.

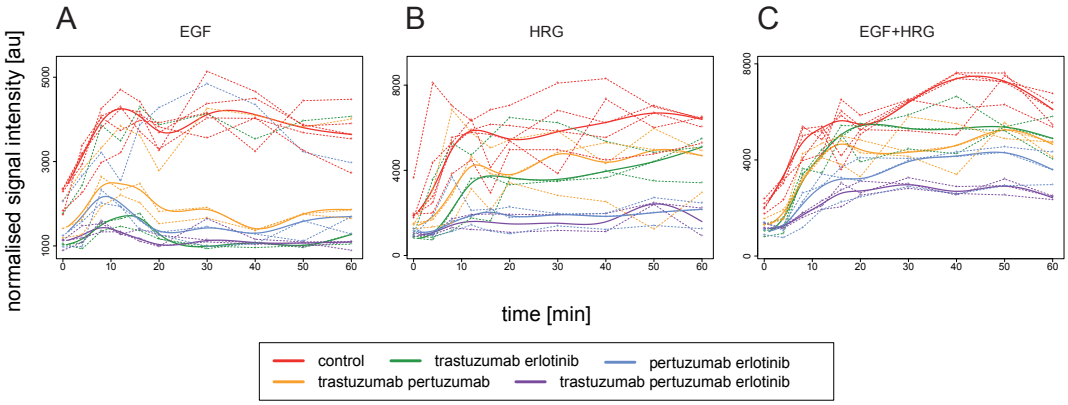

Figure 3.35: Impact of combinatorial drug treatment on AKT activation in SKBR3 cells.

Cells were preincubated with trastuzumab and pertuzumab (orange), trastuzumab and erlotinib (green), pertuzumab and erlotinib (blue) and the combination of all three inhibitors (violet) and subsequently stimulated with EGF (A), HRG (B), or EGF and HRG (C). The plots show the phosphorylation of AKT (S473). The dashed lines represent the biological replicates, the thick lines show the smoothing splines.

3.5.5 Long-term inhibition experiments

Erlotinib was the therapeutic agent which had the strongest inhibitory potential towards all pathways within the 60 min time series. To analyse if the inhibitory effects on MAPK and PI3K pathway had an extended activity, the effects of erlotinib and all possible drug combinations in full growth medium was measured up to 30 h. As one biological replicate lacked the 18 h time point, this value was set as the mean of the 12 h and the 24 h time point. In addition to HCC1954 and SKBR3 cells, the experiment was also carried out in BT474 cells. Major signalling proteins measured in short time experiments were also analysed in the long-term study. Figure 3.36 shows the combinatorial effects on ERK1/2 and AKT phosphorylation in the three cell lines. Additionally, proteins playing a role in cell cycle progression were studied. Figure 3.37 displays the phosphorylation of the ribosomal protein S6 and the retinoblastoma tumour suppressor protein (RB). Phosphorylation of S6 correlates with increased mRNA transcription in response to growth factors, an important aspect of sustained cell growth and proliferation. RB regulates cell proliferation by controlling the restriction point in G1-phase and phosphorylation of RB is correlated with cell cycle progression. With respect to ERBB receptor activation, ERBB2 phosphorylation at Y1248 was analysed, as Y1248 is one major autophosphorylation site of ERBB2 correlating well with receptor activation (Fig. 3.38). The results are described in detail for each cell line separately.

Long-term inhibitory effects in HCC1954 cells

In the control experiment without any inhibitor, ERK1/2 showed a first activation peak after 2 h with a subsequent decline until 6 h and a second long lasting activation reaching a maximum after 18 h. The erlotinib containing combinations led to an immediate downregulation of pERK1/2 and no activation was noticed for the following 30 h. In contrast, trastuzumab and pertuzumab resulted in an activation of ERK1/2 similar to the control, and ERK1/2 phosphorylation level remained elevated for 24 h and declined afterwards.

As already observed in the short time series, no clear AKT activation profile was detected in HCC1954 cells. The dual combinations containing erlotinib resulted in a general downregulation of pAKT compared to the control. The combination of pertuzumab and trastuzumab and the triple combination were

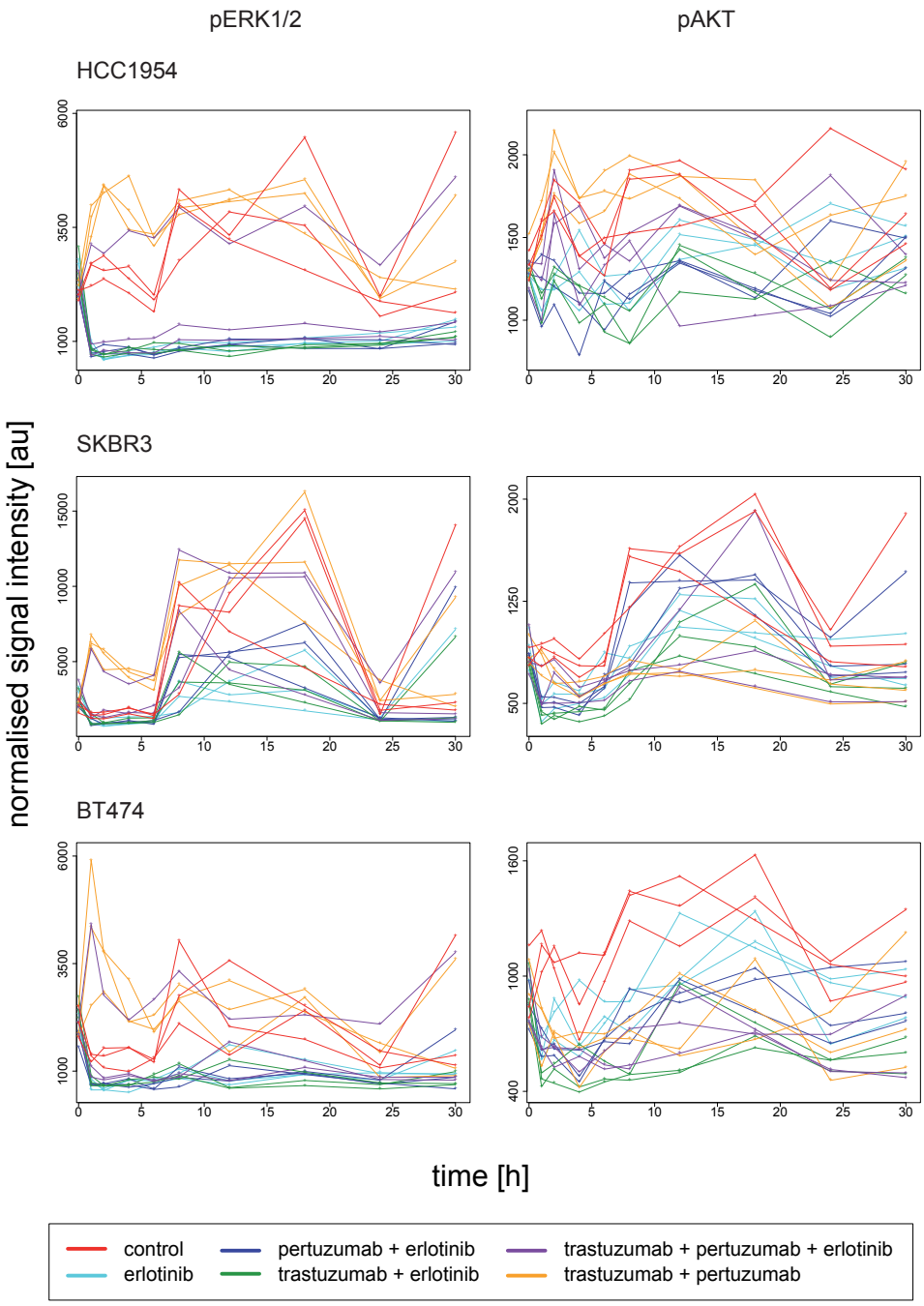

Figure 3.36: Phosphorylation of ERK1/2 and AKT after addition of inhibitors within 30 h

The figure shows the phosphorylation of ERK1/2 and AKT (S473) in response to the inhibitor combinations and the control within 30 h. The coloured lines represent the three biological replicates.

not different from the control which showed two peaks, the first after 2 h and the second after 12 h followed by a steadily increased AKT phosphorylation.

The phosphorylation of the RB protein started to decline 8 h after addition of all erlotinib containing combinations. However, the RB phosphorylation after addition of the trastuzumab and pertuzumab combinations increased compared to the control. The same effect was observed for the phosphorylation of S6 within the first 24 h. While pS6 stayed on an elevated level for the control and the trastuzumab/pertuzumab combination, all other combinations led to a downregulation of S6 phosphorylation. This effect was observed during the first 24 h but lost afterwards.

To sum up, in HCC1954 cells, the erlotinib containing combinations had indeed the strongest impact on signalling within 24–30 h. Nevertheless, no difference was observed between erlotinib alone and the combinations. The combination of trastuzumab and pertuzumab had no inhibitory effect on signalling and even resulted in elevated protein phosphorylation.

Long-term inhibitory effects in SKBR3 cells

The long term inhibitory effect on ERK1/2 looked different in SKBR3 cell compared to HCC1954 cells (Fig. 3.36). The phosphorylation level of the control weakly declined and remained on a low level for 6 h. All combinations, except trastuzumab and pertuzumab, weakly decreased ERK1/2 phosphorylation whereas addition of trastuzumab and pertuzumab immediately resulted in an increase of phosphorylation which declined within the first 6 h. Similar to the signalling in HCC1954 cells, SKBR3 cells showed a second activation cycle after 8 h which reached a peak after 18 h and returned to baseline activation after 24 h. The uninhibited control reached the highest level of ERK1/2 activation. However, trastuzumab and pertuzumab and also the triple combination were not able to inhibit the activation of ERK1/2. Erlotinib alone strongly inhibited EKR1/2 phosphorylation followed by trastuzumab/erlotinib and pertuzumab/erlotinib.

The impact of the inhibitors on AKT signalling was different. The pAKT level of the control remained constant during 6 h, followed by a strong increase peaking after 18 h. In contrast, all inhibitor combinations resulted in a immediate decline of pAKT within 1 h. The increase of AKT phosphorylation observed for the

control after 6 h was inhibited by all combinations whereas trastuzumab and pertuzumab, independent of addition of erlotinib, showed the strongest effect.

The phosphorylation of S6 resembled the AKT activation dynamics for the control experiment (Fig. 3.37). Trastuzumab and pertuzumab in combination induced a strong increase of AKT phosphorylation with a peak after 2 h. The erlotinib containing combinations resulted in an immediate dephosphorylation and kept the phosphorylation on a low level. The second activation peak approximately after 12–18 h was inhibited by the combination trastuzumab/erlotinib and the triple combination.

In HCC1954 cells, the pRB signal started to decline already after 8 h following treatment, which was also observed in the control experiment. In SKBR3 cells, RB phosphorylation of the control stayed on a high level for almost 24 h. The combination trastuzumab/erlotinib showed a strong impact in this cell line and RB phosphorylation decreased persistently within the 30 h measurement. Erlotinib alone and in combination with pertuzumab also induced RB dephosphorylation but to a weaker extent. The combination trastuzumab/pertuzumab and the triple combination showed the weakest effect in terms of downregulating the pRB level.

In summary, the combination of trastuzumab and erlotinib had a strong inhibitory effect on ERK1/2, AKT, RB and S6 phosphorylation in SKBR3 cells. This was in line with the results observed for the 60 min measurements. The combination of trastuzumab and pertuzumab only inhibited AKT activation while no inhibition of ERK1/2, S6, and RB phosphorylation was observed.

Long-term inhibitory effects in BT474 cells

In BT474 cells, a downregulation of ERK1/2 was observed for the control within the first hour (Fig. 3.36). The dephosphorylation was even stronger for erlotinib and erlotinib containing combinations. Trastuzumab and pertuzumab in combination led to an increase of ERK1/2 phosphorylation within 1 h, as seen for the other two cell lines. A second peak was observed after 8 h, likewise for the control. For the other combinations, the phosphorylation remained on the same level.

For AKT, the highest phosphorylation was observed after 18 h. At this time point, the control showed the strongest signal while trastuzumab and erlotinib

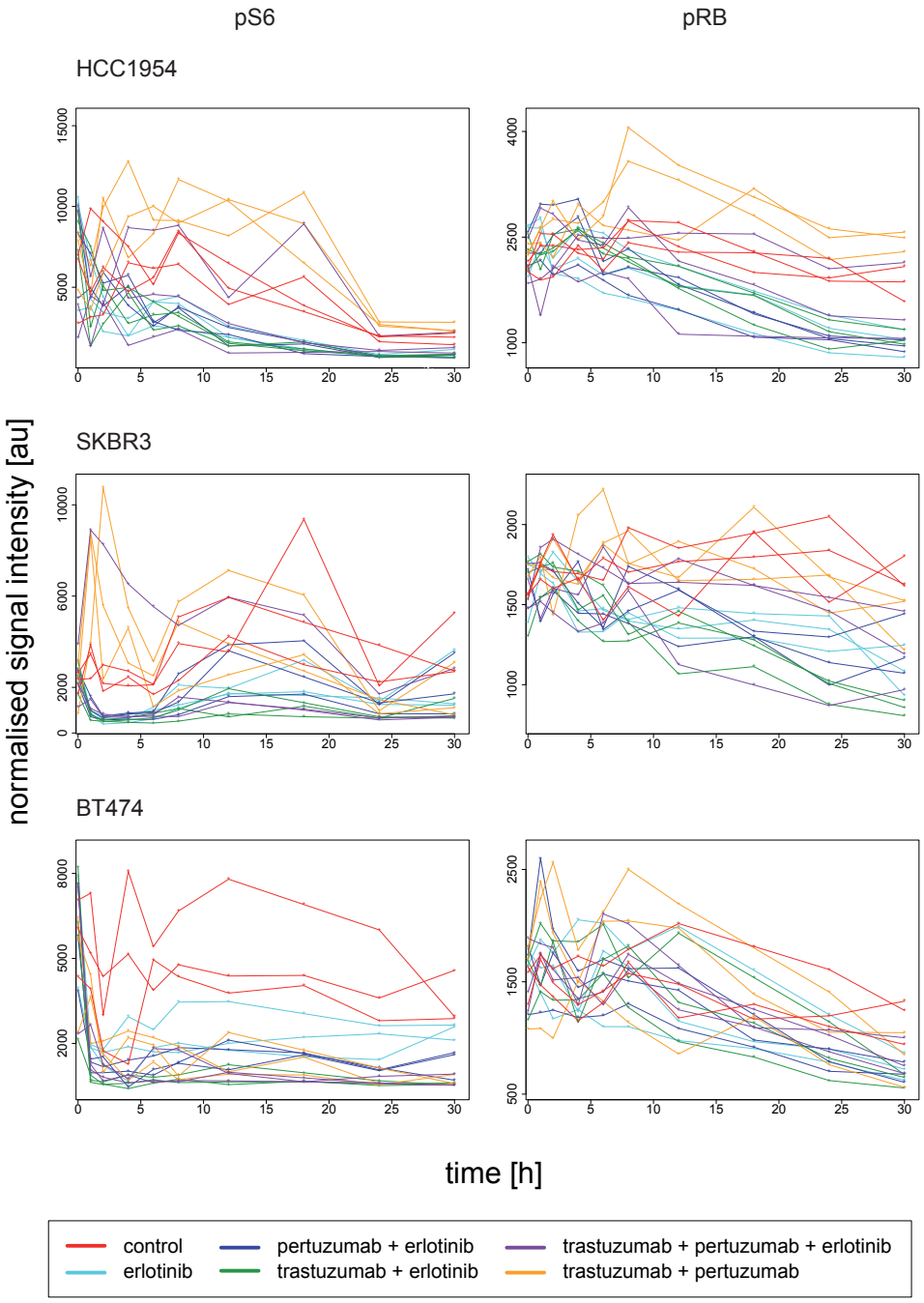

Figure 3.37: Phosphorylation of S6 and RB after addition of inhibitory drugs within 30 h

The figure shows the phosphorylation of S6 (S235/236) and RB (S807/811) after addition of inhibitor combinations in growth medium and the control within 30 h. The coloured lines represent the three biological replicates.

Table 3.12: Therapeutics effect summary

	strongest effect	**weakest effect**
HCC1954	erlotinib	trastuzumab/pertuzumab
SKBR3	trastuzumab/erlotinib	trastuzumab/pertuzumab
BT474	trastuzumab/erlotinib	erlotinib

used in combination completely inhibited AKT phosphorylation. The triple combination also revealed a strong inhibitory potential. Erlotinib alone had the weakest impact on AKT phosphorylation in BT474 cells.

Regarding S6 phosphorylation, erlotinib also had the weakest impact while trastuzumab and erlotinib and the triple combination had the strongest impact. As observed for HCC1954 cells, the phosphorylation of RB declined for all conditions analysed and significant differences were only detected after 30 h. However, S6 dephosphorylation was significantly stronger for trastuzumab and erlotinib.

In summary, trastuzumab and erlotinib in combination had the strongest inhibitory effect in BT474 cells, comparable to the effect observed for SKBR3 cells. But while AKT and ERK1/2 signalling was still active in SKBR3 cells, this was totally diminished in BT474 cells. The reduction of protein phosphorylation by erlotinib alone was weaker in BT474 cells compared to SKBR3 and HCC1954 cells. This could be due to the low expression of EGFR in this cell line (Fig. 3.11). Table 3.12 gives an overview of the strongest and weakest drug combinations for all three cell lines. The triple combination did not necessarily reveal the strongest inhibitory potential.

Noteworthy, a single biological replicate of the triple combination showed the same results as the trastuzumab/pertuzumab combination while the other two replicates were strongly inhibited. This was observed for all three cell lines. This result indicated that erlotinib might not have been present in the third replicate by mistake.

Impact of combinatorial treatment on ERBB2 receptor phosphorylation

The previous experiment revealed that ERBB2 was phosphorylated upon trastuzumab or pertuzumab treatment (section 3.5.2). The phosphorylation remained on an elevated level for 60 min (Fig. 3.28). To investigate the drug influence

on receptor phosphorylation for a longer time period, we monitored the phosphorylation of ERBB2 at Y1248 for 30 h (Fig. 3.38). The drug combinations clustered in three groups based on the phosphorylation status. Erlotinib did not induce receptor phosphorylation and was similar compared to the control. The dual combinations containing erlotinib and any of the antibody drugs induced phosphorylation within 1 h which stayed on an elevated level for the remaining 30 h.

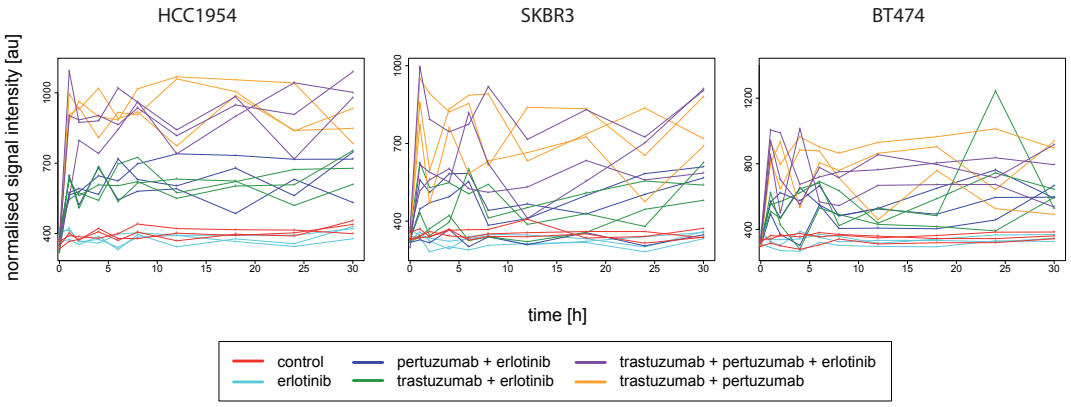

Figure 3.38: ERBB2 phosphorylation at Y1248
The plots show the phosphorylation of ERBB2 at Y1248 in the three cell lines HCC1954, SKBR3 and BT474. Drug combinations were added in growth medium and effects were measured for 30 h in comparison to the control. The coloured lines represent the three biological replicates, the dashed lines represent the splines.

Trastuzumab and pertuzumab in combination, independent of added erlotinib, caused a very strong increase of ERBB2 phosphorylation at Y1248 within the first hour. The phosphorylation maintained at a high level for 30 h. Overall, these findings were similar for the three cell lines. However, in HCC1954 cells, the biological replicates were highly reproducible and showed a sharp separation between the three clusters while the separation was not so clear in the two cell lines SKBR3 and BT474.

3.6 Cell cycle progression after drug treatment

A 7-amino-actinomycin D (7AAD) assay was performed in HCC1954 and SKBR3 cells to study the impact of treatment with drug combinations on cell cycle progression. After treatment with erlotinib alone and in combination with trastuzumab, the proportion of HCC1954 cells in G1-phase significantly increased compared to the control (Fig. 3.39). Accordingly, the proportion of cells in S-phase decreased. These results suggested an inhibition of cell cycle progression as already indicated by reduced RB phosphorylation in HCC1954 cells. In SKBR3 cells, the combination of erlotinib and trastuzumab revealed a significant decrease of cells on G1-phase as it had been observed for HCC1954 cells. In contrast, treatment with trastuzumab and pertuzumab in combinations resulted in a significant increase of cells in G1-phase. In HCC1954 cells, no significant effect was observed for this combination of both therapeutic antibodies.

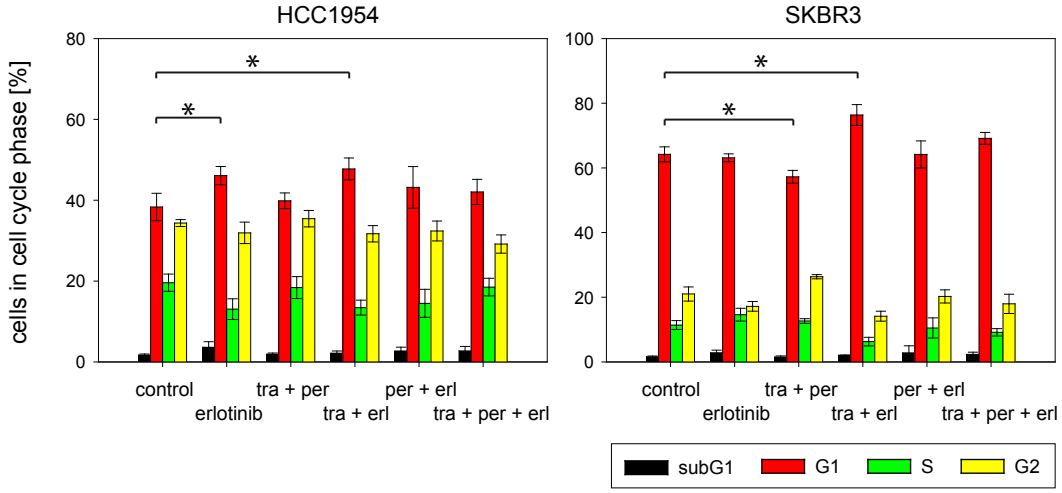

Figure 3.39: Cell cycle analysis after drug treatment
Cells were incubated with the therapeutics trastuzumab (tra), pertuzumab (per), and erlotinib (erl) in the indicated combinations in growth medium for 24 h and DNA content was analysed using 7AAD. * = $p<0.01$

In summary, the analysis of cell cycle progression confirmed the results of the long-term inhibition experiments whereas erlotinib revealed a significant inhibitory effect in HCC1954 cells and the combination of trastuzumab and erlotinib significantly inhibited cell cycle progression in both cell lines.

3.7 Regulation of p70S6K activation

The protein kinase p70S6K was reported to be phosphorylated by kinases of both major signalling pathways, MAPK and PI3K, as observed for MCF7 cells. Because no clear phosphorylation of p70S6K was detected in SKBR3 cells, analysis of BT474 cells was included in the study. In HCC1954 cells, the activation of p70S6K seemed only to be correlated to ERK1/2 activation. To analyse the contribution of the two pathways on downstream signal integration, the impact of the PI3K inhibitor LY294002 and the MEK1 inhibitor PD98059 on ligand-mediated signalling was measured. Therefore, cells were incubated with the inhibitors for 1 h prior to stimulation with 5 nM EGF. As proof of principle experiment, the phosphorylation of ERK1/2 and AKT was analysed to ensure the specificity of the inhibition. For both cell lines, LY294002 resulted in inhibition of AKT and PD98059 in inhibition of ERK1/2 as shown for SKBR3 in figure 3.40. Analysis of downstream targets revealed cell line specific effects which are presented below.

p70S6K regulation in SKBR3 cells

Phosphorylation of p70S6K was hardly detectable in SKBR3 cells. However, the impact of the two inhibitors on EGF-induced activation of ERK1/2, AKT,

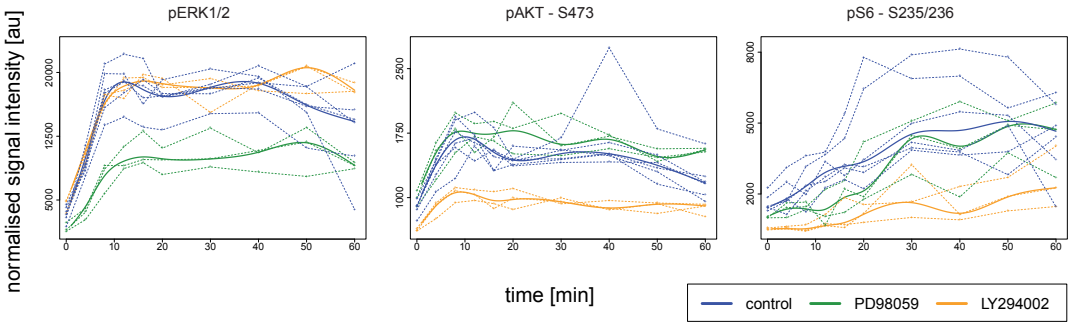

Figure 3.40: Contribution of MAPK and PI3K pathways on S6 phosphorylation in SKBR3 cells.
SKBR3 cells were preincubated with PD98059 or LY294002 and subsequently stimulated with 5 nM EGF. Phosphorylation of ERK1/2, AKT (S473), and S6 (S235/236) was measured. The dashed lines show the biological replicates, the thick lines represent the smoothing splines.

and S6 is shown in figure 3.40. LY294002 almost completely inhibited phosphorylation of S6 indicating an PI3K dependent phosphorylation. In addition, PD98059 was also able to inhibit phosphorylation of S6, although its inhibitory activity was much weaker compared to LY294002. Phosphorylation was only reduced within the first 10-20 min after stimulation and increased afterwards.

p70S6K regulation in HCC1954 cells

Previous results from experiments performed in HCC1954 cells indicated that p70S6K is under the control of ERK1/2 as both kinases revealed comparable kinetics. Experiments with PI3K and MEK1 inhibitors confirmed this assumption. PD98059 completely inhibited the phosphorylation of p70S6K at both phosphorylation sites in this cell line whereas PI3K inhibition had no influence on p70S6K activation (Fig. 3.41). However, S6 phosphorylation was dependent

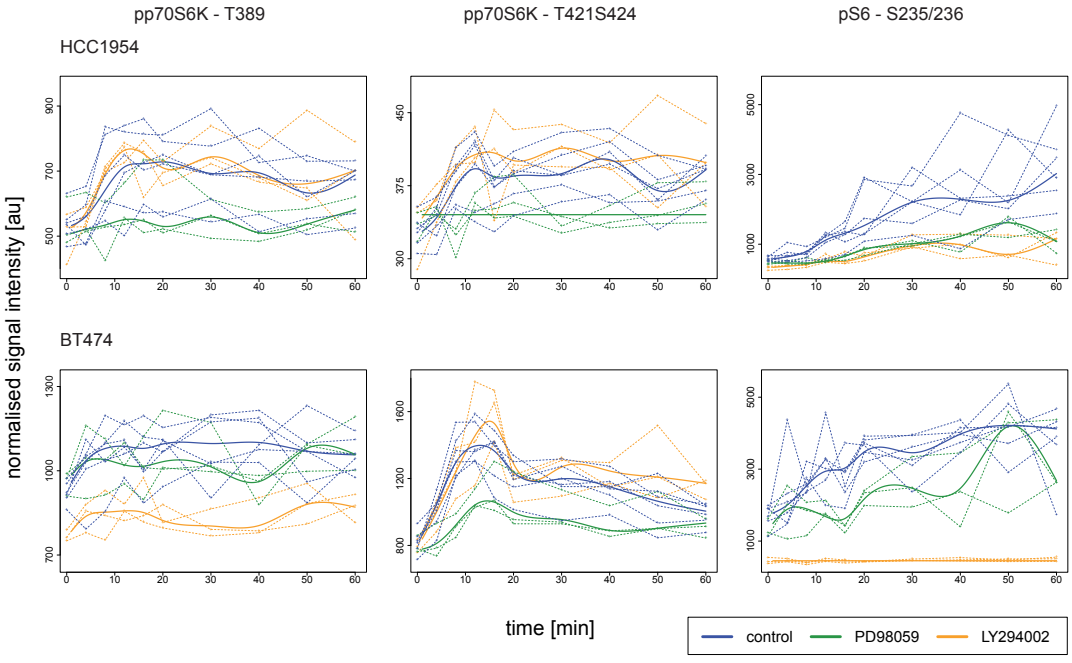

Figure 3.41: Contribution of MAPK and PI3K pathways on S6 phosphorylation in HCC1954 and BT474 cells.
Cells were preincubated with PD98059 or LY294002 and subsequently stimulated with 5 nM EGF. Phosphorylation of p70S6K (T389), p70S6K (T421/S424), and S6 (S235/236) was measured. The dashed lines show the biological replicates, the thick lines represent the smoothing splines.

on both signalling pathways. In contrast to SKBR3 cells, both inhibitors reduced the phosphorylation of S6 (S235/236) to a similar extent.

p70S6K regulation in BT474 cells

Phosphorylation of p70S6K (T389) in BT474 cells was significantly downregulated after preincubation with LY294002 while preincubation with PD98059 resulted in a significant reduction of the p70S6K (T421/S424) activation (Fig. 3.41). While inhibition of the PI3K pathway resulted in a complete downregulation and prevention of S6 phosphorylation in this cell line, inhibition of the MAPK pathway only led to a reduction of S6 phosphorylation.

Analysing the target proteins p70S6K and S6 downstream of ERK1/2 and AKT revealed differences in the wiring of the signalling networks between the cell lines. Whereas activation of p70S6K was MAPK dependent in HCC1954 cells, S6 was dependent on both pathways indicating an additional regulatory mechanism in this cell line. In SKBR3 cells, phosphorylation of S6 was mostly dependent on AKT activation reflecting the canonical PI3K/mTOR dependent pathway. However, both pathways resulted in the phosphorylation of S6 whereas inhibition of the ERK1/2 dependent activation was compensated after 30 min. In BT474 cells, p70S6K (T389) and S6 phosphorylation were PI3K pathway dependent, while inhibition MAPK pathway only reduced phosphorylation of p70S6K (T421/S424) and S6.

3.7.1 Impact of rapamycin on p70S6K phosphorylation

The phosphorylation of p70S6K at T389 seemed to be MAPK pathway dependent in HCC1954 cells, although this particular phosphorylation site was reported to be rapamycin sensitive. Therefore, HCC1954 cells were preincubated with 10 nM rapamycin and subsequently stimulated with EGF. Preliminary results indicated that both phosphorylation sites of p70S6K were rapamycin insensitive. As shown in figure 3.42, preincubation with rapamycin led to an upregulation of p70S6K and ERK1/2 phosphorylation. Western blot analysis revealed that mainly p85S6K but not p70S6K was phosphorylated upon EGF treatment (Fig. 3.43). In contrast to p70S6K, the corresponding phosphorylation site of p85S6K seemed to be rapamycin insensitive and this isoform was mainly measured on RPPA.

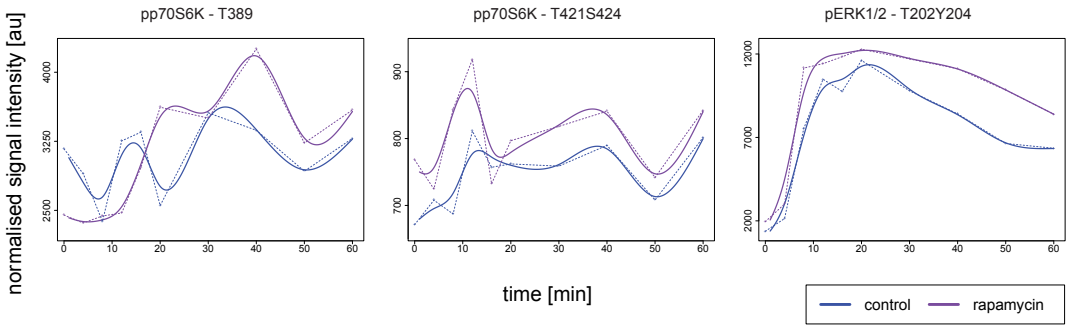

Figure 3.42: Rapamycin incubation prior to EGF stimulation in HCC1954 cells.
The plots show the activation of p70S6K and ERK1/2 with (violet) and without (blue) preincubation with 10 nM rapamycin and subsequent stimulation with 5 nM EGF.

For comparison, the experiment was repeated in MCF7 cells. In this cell line, both isoforms were phosphorylated in response to EGF but p70S6K to a higher degree (Fig. 3.44). In contrast to HCC1954 cells, the phosphorylation of both isoforms was inhibited by rapamycin. Nevertheless, rapamycin inhibited S6 phosphorylation in a comparable manner in both cell lines.

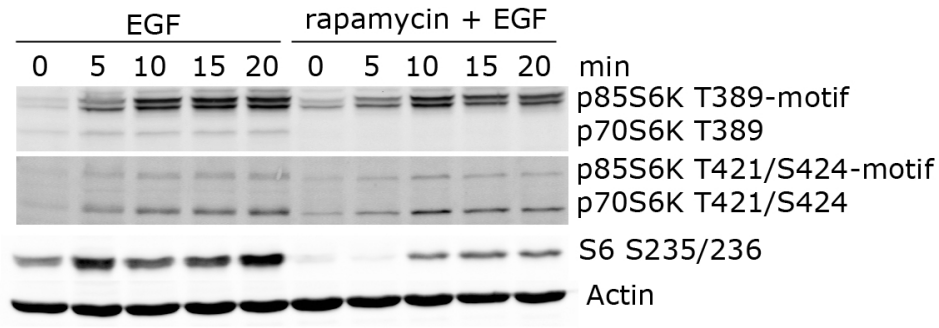

Figure 3.43: Isoform specific analysis of p70S6K/p85S6K phosphorylation in HCC1954 cells

Cells were preincubated with 10 nM rapamycin for 1 h and subsequently stimulated with EGF. Phosphorylation of p70S6K (T389), p70S6K (T421/S424), the corresponding phosphorylation sites of p85S6K, and S6 (S235/236) are shown.

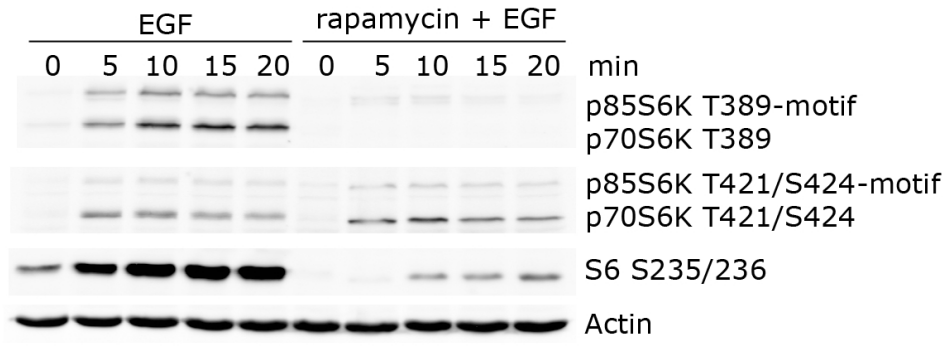

Figure 3.44: Isoform specific analysis of p70S6K/p85S6K phosphorylation in MCF7 cells

Cells were preincubated with 10 nM rapamycin for 1 h and subsequently stimulated with EGF. Phosphorylation of p70S6K (T389), p70S6K (T421/S424), the corresponding phosphorylation sites of p85S6K, and S6 (S235/236) are shown.

4 Discussion

Breast cancer is the most frequent cancer in women and five molecular subtypes have been identified so far. The orphan receptor ERBB2 characterises a particular subtype which is associated with poor prognosis and short overall survival (Sorlie et al., 2001). To treat ERBB2-positive breast cancer, the humanised monoclonal antibody trastuzumab, targeting ERBB2, was clinically approved. However, only one third of the ERBB2-positive patients respond to trastuzumab (Baselga et al., 1996, Cobleigh et al., 1999, Vogel et al., 2002) and nearly all develop resistance within the first year of treatment (Esteva et al., 2002). Several molecular factors were discussed as possible cause for *de novo* therapy resistance. Constitutive activation of the PI3K pathway due to loss of PTEN or activating mutations in the catalytical domain of PI3K were associated with trastuzumab resistance (Berns et al., 2007, Gymnopoulos et al., 2007, Isakoff et al., 2005, Kataoka et al., 2009). Although many diseases like cancer are associated with alterations of particular proteins, little is known how these alterations impact cellular proteomes. Therefore, ERBB receptor mediated signal transduction was quantitatively assessed in breast cancer cell lines. In a systematic set of experiments, dynamic measurements were carried out in HCC1954 and SKBR3 cells, which exhibit ERBB2 overexpression. Additionally, MCF7 cells were chosen as cell line representative for low level ERBB2 expression. Proteome profiling of dynamic measurements was carried out using protein microarrays.

4.1 Advancement of protein microarray technology

Two approaches were employed for the analysis of signalling networks, microspot immunoassay (MIA) and reverse phase protein array (RPPA). MIA is a very sensitive tool for the quantitative analysis of protein phosphorylation. A major bottleneck for the development of new MIA assays is the identification of suitable antibody pairs. Performing assays on a long-term basis requires access

to reliable antibody resources. However, lot-specific changes were observed even for monoclonal antibodies which hampered the assay quality. An example was the pAKT (S473) specific capture antibody BD558368. This antibody showed the best results during the development of the assay and was therefore used for the analysis of biological samples. Nevertheless, a different pAKT specific antibody, 05-669, was spotted along with other capture antibodies and gave comparable results to BD558368. A new lot of this antibody caused poor results. The fit of the calibrator revealed very low signal intensities and almost no signal was detected in biological samples. Therefore, the measurements differed significantly from those obtained for 05-669. As testing further lots of BD558368 did not improve the assay outcome, this antibody was omitted and antibody 05-669 was used as capture antibody for the analysis of AKT signalling. Being aware of these challenges, data quality was assessed very carefully in all protein microarray experiments. Whenever possible, each newly established assay was based on two different capture antibodies detecting a certain phosphosite to reduce the risk of measurement artefacts.

The quality of nitrocellulose coated slides used for antibody immobilisation also presented an additional challenge. Initially, slides with 16 single pads were used. Robust measurements were possible as long as antibody pairs of high dynamic range were used. However, measurements of low abundant proteins, like pAKT and pSTAT3, resulted in low dynamic range measurements and exposed inconsistencies between different pads on the same slide so that a quantitative analysis was not possible. Further analysis revealed that inhomogeneous nitrocellulose coating of the slides resulted in immobilisation of differing amounts of capture antibodies this way causing a high variation of signals. The technical problem was solved by using slides with an overall nitrocellulose coating.

Antibody specificity is also the most important factor for RPPA analysis. Each project started with the Western blot validation of antibodies using a suitable set of samples. However, not all antibodies resulting in specific bands on Western blot performed well on RPPA and for this reason serial dilutions of control samples were spotted to assess the linear correlation between signal intensity and target protein concentration. The major difference between both techniques is that the Western blot is denaturating while the proteins on RPPAs are almost native. Therefore, an epitope might not be exposed properly in the native state. Good results were obtained with antibodies certified to work for immunoprecipitations by the supplier. In this case, the antibody has to bind the native protein

and is likely to work also on RPPA. For both protein microarray approaches, it was observed that phosphospecific antibodies showed a higher specificity than total-protein antibodies. In general, data from measurements with total-protein antibodies were highly variable and were therefore not applied for the normalisation of phosphoprotein signals. An additional observation was that certain total-protein antibodies, detecting STAT5, AKT, and ERBB2, preferably bound to the phosphorylated protein (data not shown).

Biological samples from cells incubated with antibody therapeutics revealed cross-reactivity with the secondary anti-rabbit antibody on RPPA although this cross-reactivity was not detected by Western blots. For this reason, only antibodies showing signal intensities clearly higher than those of the blank were considered as valid.

The microspot immunoassay was successfully established for the absolute quantification of three phosphoproteins: pAKT (S473), pAKT (T308), and pSTAT3 (S727). This new assay and the previously developed pERK1/2 assay were applied to generate quantitative data on ligand- and dose-dependent signalling in MCF7 cells. RPPAs were efficiently adapted to the requirements of high throughput analysis of signal transduction networks for more than 40 phosphoproteins. Using phosphospecific antibodies, RPPA enabled the reproducible generation of quantitative data and the analysis of more than 1,000 biological samples in parallel. The high sensitivity and the robust technology of this approach allowed the detection of small changes in the dynamic network of protein phosphorylation. To sum up, protein microarrays were established for the generation of large high quality data sets suitable for systems biology approaches.

ERBB receptor signalling in MCF7 cells was analysed quantitatively using the microspot immunoassay. Additionally, RPPAs were performed on the MCF7 samples to analyse additional phosphoproteins known to be involved in signalling downstream of ERBB receptors. In ERBB2 overexpressing cell lines, the influence of the ERBB receptors targeting therapeutics trastuzumab, pertuzumab, and erlotinib on ligand induced signalling was analysed using reverse phase protein arrays.

4.2 Statistical analysis of time-resolved data

The statistical analysis of time series experiments was a challenging task. The question of how to identify significant differences in the time-dependent expression or activation of markers under different conditions has to be solved. Tai and Speed (2009) discussed this problem for microarray data comprising several thousand genes and suggested to rank the features instead of testing for significance. This method is not applicable to the analysis of time-dependent changes in the phosphorylation status of proteins since here the number of different features is much lower, e.g. limited to 40 different antibodies. Moreover, the kinetics of protein phosphorylation differ immensely from that of gene expression due to rapid dephosphorylation events induced by feedback loops. In most cases, the effects of external stimuli on the phosphorylation status is visible only for a very limited timeframe whereas differences in gene expression tend to be evident for a larger time period. Here, a t-test for each time point was used, decoupling the multivariate problem into single test problems. However, analysing the significance of changes in the phosphorylation status of proteins over time remains a challenge. To further analyse the data, dynamic modelling approaches and signalling network reconstruction were performed (Bender et al., 2010).

4.3 Quantitative analysis of ERBB receptor signalling in breast cancer cell lines

The human breast cancer cell line MCF7 was used to analyse ERBB signalling without the dominant impact of an overexpressed receptor. Comparing the activation potential of the three ligands EGF, BTC, and HRG at a concentration of 1 nM revealed that HRG had the strongest impact on ERBB receptor signalling in MCF7 cells. It strongly induced receptor phosphorylation and a higher and more sustained activation of targets of the MAPK and the PI3K pathway, like ERK1/2 and AKT, compared to both other ligands (Fig. 3.19). Analysing the simultaneous stimulation with two different ligands revealed that HRG was the dominant ligand as the HRG-containing combinations resembled downstream signalling mediated by HRG alone (Fig. 3.18). In a systems biology approach, a similar observation was made for increasing EGF and HRG concentrations

in MCF7 cells (Birtwistle et al., 2007). HRG binds to ERBB3, which has a non-functional kinase domain and therefore depends on transphosphorylation by other receptors, mainly ERBB2. However, it has been reported that ERBB3 exhibits very weak kinase activity and can only weakly phosphorylate its dimerisation partner (Shi et al., 2010). On the other hand, the ERBB2/ERBB3 dimer, which is activated by HRG, is the dimer with the strongest oncogenic potential (Citri et al., 2003). RPPA data revealed that HRG induced not only phosphorylation of ERBB2 but also of EGFR in MCF7 cells. Riese et al. (1995) showed that HRG can indeed regulate EGFR signalling in the mouse pro-B-lymphocyte cell line Ba/F3 transfected with exogenous ERBB receptors. The same effect was reported for Tamoxifen resistant MCF7 (Hutcheson et al., 2007) and for melanoma cells (Ueno et al., 2008) and in ERBB2-positive pancreatic cells, only EGFR/ERBB3 dimers were formed upon EGF or HRG treatment (Frolov et al., 2007). The reports demonstrated that EGFR/ERBB3 dimers exist in cells which are not overexpressing ERBB2. However, other studies described that these dimers are relatively weak (Wehrman et al., 2006) and that their transphosphorylation activity is limited (Tzahar et al., 1996). A second mechanism of HRG-induced EGFR activation is the formation of secondary dimers, as reported to occur in PC12 cells by Gamett et al. (1997). After HRG-mediated activation, the transiently formed ERBB3/ERBB2 dimers dissociate and the phosphorylated ERBB2 monomers interact with unphosphorylated receptors to form secondary ERBB2/EGFR dimers. Additionally, an EGF-induced formation of ERBB2/ERBB3 dimers was observed in SKBR3 cells (Graus-Porta et al., 1997). To determine the influence of the single ERBB receptors on downstream kinase activation, ligand induced signalling was analysed after knockdown of the single receptors EGFR, ERBB2, ERBB3, and ERBB4 in MCF7 cells. The knockdown of ERBB2 and ERBB3 caused an equal reduction of HRG-induced MAPK and PI3K pathway activation, namely MEK1/2, ERK1/2, AKT, p70S6K (Fig. 3.23), and S6 (data not shown), confirming the co-dependency on both receptors. Signalling via EGFR was not able to compensate for the loss of ERBB2. Instead, knockdown of EGFR slightly enhanced HRG-mediated activation of the MAPK and PI3K pathways. In contrast, addition of gefitinib, an EGFR inhibitor, resulted in inhibition of EGFR, ERBB2, and ERBB3 phosphorylation and prevented downstream pathway activation. This has also been shown by Yang et al. (2006) and was interpreted as an essential role of EGFR in HRG signalling. However, the knockdown of EGFR did not

support a role of EGFR in HRG signalling since knockdown of EGFR did not reduce HRG-mediated pathway activation in MCF7 cells. The different effects obtained from gefitinib-mediated EGFR inhibition and siRNA-mediated EGFR knockdown could result from sequestration of ERBB receptors by formation of inactive dimers with the inhibited EGFR acting as a dominant negative receptor (Moulder et al., 2001). In the presence of EGFR, this receptor is involved in HRG-induced receptor dimerisation and signalling. If inhibited, EGFR still forms dimers as described before, but downstream signalling is not possible. However, the lack of EGFR steers the increased formation of ERBB2/ERBB3 dimers, which results in enhanced pathway activation. The knockdown of EGFR and ERBB2 had the strongest impact on EGF mediated signalling. AKT and STAT3 phosphorylation was reduced equally after knockdown of both receptors, whereas ERK1/2 activation was stronger influenced by EGFR than by ERBB2 knockdown (Fig. 3.23). In cell lines expressing several different ERBB receptors, EGF mainly induces EGFR/ERBB2 heterodimer formation (Lenferink et al., 1998), leading to the activation of both pathways, MAPK and PI3K. Knockdown of ERBB2 forced the formation of EGFR homodimers which mainly induced ERK1/2 activation. Additionally, homodimers produce weaker signals than heterodimers, they are less mitogenic and transforming (Kokai et al., 1989, Pinkas-Kramarski et al., 1996). In summary, AKT signalling in response to EGF is dependent on ERBB2 activation while EGFR homodimers are still able to induce ERK1/2 phosphorylation although to a lesser extent. It is well known, that ERBB2, as the preferred dimerisation partner of ERBB receptors, enhances and prolongs signalling. However, the dynamics of ligand induced protein phosphorylation in MCF7 cells did not change after the ERBB2 knockdown. It solely reduced the absolute amount of phosphorylated proteins. In conclusion, in MCF7 cells, ERBB2 indeed enhanced the amplitude of downstream signalling but did not prolong the pathway activation and the signal-amplifying role of ERBB2 was ligand-independent.

In SKBR3 cells, no ligand-dependent differences were observed with respect to the activation of ERK1/2, indicating a saturated response. HRG and the combination of EGF+HRG induced a stronger AKT phosphorylation compared to EGF alone, as seen also in MCF7 cells. In HCC1954 cells, EGF induced strong MAPK signalling in contrast to HRG. Both ligands did not induce AKT phosphorylation in HCC1954 cells but starvation resulted in an upregulation of baseline pAKT (Fig. 3.12). This has also been reported by Chakrabarty et al.

(2010) and was correlated with oncogenic PI3K mutations leading to increased HRG expression. Consequently, secretion of HRG resulted in an autocrine loop activating ERBB3 and subsequently AKT. Interestingly, the combination of both ligands in HCC1954 cells decreased the phosphorylation of ERK1/2 and p70S6K compared to stimulation with EGF alone. These observations can solely be explained by the expression pattern of ERBB receptors in the two cell lines. SKBR3 cells express high levels of EGFR and ERBB3 and therefore EGF- and HRG-induced signalling resulted in a strong ERK1/2 activation, probably reaching saturation as no additive effect was caused by the addition of both ligands in parallel. In contrast, HCC1954 cells barely expressed ERBB3 but instead high amounts of EGFR. Therefore, EGF was the predominant ligand in HCC1954 cells and simultaneous stimulation with EGF and HRG even resulted in a reduction of ERK1/2 activation compared to EGF alone, as HRG leads to the formation of ERBB3 containing dimers not contributing to the activation of the MAPK pathway. To sum up, the differential expression of the ERBB receptors resulted in different ligand-induced activation of the two major downstream pathways, MAPK and PI3K, in the three breast cancer cell lines.

4.4 Impact of targeted therapeutics on ERBB mediated signal transduction

Therapeutic antibodies exhibit high target specificity, whereas ATP-competitive small molecule inhibitors often possess off-site effects, as the ATP binding pockets of related kinases are very similar (Karaman et al., 2008). Therefore, it cannot be ruled out that the clinical benefit is indeed at least partly caused by unspecific effects (Jimeno and Hidalgo, 2006). Recently, Kriegs et al. (2010) postulated that the different effects of cetuximab, a chimeric monoclonal antibody against EGFR, and erlotinib, a small molecule drug inhibiting EGFR, on DNA repair might be due to the low specificity of the small molecule inhibitor erlotinib. The impact of three targeted therapeutics, trastuzumab, pertuzumab, and erlotinib on ligand induced signalling was analysed in two ERBB2 overexpressing cell lines, SKBR3 and HCC1954. The aim was to delineate whether a combinatorial use of the drugs would yield any evidence to suggest also a possible clinical beneficial which could then be addressed in clinical studies. HCC1954 cells are resistant to trastuzumab (O'Brien et al., 2010, Sahin et al., 2009), which was of-

ten correlated with activating mutations of the PI3K pathway. While HCC1954 as well as SKBR3 cells express *wt*-PTEN in a comparable amount (Fig. 3.13), the cell line HCC1954 harbours a H1047R mutation in the kinase domain of catalytical subunit p110α of PI3K. Additionally, very low levels of p27 were present and not upregulated upon trastuzumab treatment in HCC1954 cells, in contrast to the other ERBB2 overexpressing cell lines SKBR3 and BT474 (Fig. 3.14). In trastuzumab sensitive cells, treatment leads to an upregulation of p27 and a downregulation of cyclinD1 and therefore low p27 abundance has been associated with trastuzumab resistance (Nahta et al., 2004).

4.4.1 Protein phosphorylation upon drug treatment

Amino acid Y1248 is one of the major autophosphorylation sites of the ERBB2 receptor and was correlated with ERBB2 activation (Akiyama et al., 1991). After ligand binding, proliferation is induced by recruiting SHC, thus activating the MAPK pathway. Phosphorylation of ERBB2 at Y1248 has already been associated with poor clinical prognosis (Cicenas et al., 2006, Thor et al., 2000). However, a high phosphorylation of ERBB2 indicates a strong signalling activity and growth dependency of the tumour on this signalling pathway. Therefore, response rates to trastuzumab tend to be higher in patients with tumours exhibiting phosphorylated ERBB2 (Hudelist et al., 2003). Additionally, activation of EGFR in tumours enhances the significance of the predictive role of pERBB2 (Hudelist et al., 2006). This is in line with *in vitro* experiments as studies in a set of breast cancer cell lines revealed that not only overexpression of ERBB2 but also the phosphorylation status of the ERBB2 receptor is an important factor for trastuzumab sensitivity (Ginestier et al., 2007).

A controversy still exists if antibody drugs exhibit activating potential on the targeted receptor or not. Nagata et al. (2004) reported no change of ERBB2 phosphorylation within 1 h of trastuzumab treatment in BT474 and SKBR3 cells. Lane et al. (2000) reported that ERBB2 was rapidly dephosphorylated after addition of 4D5, the murine precursor of trastuzumab. In contrast, Sarup et al. (1991) showed that 4D5 acts as partial agonist and rapidly induced receptor phosphorylation in SKBR3 cells. Additionally, Scott et al. (1991) reported that PI3K was activated after addition of 4D5. Moreover, Diermeier et al. (2005) reported that treatment of SKBR3 cells with trastuzumab led to an increase in ERBB2 phosphorylation. However, despite the controversy on

ERBB2 activation, an inhibition of cell proliferation in SKBR3 cells was seen in all these studies. The reports of receptor phosphorylation and subsequent inhibition of cell proliferation are in line with the observed results that addition of both antibody agents trastuzumab and pertuzumab resulted in a strong increase of receptor phosphorylation in BT474, SKBR3, and HCC1954 cells, which was even stronger than after addition of a ligand. Despite the phosphorylation of ERBB2 at Y1248, the cell cycle regulator RB and the ribosomal protein S6 were dephosphorylated after treatment with trastuzumab or pertuzumab if the antibody therapeutics applied were in combination with erlotinib. A possible explanation for reduced cell cycle progression in the context of sustained receptor phosphorylation is supported by the report that sustained activation of ERBB2 can result in apoptosis instead of proliferation (Tikhomirov and Carpenter, 2004). In contrast, addition of EGF leads only to transient receptor phosphorylation, subsequent receptor internalisation and induction of proliferation. Therefore, the cellular response to receptor phosphorylation might be dependent on the strength and duration of receptor phosphorylation.

Although the main focus of this study was the analysis of the MAPK and PI3K signalling pathway activation downstream of ERBB receptors, further proteins were monitored as well. For example, the ERBB effectors SRC, PLCγ, and STAT5, which directly bind to the receptors via their SH2 domains (Rotin et al., 1992, Schulze et al., 2005) were strongly phosphorylated after exposure to therapeutic antibodies.

Phosphorylated PLCγ catalyses the hydrolysis of phosphatidylinositol-trisphosphate (PIP_3) to inositol triphosphates (IP_3). Sarup et al. (1991) reported increased levels of IP_3 5 min after addition of 4D5 to SKBR3 cells which is in line with the observed phosphorylation of PLCγ in response to both antibody drugs. Furthermore, a different monoclonal antibody against ERBB2 (ID5) activated PLCγ in SKBR3 cells but this activation had no impact on ID5 induced G1 arrest (Le et al., 2000). Therefore, the role of PLCγ in trastuzumab mediated cell cycle arrest remains unclear. Activation of PLCγ has been associated with migration, and phosphorylation of ERBB2 at Y1248 was proposed to initiate this signalling cascade (Dittmar et al., 2002). However, transient rather than sustained PLCγ activation attributed to migration.

SRC plays a role in development, progression, and metastasis of breast cancer (Biscardi et al., 2000, Di Cosimo and Baselga, 2008). In addition, it has

been described that metastasis of ERBB2 overexpressing cells is correlated with increased SRC activity *in vivo* and this was confirmed by cell invasion assays *in vitro* (Tan et al., 2005). However, it has also been reported that inhibition of SRC activation has no effect on ERBB2-mediated oncogenesis in transgenic mice, and that SRC expression rather than activation is important (Kaminski et al., 2006). Results observed for SRC phosphorylation in this study are in contrast to those reported by Nagata et al. (2004). In that case a dephosphorylation of SRC after trastuzumab treatment but also no increase of ERBB2 phosphorylation was observed. Therefore, the role of SRC in response targeted therapy remains to be elucidated.

STAT proteins are involved in cellular differentiation, proliferation, and survival and play a role in the differentiation of the breast epithelium (Liu et al., 1996). Nevalainen et al. (2004) reported that STAT5 phosphorylation is a marker of favourable prognosis in breast cancer. However, involvement of STAT5 in breast cancer progression is still unclear.

To sum up, a role of signalling proteins such as SRC, STAT5, and PLCγ in mediating the functionality of the drugs has to be addressed by further studies.

4.4.2 Impact of drug treatment on ligand-induced signalling

The two major pathways downstream of the ERBB receptor family are the MAPK and the PI3K pathway. Both contribute to cancer growth as described in detail in section 1.4. Regarding single drug treatments, results obtained in this thesis suggest that both antibody drugs had only minimal effects on ERK1/2 activation. This was observed for both cell lines, HCC1954 and SKBR3. Erlotinib, on the other hand, was able to inhibit the EGF mediated activation of all measured proteins. The AKT phosphorylation dynamics were very different in both cell lines. In HCC1954 cells, no inhibition of AKT was evident (Fig. 3.30). Preincubation with antibody therapeutics revealed no influence while erlotinib was able to downregulate, but not to inhibit, phosphorylation of AKT at position S473. AKT phosphorylation at T308 seemed to be unaffected in this cell line. PI3K mutations, as reported for HCC1954 cells, decouple the activation of AKT from the receptor level. Therefore, the inhibition of ERBB2 had no inhibitory potential towards the activation of AKT in this cell line. This is in line with the previously reported trastuzumab resistance of HCC1954 cells. However, erlotinib alone was able to reduce cell cycle progression in this cell line (Fig. 3.39).

In SKBR3 cells, all three drugs resulted in a downregulation of EGF mediated AKT activation but with different impact on the phosphorylation dynamics. For example, trastuzumab did not reduce the amount of phosphorylated protein formed at the activation peak after 12 min, but it was able to subsequently downregulate pAKT so that the steady state level was reached again after 20 min while the control showed a sustained AKT activation for at least 60 min. Furthermore, pertuzumab significantly reduced the activation of AKT and resulted in a downregulation of AKT phosphorylation after 20 min (Fig. 3.31). Thus, the data reflect previously reported mechanisms of both drugs. Pertuzumab is known to prevent dimerisation of ERBB2 with other receptors, for example the formation of EGFR/ERBB2 dimers in response to EGF stimulation. As ERBB2 is more potent in activating AKT than EGFR, lower AKT activation was due to a shift from EGFR/ERBB2 heterodimer to EGFR homodimer formation which was already shown in pertuzumab-treated SKBR3 cells (Hughes et al., 2009). Junttila et al. (2009) reported that trastuzumab was not able to prevent a ligand-induced dimerisation but instead disrupted ligand-independent dimers. The activation peak at 12 min after stimulation with EGF observed in the time-resolved data matched to the single time point analysed in the study performed by Junttila et al. (2009). After 12 min, no difference between trastuzumab and the uninhibited control was observed with respect to AKT phosphorylation, confirming that trastuzumab had no effect on the initial receptor heterodimer formation. Measuring the effects of the inhibitors in a time-resolved manner revealed the differences between both therapeutic antibodies. Although trastuzumab did not prevent the ligand-induced activation, it downregulated AKT phosphorylation probably by inducing a disruption of ERBB2 heterodimers and prevented a sustained activation. The effects of the inhibitors are illustrated in figure 4.1. The impact of inhibitors on S6 phosphorylation resembled the effects observed for the upstream proteins pAKT, pERK1/2, and p70S6K. While erlotinib was able to entirely inhibit S6 phosphorylation in both cell lines, both antibody drugs downregulated the phosphorylation of S6 in SKBR3 (Fig. 3.31), but not in HCC1954 cells (Fig. 3.30).

While both antibody drugs altered EGF-mediated AKT signalling, HRG-induced AKT activation was not influenced. On the contrary, trastuzumab pretreatment resulted in a slight upregulation of AKT activation. The fact, that trastuzumab had only a weak impact on fast signalling is in line with reports that it inhibits the interaction of EGFR and ERBB2 but not of ERBB2

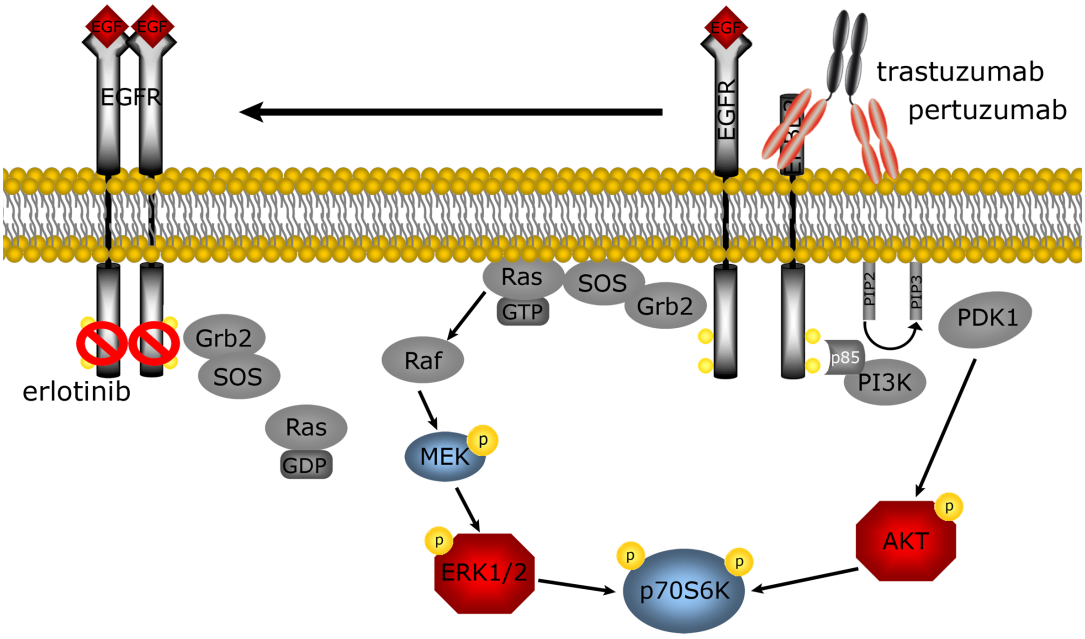

Figure 4.1: Impact of targeted therapeutics on EGF signalling
Schematic overview of inhibitory effects of trastuzumab, pertuzumab, and erlotinib on EGF induced signalling.

and ERBB3 (Wehrman et al., 2006). It was reported, that HRG is able to compensate the inhibitory effect of trastuzumab on cell proliferation (Diermeier et al., 2005). The main feature of pertuzumab, however, is to prevent ERBB2 receptor dimerisation with any other receptor. It has been reported several times, that pertuzumab is able to inhibit HRG-induced signalling in breast, prostate, (Agus et al., 2002), and colon carcinoma cells (Jackson et al., 2004). However, in this study, pertuzumab did not prevent HRG-induced ERBB2 dimerisation as it did not inhibit HRG mediated AKT signalling in SKBR3 cells (Fig. 3.32). In contrast to previous reports, Cai et al. (2008) demonstrated, that pertuzumab prevented a dimerisation of ERBB2 with EGFR, but that it only reduced the extent of HRG-induced ERBB2/ERBB3 dimer formation in SKBR3 cells. This is in line with the observation made in this thesis that pertuzumab decreased EGF- but not HRG induced AKT signalling. It was anticipated that simultaneous stimulation with EGF and HRG will additionally induce EGFR/ERBB3 heterodimers if ERBB2 is excluded from dimerisation after preincubation with pertuzumab or trastuzumab. The combination of both ligands resulted in a slightly stronger AKT phosphorylation compared to HRG alone and the impact of the inhibitors was even weaker. Both ligands when applied in combination

can induce activation of dimers involving EGFR, ERBB2, ERBB3 and thereby circumvent the inhibition of single receptors.

Franklin et al. (2004) have shown that pertuzumab binds to the dimerisation arm of ERBB2. However, this study was carried out with the extracellular domain of ERBB2 and not with the membrane-spanning full-length receptor. Although the extracellular domain is responsible for homodimerisation, other regions of the receptor, like the transmembrane domain or the intracellular domain, play a crucial role for the formation of heterodimers as reviewed by Lemmon (2009). For example, Duneau et al. (2007) showed that transmembrane domains of the ERBB receptors governed a hierarchy of receptor interactions which reflected the dimerisation preferences of the full length receptors in the cellular context. Certainly, dimers can form due to multiple mechanisms which influence the particular binding preferences of the individual receptors. ERBB3 does not form homodimers while ERBB2 only forms homodimers when it is overexpressed (Tzahar et al., 1996, Yarden and Sliwkowski, 2001). On the contrary, both receptors form the strongest heterodimers in response to ERBB3 stimulation (Ferguson et al., 2000), an effect mediated by other domains apart from the dimerisation loop. Domain IV plays a role in receptor heterodimerisation of ERBB2 with EGFR. Therefore, binding of trastuzumab to domain IV of ERBB2 leads to disruption of heterodimers. Hence, the binding of pertuzumab to the dimerisation domain of ERBB2 did not categorically prevent ligand-induced heterodimerisation, as suggested by the data generated in this study.

4.4.3 Effects of combinatorial drug treatment

Drug resistance can be due to an upregulation of non-targeted receptor tyrosine kinases, for example MET (Shattuck et al., 2008), VEGFR (Bianco et al., 2008), and IGFR (Lu et al., 2001, Nahta et al., 2005). Therefore, targeting more than a single receptor is a promising strategy. Several inhibitors are already clinically approved (lapatinib: targeting EGFR and ERBB2) or are in clinical studies (vandetanib: targeting EGFR, VEGFR, and RET (Alferez et al., 2008, Pennell and Lynch, 2009, Ryan and Wedge, 2005)). Another promising approach is the development of dual PI3K and mTOR inhibitors (Maira et al., 2008), since inhibition of mTOR results in upregulation of AKT signalling due to a feedback loop including p70S6K (Yang and Guan, 2007). Therefore, the dual inhibition of mTOR and PI3K was demonstrated to disable this feedback loop and induce

apoptosis *in vitro* (Brachmann et al., 2009) and inhibit tumour growth *in vivo* (Mallon et al., 2010).

In *in vivo* models and clinical trials, the combination of the two therapeutical antibodies trastuzumab and pertuzumab promised to be beneficial for trastuzumab resistant patients (Baselga et al., 2010, Scheuer et al., 2009). However, according to data on signalling dynamics in ERBB2 overexpressing breast cancer cell lines obtained in this thesis, this drug combination did not improve the efficiency of the single agents. The combination of trastuzumab and pertuzumab reduced the fast ligand-induced activation of ERK1/2 and S6 in both cell lines and also of AKT in SKBR3 cells (Fig. 3.33, 3.34). However, in a long-term experiment applying both antibody drugs in full growth medium, the combination of trastuzumab and pertuzumab seemed to be rather activating as it increased receptor phosphorylation and resulted in the activation of RB and S6 compared to the control. Furthermore, this combination significantly induced cell cycle progression in SKBR3 cells (Fig. 3.39). In cell culture experiments, no increased antibody-dependent cellular cytotoxicity (ADCC) was observed for the combination trastuzumab/pertuzumab (Scheuer et al., 2009). However, *in vitro* studies certainly miss the impact of the tumour microenvironment. Thus, the clinical benefit observed for the combination of trastuzumab and pertuzumab might therefore result from a combination of impact on signalling and ADCC which can only be approached *in vivo*. In contrast, the combination trastuzumab/erlotinib or pertuzumab/erlotinib showed a strong inhibition of signalling in both short and long term experiments. Cell cycle analysis revealed that the combination of trastuzumab and erlotinib significantly reduced cell cycle progression in both cell lines. With respect to the fact, that pertuzumab and also trastuzumab shift the dimer equilibrium from ERBB2 containing heterodimers towards formation of EGFR homodimers (Hughes et al., 2009), the addition of erlotinib to inhibit specifically EGFR signalling prevents the cell from taking an alternative route to activate downstream signalling (Fig. 4.1). This was shown for EGF as well as HRG induced AKT (S473) phosphorylation in SKBR3 cells (Fig. 3.35) which was significantly inhibited by pertuzumab and erlotinib applied in combination. As ADCC is important for the clinical outcome, combinatorial therapies combining a small molecule inhibitor and a monoclonal antibody might be superior compared to dual small molecule inhibitors, like lapatinib, targeting EGFR and ERBB2 in parallel. The combination of trastuzumab and erlotinib is already in clinical trials in phase II studies as

therapy of breast cancer (NCT00033514). Another study was closed before meeting its accrual goal due to the introduction of other combinatorial therapies, for example of trastuzumab with bevacizumab, a VEGFR specific antibody, or the dual specific inhibitor lapatinib (Britten et al., 2009). The combination of pertuzumab and erlotinib was superior when compared to monotherapy with either substance alone in human tumour xenografts of breast and lung cancer cells (Friess et al., 2005).

The results obtained in this study implied that HCC1954 cells were dependent on ERK1/2 signalling, but not on AKT signalling, and were therefore responsive to erlotinib treatment. Breast tumour are very heterogenous and in tumours with PI3K mutations or loss of PTEN, which are resistant to trastuzumab, the addition of erlotinib in combination with trastuzumab or pertuzumab might not be sufficient to inhibit tumour growth. In these tumours, combinations with PI3K/mTOR inhibitors might be more promising. However, the combination of trastuzumab and erlotinib revealed downregulation of signalling and of cell cycle progression in both cell lines, trastuzumab sensitive and resistant cells, and should therefore be addressed by further clinical studies.

4.5 Regulation of p70S6K activation in breast cancer cell lines

ERK1/2 and AKT are key intermediates upon EGF and HRG stimulation. However, the activation or inhibition of these two proteins can not always be correlated with the clinical outcome. Therefore, phosphoproteins further downstream integrating signals from different pathways were investigated to identify targets of clinical relevance. Klos et al. (2006) reported that breast cancer patients with increased p70S6K phosphorylation revealed worse disease-free survival and increased metastasis. Recently, it was shown that growth inhibition is more closely correlated with p70S6K than with AKT phosphorylation (Kataoka et al., 2009). Therefore, mechanisms for the activation of p70S6K signalling were analysed in more detail. In general, activation of p70S6K is a complex process. Phosphorylation of p70S6K at the dual site T421/S424, which is located in the autoinhibitory pseudosubstrate segment in the noncatalytic tail of p70S6K, is the first step of activation as it releases autoinhibition. Phosphorylation of

p70S6K at position T389 is the last step and leads to full kinase activity (Weng et al., 1998).

The four cell lines MCF7, HCC1954, SKBR3, and BT474 showed different effects regarding the regulation of p70S6K phosphorylation. Preincubation with different inhibitors targeting ERK1/2 and AKT signalling, revealed that indeed both pathways were involved in the phosphorylation of p70S6K at the two distinct phosphorylation sites. In MCF7 cells, the phosphorylation of p70S6K at position T389 was dependent on PI3K/mTOR signalling, while the p70S6K dual phosphorylation site T421/S424 was ERK1/2 dependent, as revealed by the specific inhibition with LY292004 (PI3K inhibitor) and PD98059 (MEK1 inhibitor), respectively (Fig. 3.21). This is in line with the reported crosstalk of the MAPK and the PI3K pathways merging in p70S6K activation. For example, Ahmed and Kundu (2010) recently reported that p70S6K is phosphorylated at T421/S424 via the MAPK pathway upon osteopontin stimulation in MCF7 cells, while the main phosphorylation site of p70S6K, T389, remained unaffected. Additionally, it has been reported that in neutrophils, p70S6K is phosphorylated at position T421/S424 via a MAPK dependent pathway while phosphorylation of p70S6K at T389 is rapamycin sensitive (Lehman et al., 2003). As shown here, the rapamycin sensitive phosphorylation site T389 was indeed not phosphorylated after rapamycin treatment of MCF7 cells. However, rapamycin also increased phosphorylation rate of AKT, ERK1/2, and p70S6K (T421/S424). This is in line with the observation that inhibition of mTORC1 by rapamycin can lead to PI3K pathway activation due to inhibition of a p70S6K dependent negative feedback loop (O'Reilly et al., 2006). Furthermore, activation of ERK1/2 signalling after addition of rapamycin has also been shown. For example, treatment of breast tumours with RAD001, a rapamycin analog, resulted in increased ERK1/2 phosphorylation so that a p70S6K dependent feedback loop activating ERK1/2 via a RAS dependent pathway was postulated (Carracedo et al., 2008). Furthermore, Kinkade et al. (2008) showed that a combinatorial inhibition of mTOR and MAPK pathways synergistically prevented prostate cancer cell growth, both, *in vitro* and *in vivo*.

In SKBR3 cells, p70S6K phosphorylation was not detected by RPPA. However, the downstream target S6 was strongly affected by AKT inhibition while ERK1/2 inhibition had only minor inhibitory effects. Inhibition of MEK1/2 delayed only the initial activation of S6 within the first 10-20 min and full S6 phosphorylation was reached after 30 min. Roux et al. (2007) reported that

both pathways can result in phosphorylation of S6 (S235/236) via p70S6K and p90RSK in HEK293E and HeLa cells. Furthermore, inhibition of the MAPK pathway resulted in a strong decrease of S6 phosphorylation during the first 10 min which corresponded to the activation peak of ERK1/2 and p90RSK. In conclusion, in SKBR3 cells, the MAPK pathway seemed to be involved in the initial S6 phosphorylation, however, the PI3K pathway is mandatory and sufficient for the sustained activation of S6. In BT474 cells, p70S6K phosphorylation was AKT dependent at T389 and MAPK dependent at T421/S424, as observed for MCF7 cells. S6 phosphorylation was significantly downregulated upon PI3K inhibition and ligand-induced activation was entirely prevented. In contrast, MEK1 inhibition had only a temporary impact on S6 phosphorylation as observed for SKBR3 cells.

In HCC1954 cell, RPPA data suggested that both phosphorylation sites of p70S6K were dependent on ERK1/2 activation, since MEK1 inhibition by PD98059 inhibited phosphorylation at both phosphorylation sites. In contrast, the PI3K inhibitor LY292004 was not able to inhibit p70S6K phosphorylation at all (Fig. 3.41). In contrast, the phosphorylation of S6 (S235/236) was equally dependent on AKT and ERK1/2 activation as both inhibitors, LY292004 and PD98059, inhibited the phosphorylation to a comparable extent. Preliminary results of an additional experiment applying rapamycin in HCC1954 cells showed that both phosphorylation sites of p70S6K were indeed rapamycin insensitive (Fig. 3.42). In contrast, the phosphorylation of ERK1/2 and p70S6K increased after preincubation with rapamycin. Western blot analysis revealed that the p85S6K isoform was predominantly activated in HCC1954 and that only phosphorylation of p70S6K but not p85S6K was inhibited by rapamycin treatment (Fig. 3.43). Thus, p85S6K phosphorylation was MAPK pathway dependent while p70S6K was PI3K pathway dependent. Although p85S6K was prominently activated in HCC1954 cells, S6 seemed to be phosphorylated by both isoforms, as inhibition of the both pathways resulted in a reduced of S6 phosphorylation. Except for the nuclear localisation, little is known about the function of p85S6K. S6 has been shown to reside and to be phosphorylated in the nucleus as well as in the cytoplasm (Franco and Rosenfeld, 1990). Additionally, it has been reported that p85S6K is required for S-phase entry (Reinhard et al., 1994). However, it was suggested that both S6K isoforms lie on the same pathway and that p85S6K parallels p70S6K regulation (Dennis et al., 1998, Ming et al., 1994). This is in contrast to the results obtained in this study, which

indicated a differential regulation of both S6K isoforms at least in HCC1954 cells.

Cells overexpressing ERBB2 or harbouring an oncogenic PI3K mutation like HCC1954 cells are selectively dependent on PI3K signalling (She et al., 2008). It has been reported that trastuzumab or lapatinib resistance are due to PI3K mutations and that resistance can be reversed by PI3K or mTOR inhibition (Berns et al., 2007, Eichhorn et al., 2008, Serra et al., 2008). Therefore, it was surprising that the p70S6K phosphorylation seemed to be ERK1/2 and not PI3K/mTOR dependent in HCC1954 cells while S6 phosphorylation was dependent on both pathways. However, the co-dependency on two survival pathways may present a benefit for cancer cells and insures that lethal interruption of one pathway can be overcome. The results on p70S6K regulation indicated that the crosstalk between these two major pathways to activate downstream targets differs between the cell lines. Apart from the data shown here, there is further evidence that the MAPK and the PI3K pathway converge on S6 phosphorylation and the inhibition of one pathway might not be sufficient. For example, Faber et al. (2009) reported that ERBB2 amplified breast cancer cell lines are sensitive to treatment with NVP-BEZ235, a dual PI3K/mTOR inhibitor. The ERBB2 amplified cell lines used were SKBR3 and BT474 cells. In contrast, EGFR mutant lung cancer cell lines additionally required MEK inhibition as they were dependent on both pathways. This is in line with the results, that both cell lines, SKBR3 and BT474, revealed AKT dependency for S6 phosphorylation. In insensitive cells, e.g. MDA-MB231 cells which harbour a KRAS mutation, co-treatment with a MEK inhibitor restored sensitivity (Brachmann et al., 2009). Meaningful clinical progress for drugs targeting only a single kinase or just one molecular pathway is limited to a few examples (van der Heijden and Bernards, 2010). The concept of synthetic lethality, where two pathways are targeted, might be a promising tool (Hartwell et al., 1997). This has already been shown for KRAS mutant lung cancer (Brachmann et al., 2009, Engelman et al., 2008). In the latter report, insensitivity was associated with residual S6 phosphorylation as a result of ERK1/2 pathway activation. Therefore, the ribosomal protein S6 seems to be an appropriate readout for the efficacy of targeted therapeutics.

A Appendix

A.1 ERBB signalling in MCF7 cells

A.1.1 Dose-dependent signalling

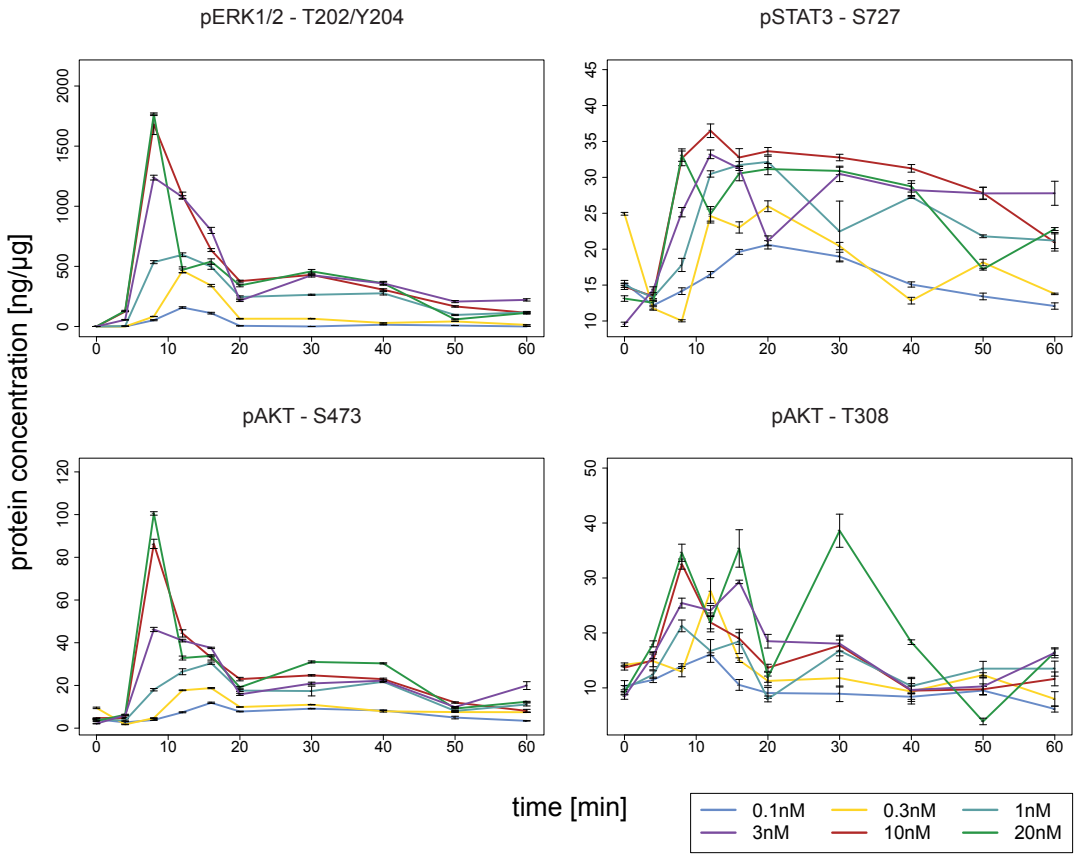

Figure A.1: Dose-dependent stimulation with EGF in MCF-7 cells. MCF7 cells were stimulated with EGF in concentrations ranging from 0.1 nM to 20 nM. Phosphorylation of ERK1/2, STAT3 (S727), AKT (S473), and AKT (T308) was quantified.

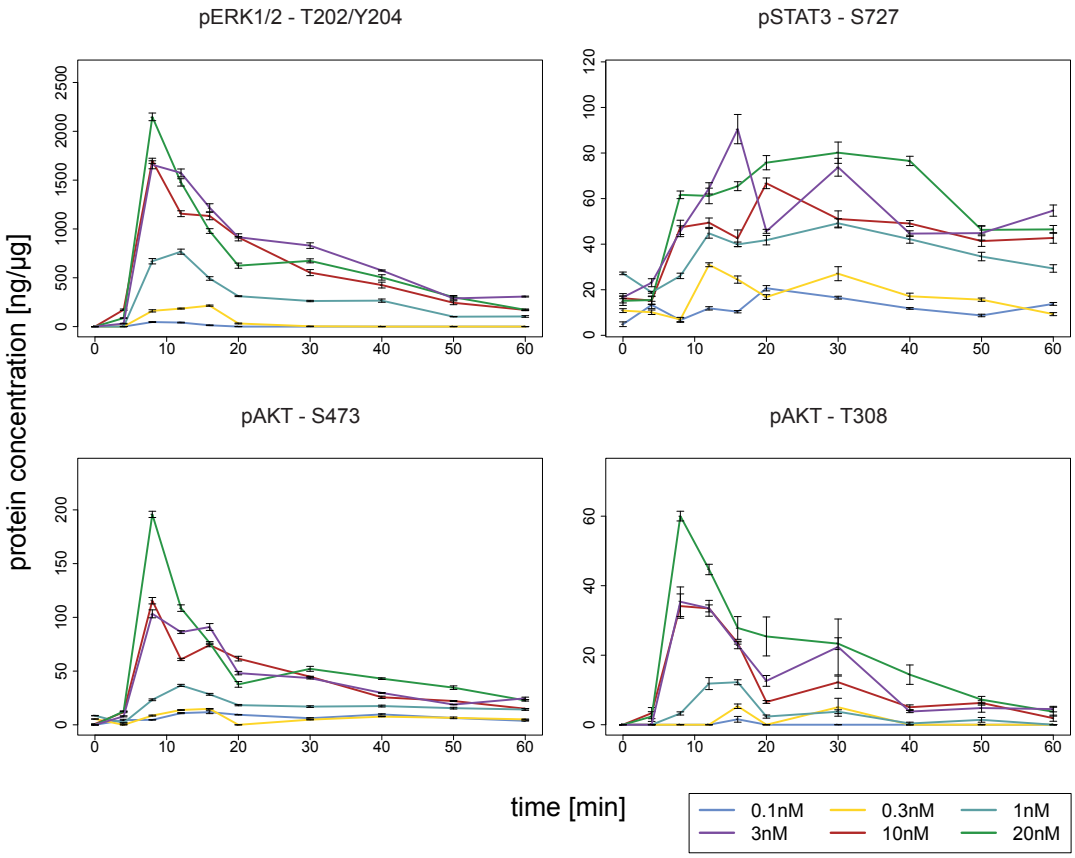

Figure A.2: Dose-dependent stimulation with BTC in MCF-7 cells
MCF7 cells were stimulated with BTC in concentrations ranging from 0.1 nM to 20 nM. Phosphorylation of ERK1/2, STAT3 (S727), AKT (S473), and AKT (T308) was quantified.

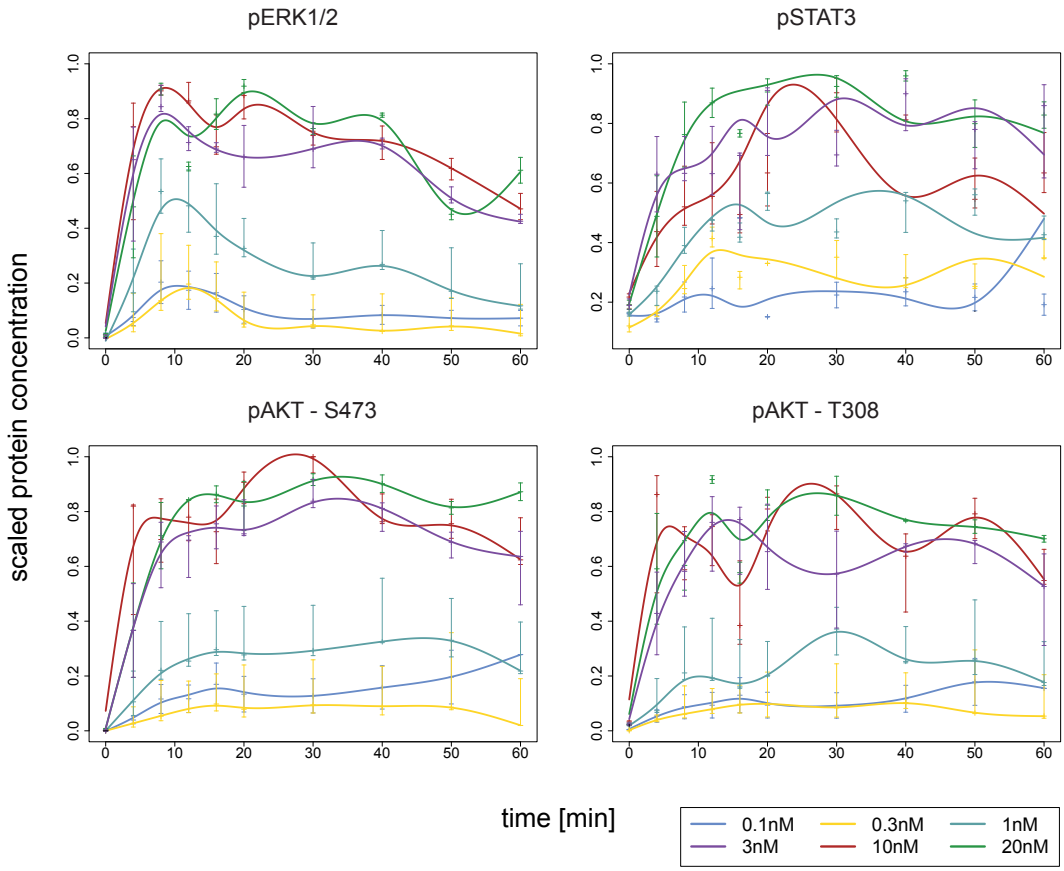

Figure A.3: Scaled data of dose-dependent stimulation of MCF7 cells with HRG

MCF7 cells were stimulated with HRG in a concentration ranging from 0.1 nM to 20 nM. Phosphorylation of ERK1/2, STAT3 (S727), AKT (S473), and AKT (T308) was quantified. The three biological replicates were scaled to the maximum value of each replicate. A cross marks the median of the replicates.

A.1.2 Impact of inhibitors on ligand-induced signalling

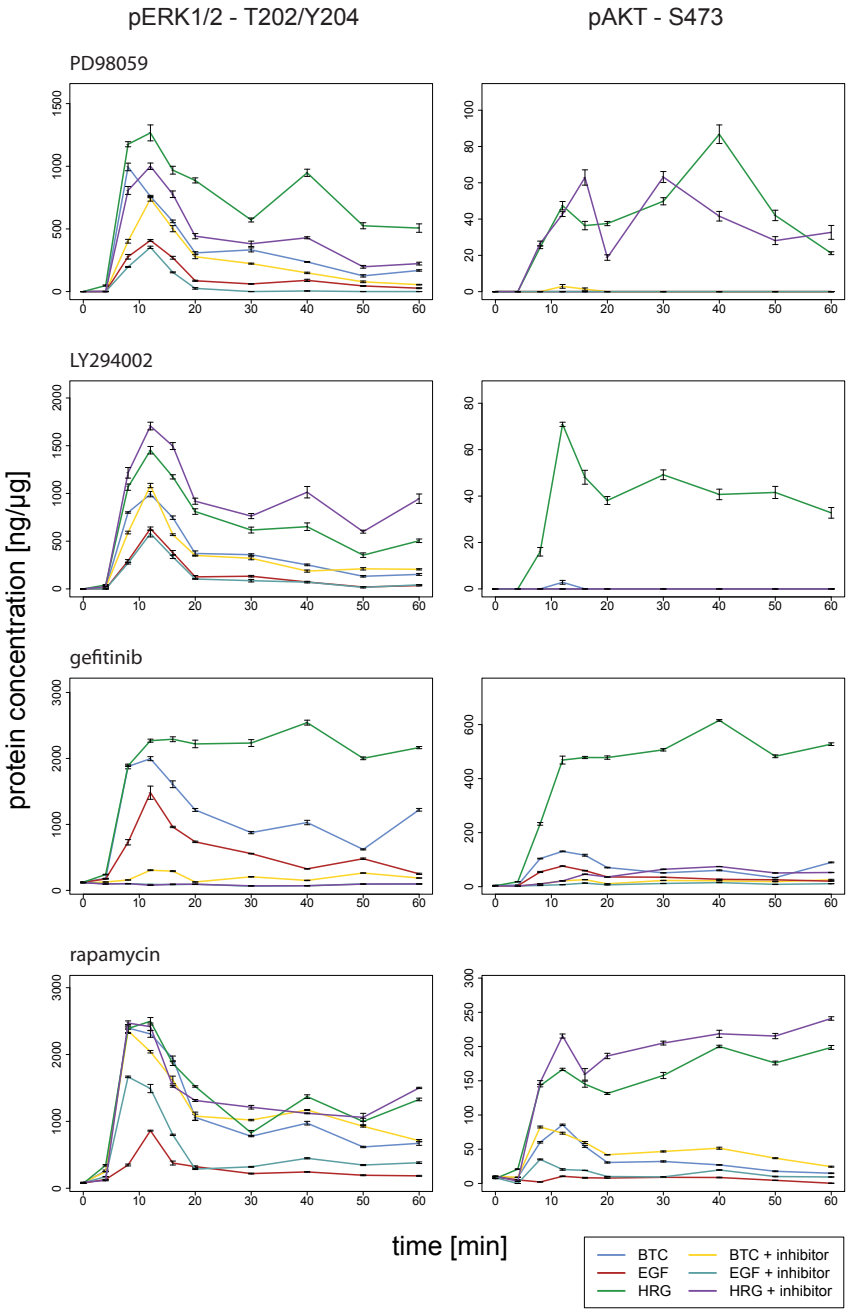

Figure A.4: Impact of inhibitors on ligand-mediated signalling in MCF7 cells

Cells were preincubated with the inhibitors PD98059, LY294002, gefitinib, or rapamycin for 1 h and subsequently stimulated with BTC, EGF, or HRG. The phosphorylation of ERK1/2 and AKT (S473) is shown.

A.1.3 Ligand-induced signalling after receptor knockdown

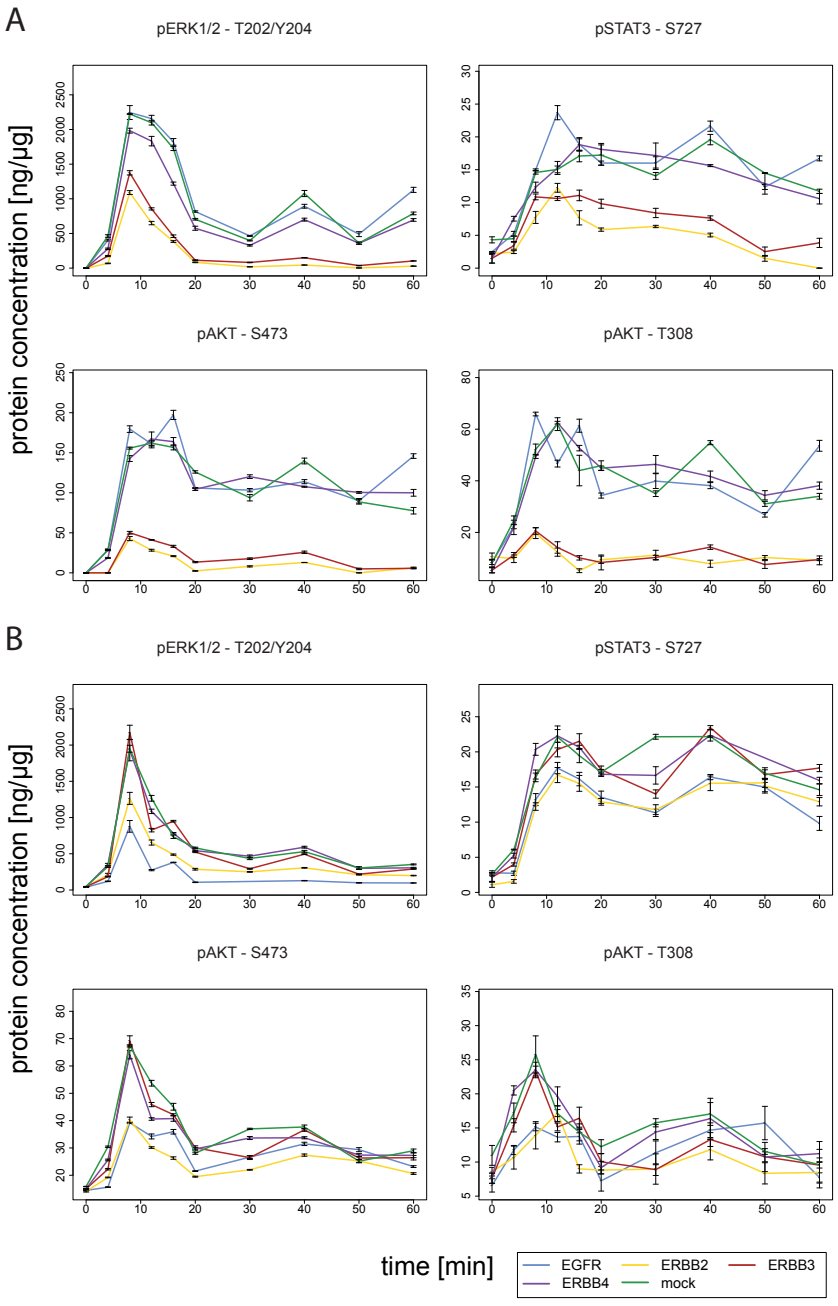

Figure A.5: Stimulation in MCF7 cells after siRNA-mediated knockdown of ERBB receptors

MCF7 cells were transfected with siRNA targeting the four ERBB receptors and subsequently stimulated with 1 nM HRG (A) or EGF (B). The diagrams show the phosphorylation of ERK1/2, STAT3, AKT (S73), and AKT (T308).

A.2 Effects of targeted therapeutics

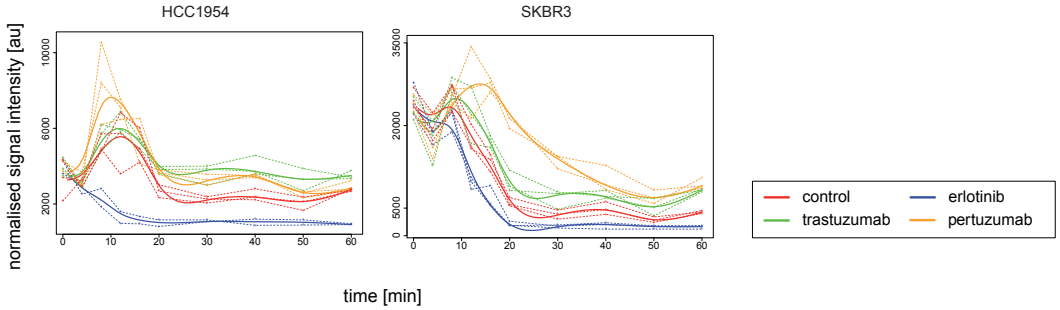

Figure A.6: Immediate ERK1/2 phosphorylation after drug treatment
HCC1954 and SKBR3 cells were incubated with the therapeutics for the indicated time points. The dashed lines represent the biological replicates while the thick lines show the fit of the smoothing splines.

A.2.1 Impact of therapeutics on HRG-induced signalling

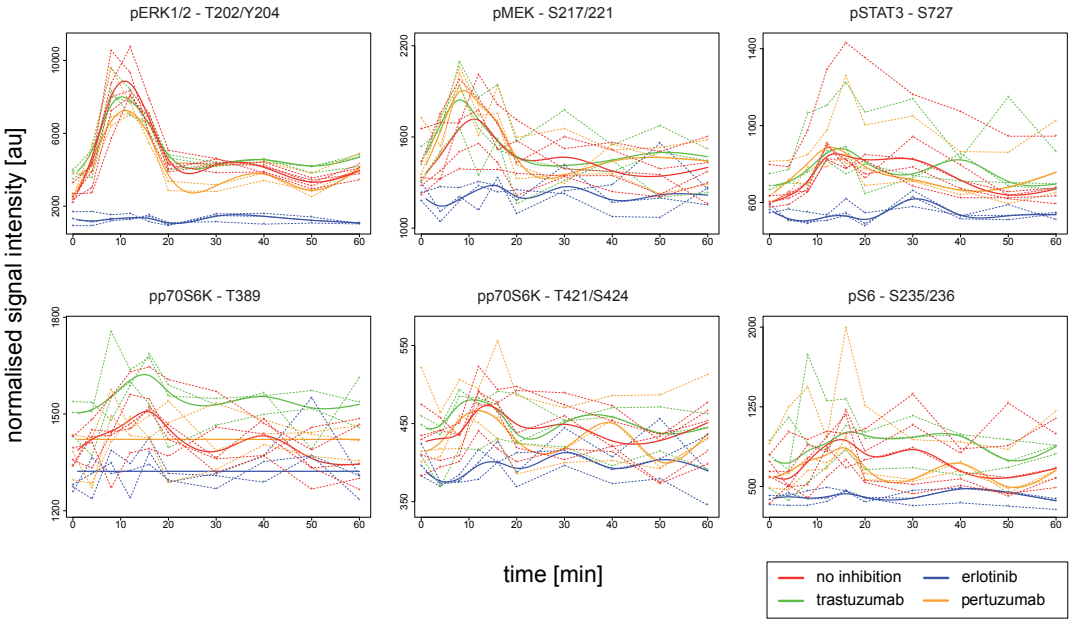

Figure A.7: Impact of targeted therapeutics on HRG-induced signalling in HCC1954 cells
HCC1954 cells were preincubated with the therapeutics and subsequently stimumation with HRG. The dashed lines represent the biological replicates while the thick lines show the fit of the smoothing splines.

Glossary

AKT (v-akt murine thymoma viral oncogene)
key modulator of PI3K-AKT-mTOR pathway, three isoforms,
phosphorylated by mTORC2 (S473) and PDK1 (T308)
regulates cell survival, insulin signalling, angiogenesis, tumour formation

eIF4B (eukaryotic translation initiation factor 4B)
required for the binding of mRNA to ribosomes

ERBB (erythroblastic leukemia viral oncogene) receptor family
family of receptor tyrosine kinases (EGF receptor family)
frequently deregulated in cancer

ERK1/2 (extracellular regulated kinase 1/2) (MAPK3/1)
key modulator of MAPK pathway, translocates to the nucleus,
regulates proliferation, differentiation, transcription and development

MEK1/2 (mitogen-activated protein kinase kinase 1/2)
dual specific protein kinase family, essential component of MAPK signal transduction pathway, phosphorylates ERK1/2

mTOR (mammalian target of rapamycin)
kinase subunit of mTORC1 and mTORC2,
regulates cell growth and survival in response to growth factors and nutrients, phosphorylates p70S6K at T389

p27 (cyclin-dependent kinase inhibitor p27)
binds to and prevents the activation of cyclin E-CDK2 or cyclin D-CDK4 complexes, controls cell cycle progression at G1,
regulated by phosphorylation and degradation

p70S6K (p70 S6 kinase)
phosphorylates ribosomal protein S6, isoform p85S6K

p90RSK (p90 S6 kinase)
directly activated by ERK1/2, downstream effector of MAPK pathway, phosphorylates numerous cytosolic and nuclear targets

PDK1 (3-phosphoinositide-dependent protein kinase-1)
phosphorylates and activates AKT, phosphorylates p70S6K at T229

PI3K (phosphoinositide 3-kinase)
lipid kinase consisting of regulatory p85 and catalytical p110 subunit, phosphorylates PIP_2

PLCγ (phospholipase C gamma)
catalyses hydrolysis of PIP_3 to IP_3, a second messenger molecule

PRAS40 (40 kDa proline-rich AKT substate)
inhibitory component of mTORC1, phosphorylation by AKT relieves inhibition

PTEN (phosphatase and tensin homolog)
dephosphorylates PIP3, negative regulator of PI3K pathway, tumour suppressor

RAF (v-raf murine sarcoma viral oncogene homolog)
plays role in regulating the MAPK/ERK signalling pathway

RAS (rat sarcoma viral oncogene homolog)
monomeric G-protein, GTPase activity, attached to the cell membrane, mutated in 20–30% of cancers

RB (retinoblastoma tumor suppressor protein)
hypophosphorylated form binds transcription factor E2F1 and leads to cell cycle arrest, phosphorylation by cyclinD1/CDK4/CDK6 and cyclinE/CDK2 inactivates RB and initiates S-phase entry

S6 (ribosomal protein S6)
component of the 40S ribosomal subunit, major substrate of kinases in ribosomes contributing to control of cell growth and proliferation

SOS (son of sevenless homolog)
guanine nucleotide exchange factor for RAS proteins

SRC (v-src sarcoma viral oncogene homolog)
non-receptor tyrosin kinase, interact with the intracellular domains of growth factor/cytokine receptors, GPCRs and integrins, key upstream mediators of both the PI3K and MAPK signalling pathways, play important role in cell proliferation, migration and survival

TSC2 (tuberous sclerosis 2)
negatively regulates mTORC1 signalling, implicated as tumour surpressor

Abbreviations

°C ..... degree celsius
µ ..... micro
7AAD ..... 7-amino-actinomycin D
ADCC ..... antibody-dependent cellular cytotoxicity
AMSA ..... antibody mediated signal amplification
ANOVA ..... analysis of variance
BD ..... Becton Dickinson
BSA ..... bovine serum albumine
BTC ..... betacellulin
CST ..... Cell Signaling Technology
DMEM ..... Dulbecco's modified eagle medium
DMSO ..... dimethylsulfoxid
DTT ..... 1,4-Bis(sulfanyl)butan-2,3-diol
DTT ..... dithiothreitol
EDTA ..... ethylendiamintetraacetat
EGF ..... epidermal growth factor
EGFR ..... EGF receptor
ELISA ..... enzyme-linked immunosorbent assay
ER ..... oestrogen receptor
FBS ..... fetal bovine serum
fig ..... figure
g ..... gramm; acceleration of gravity
GDP ..... guanosine diphosphate
GTP ..... guanosine triphosphate
h ..... hours

HRG	heregulin-β1
IGFR	insulin-like growth factor receptor
IP_3	inositol-1,4,5-triphosphates
IPTG	isopropyl β-D-1-thiogalactopyranoside
kDa	kilo Dalton
l	liter
LB	lysogeny broth
M	Mol, molar
m	milli
MET	met proto-oncogene (hepatocyte growth factor receptor)
MIA	microspot immunoassay
min	minute
miRNA	micro RNA
mRNA	messenger RNA
n	nano
NEAA	non essential amino acids
NP-40	nonident P-40
OD	optical density
PBS	phosphate buffered saline
PCR	polymerase chain reaction
PIP_2	Phosphatidylinositol-4,5-bisphosphate
PIP_3	phosphatidylinositol-3,4,5-trisphosphate
PMSF	phenylmethanesulfonylfluoride
qRT-PCR	quantitative realtime PCR
RET	ret proto-oncogene
RNA	ribonucleic acid
RPMI 1640	Roswell Park Memorial Institute 1640
RPPA	reverse phase protein array
RT	room temperature
RTK	receptor tyrosin kinase
SDS	sodium sodecylsulfatae

sec	second
SERM	selective estrogen receptor modulator
SH2	SRC-homology 2
siRNA	small interfering RNA
TBS	tris buffered saline
TBST	tris buffered saline with 0.1% Tween®20
U	unit
v/v	volume per volume
VEGFR	vascular endothelial growth factor
w/v	weight per volume
wt	wild-type

References

Adams, C. W., Allison, D. E., Flagella, K., Presta, L., Clarke, J., Dybdal, N., McKeever, K., and Sliwkowski, M. X. (2006). Humanization of a recombinant monoclonal antibody to produce a therapeutic HER dimerization inhibitor, pertuzumab. *Cancer Immunol Immunother*, 55(6):717–27.

Agus, D. B., Akita, R. W., Fox, W. D., Lewis, G. D., Higgins, B., Pisacane, P. I., Lofgren, J. A., Tindell, C., Evans, D. P., Maiese, K., Scher, H. I., and Sliwkowski, M. X. (2002). Targeting ligand-activated ErbB2 signaling inhibits breast and prostate tumor growth. *Cancer Cell*, 2(2):127–37.

Ahmed, M. and Kundu, G. C. (2010). Osteopontin selectively regulates p70S6K/mTOR phosphorylation leading to NF-kappaB dependent AP-1-mediated ICAM-1 expression in breast cancer cells. *Mol Cancer*, 9:101.

Akiyama, T., Matsuda, S., Namba, Y., Saito, T., Toyoshima, K., and Yamamoto, T. (1991). The transforming potential of the c-erbB-2 protein is regulated by its autophosphorylation at the carboxyl-terminal domain. *Mol Cell Biol*, 11(2):833–42.

Alferez, D., Wilkinson, R. W., Watkins, J., Poulsom, R., Mandir, N., Wedge, S. R., Pyrah, I. T., Smith, N. R., Jackson, L., Ryan, A. J., and Goodlad, R. A. (2008). Dual inhibition of VEGFR and EGFR signaling reduces the incidence and size of intestinal adenomas in Apc(Min/+) mice. *Mol Cancer Ther*, 7(3):590–8.

Alley, S. C., Okeley, N. M., and Senter, P. D. (2010). Antibody-drug conjugates: targeted drug delivery for cancer. *Curr Opin Chem Biol*.

Arap, W., Haedicke, W., Bernasconi, M., Kain, R., Rajotte, D., Krajewski, S., Ellerby, H. M., Bredesen, D. E., Pasqualini, R., and Ruoslahti, E. (2002). Targeting the prostate for destruction through a vascular address. *Proc Natl Acad Sci U S A*, 99(3):1527–31.

Austin, C. D., De Maziere, A. M., Pisacane, P. I., van Dijk, S. M., Eigenbrot, C., Sliwkowski, M. X., Klumperman, J., and Scheller, R. H. (2004). Endocytosis and sorting of ErbB2 and the site of action of cancer therapeutics trastuzumab and geldanamycin. *Mol Biol Cell*, 15(12):5268–82.

Bader, A. G., Kang, S., and Vogt, P. K. (2006). Cancer-specific mutations in PIK3CA are oncogenic in vivo. *Proc Natl Acad Sci U S A*, 103(5):1475–9.

Barlund, M., Forozan, F., Kononen, J., Bubendorf, L., Chen, Y., Bittner, M. L., Torhorst, J., Haas, P., Bucher, C., Sauter, G., Kallioniemi, O. P., and Kallioniemi, A. (2000). Detecting activation of ribosomal protein S6 kinase by complementary DNA and tissue microarray analysis. *J Natl Cancer Inst*, 92(15):1252–9.

Baselga, J., Gelmon, K. A., Verma, S., Wardley, A., Conte, P., Miles, D., Bianchi, G., Cortes, J., McNally, V. A., Ross, G. A., Fumoleau, P., and Gianni, L. (2010). Phase II trial of pertuzumab and trastuzumab in patients with human epidermal growth factor receptor 2-positive metastatic breast cancer that progressed during prior trastuzumab therapy. *J Clin Oncol*, 28(7):1138–44.

Baselga, J. and Swain, S. M. (2009). Novel anticancer targets: revisiting ERBB2 and discovering ERBB3. *Nat Rev Cancer*, 9(7):463–75.

Baselga, J., Tripathy, D., Mendelsohn, J., Baughman, S., Benz, C. C., Dantis, L., Sklarin, N. T., Seidman, A. D., Hudis, C. A., Moore, J., Rosen, P. P., Twaddell, T., Henderson, I. C., and Norton, L. (1996). Phase II study of weekly intravenous recombinant humanized anti-p185HER2 monoclonal antibody in patients with HER2/neu-overexpressing metastatic breast cancer. *J Clin Oncol*, 14(3):737–44.

Bender, C., Henjes, F., Fröhlich, H., Wiemann, S., Korf, U., and Beißbarth, T. (2010). Dynamic deterministic effects propagation networks: learning signalling pathways from longitudinal protein array data. *Bioinformatics*, 26(18):i596–i602.

Berns, K., Horlings, H. M., Hennessy, B. T., Madiredjo, M., Hijmans, E. M., Beelen, K., Linn, S. C., Gonzalez-Angulo, A. M., Stemke-Hale, K., Hauptmann, M., Beijersbergen, R. L., Mills, G. B., van de Vijver, M. J., and Bernards, R. (2007). A functional genetic approach identifies the PI3K pathway as a major determinant of trastuzumab resistance in breast cancer. *Cancer Cell*, 12(4):395–402.

Bianco, R., Rosa, R., Damiano, V., Daniele, G., Gelardi, T., Garofalo, S., Tarallo, V., De Falco, S., Melisi, D., Benelli, R., Albini, A., Ryan, A., Ciardiello, F., and Tortora, G. (2008). Vascular endothelial growth factor receptor-1 contributes to resistance to anti-epidermal growth factor receptor drugs in human cancer cells. *Clin Cancer Res*, 14(16):5069–80.

Biczok, R., Ruschhaupt, M., and Zhang, J. D. (2010). *ddCt: The ddCt Algorithm for the Analysis of Quantitative Real-Time PCR (qRT-PCR)*. R package version 1.2.0.

Birtwistle, M. R., Hatakeyama, M., Yumoto, N., Ogunnaike, B. A., Hoek, J. B., and Kholodenko, B. N. (2007). Ligand-dependent responses of the ErbB signaling network: experimental and modeling analyses. *Mol Syst Biol*, 3:144.

Biscardi, J. S., Ishizawar, R. C., Silva, C. M., and Parsons, S. J. (2000). Tyrosine kinase signalling in breast cancer: epidermal growth factor receptor and c-Src interactions in breast cancer. *Breast Cancer Res*, 2(3):203–10.

Black, R. A., Rauch, C. T., Kozlosky, C. J., Peschon, J. J., Slack, J. L., Wolfson, M. F., Castner, B. J., Stocking, K. L., Reddy, P., Srinivasan, S., Nelson, N., Boiani, N., Schooley, K. A., Gerhart, M., Davis, R., Fitzner, J. N., Johnson, R. S., Paxton, R. J., March, C. J., and Cerretti, D. P. (1997). A metalloproteinase disintegrin that releases tumour-necrosis factor-alpha from cells. *Nature*, 385(6618):729–33.

Blume-Jensen, P. and Hunter, T. (2001). Oncogenic kinase signalling. *Nature*, 411(6835):355–65.

Brachmann, S. M., Hofmann, I., Schnell, C., Fritsch, C., Wee, S., Lane, H., Wang, S., Garcia-Echeverria, C., and Maira, S. M. (2009). Specific apoptosis induction by the dual PI3K/mTor inhibitor NVP-BEZ235 in HER2 amplified and PIK3CA mutant breast cancer cells. *Proc Natl Acad Sci U S A*, 106(52):22299–304.

Brase, J. C., Mannsperger, H., Frohlich, H., Gade, S., Schmidt, C., Wiemann, S., Beissbarth, T., Schlomm, T., Sultmann, H., and Korf, U. (2010). Increasing the sensitivity of reverse phase protein arrays by antibody-mediated signal amplification. *Proteome Sci*, 8(1):36.

Britten, C. D., Finn, R. S., Bosserman, L. D., Wong, S. G., Press, M. F., Malik, M., Lum, B. L., and Slamon, D. J. (2009). A phase I/II trial of trastuzumab plus erlotinib in metastatic HER2-positive breast cancer: a dual ErbB targeted approach. *Clin Breast Cancer*, 9(1):16–22.

Cai, Z., Zhang, G., Zhou, Z., Bembas, K., Drebin, J. A., Greene, M. I., and Zhang, H. (2008). Differential binding patterns of monoclonal antibody 2C4 to the ErbB3-p185her2/neu and the EGFR-p185her2/neu complexes. *Oncogene*, 27(27):3870–4.

Carracedo, A., Baselga, J., and Pandolfi, P. P. (2008). Deconstructing feedback-signaling networks to improve anticancer therapy with mTORC1 inhibitors. *Cell Cycle*, 7(24):3805–9.

Chakrabarty, A., Rexer, B. N., Wang, S. E., Cook, R. S., Engelman, J. A., and Arteaga, C. L. (2010). H1047R phosphatidylinositol 3-kinase mutant enhances HER2-mediated transformation by heregulin production and activation of HER3. *Oncogene*.

Chambers, J. M. (1991). *Statistical Models in S*. CRC Press, Inc., Boca Raton, FL, USA.

Cho, H. S., Mason, K., Ramyar, K. X., Stanley, A. M., Gabelli, S. B., Denney, D. W., J., and Leahy, D. J. (2003). Structure of the extracellular region of HER2 alone and in complex with the Herceptin Fab. *Nature*, 421(6924):756–60.

Christianson, T. A., Doherty, J. K., Lin, Y. J., Ramsey, E. E., Holmes, R., Keenan, E. J., and Clinton, G. M. (1998). NH2-terminally truncated HER-2/neu protein: relationship with shedding of the extracellular domain and with prognostic factors in breast cancer. *Cancer Res*, 58(22):5123–9.

Cicenas, J., Urban, P., Kung, W., Vuaroqueaux, V., Labuhn, M., Wight, E., Eppenberger, U., and Eppenberger-Castori, S. (2006). Phosphorylation of tyrosine 1248-ERBB2 measured by chemiluminescence-linked immunoassay is an independent predictor of poor prognosis in primary breast cancer patients. *Eur J Cancer*, 42(5):636–45.

Citri, A., Skaria, K. B., and Yarden, Y. (2003). The deaf and the dumb: the biology of ErbB-2 and ErbB-3. *Exp Cell Res*, 284(1):54–65.

Citri, A. and Yarden, Y. (2006). EGF-ERBB signalling: towards the systems level. *Nat Rev Mol Cell Biol*, 7(7):505–16.

Clynes, R. A., Towers, T. L., Presta, L. G., and Ravetch, J. V. (2000). Inhibitory Fc receptors modulate in vivo cytoxicity against tumor targets. *Nat Med*, 6(4):443–6.

Cobleigh, M. A., Vogel, C. L., Tripathy, D., Robert, N. J., Scholl, S., Fehrenbacher, L., Wolter, J. M., Paton, V., Shak, S., Lieberman, G., and Slamon, D. J. (1999). Multinational study of the efficacy and safety of humanized anti-HER2 monoclonal antibody in women who have HER2-overexpressing metastatic breast cancer that has progressed after chemotherapy for metastatic disease. *J Clin Oncol*, 17(9):2639–48.

Cooley, S., Burns, L. J., Repka, T., and Miller, J. S. (1999). Natural killer cell cytotoxicity of breast cancer targets is enhanced by two distinct mechanisms of antibody-dependent cellular cytotoxicity against LFA-3 and HER2/neu. *Exp Hematol*, 27(10):1533–41.

Couch, F. J., Wang, X. Y., Wu, G. J., Qian, J., Jenkins, R. B., and James, C. D. (1999). Localization of PS6K to chromosomal region 17q23 and determination of its amplification in breast cancer. *Cancer Res*, 59(7):1408–11.

Dennis, P. B., Pullen, N., Pearson, R. B., Kozma, S. C., and Thomas, G. (1998). Phosphorylation sites in the autoinhibitory domain participate in p70(s6k) activation loop phosphorylation. *J Biol Chem*, 273(24):14845–52.

Dent, R., Trudeau, M., Pritchard, K. I., Hanna, W. M., Kahn, H. K., Sawka, C. A., Lickley, L. A., Rawlinson, E., Sun, P., and Narod, S. A. (2007). Triple-negative breast cancer: clinical features and patterns of recurrence. *Clin Cancer Res*, 13(15 Pt 1):4429–34.

Depowski, P. L., Rosenthal, S. I., and Ross, J. S. (2001). Loss of expression of the PTEN gene protein product is associated with poor outcome in breast cancer. *Mod Pathol*, 14(7):672–6.

Dhillon, A. S., Hagan, S., Rath, O., and Kolch, W. (2007). MAP kinase signalling pathways in cancer. *Oncogene*, 26(22):3279–90.

Di Cosimo, S. and Baselga, J. (2008). Targeted therapies in breast cancer: where are we now? *Eur J Cancer*, 44(18):2781–90.

Dickler, M. N., Cobleigh, M. A., Miller, K. D., Klein, P. M., and Winer, E. P. (2009). Efficacy and safety of erlotinib in patients with locally advanced or metastatic breast cancer. *Breast Cancer Res Treat*, 115(1):115–21.

Diermeier, S., Horvath, G., Knuechel-Clarke, R., Hofstaedter, F., Szollosi, J., and Brockhoff, G. (2005). Epidermal growth factor receptor coexpression modulates susceptibility to Herceptin in HER2/neu overexpressing breast cancer cells via specific erbB-receptor interaction and activation. *Exp Cell Res*, 304(2):604–19.

Dittmar, T., Husemann, A., Schewe, Y., Nofer, J. R., Niggemann, B., Zanker, K. S., and Brandt, B. H. (2002). Induction of cancer cell migration by epidermal growth factor is initiated by specific phosphorylation of tyrosine 1248 of c-erbB-2 receptor via EGFR. *FASEB J*, 16(13):1823–5.

Duneau, J. P., Vegh, A. P., and Sturgis, J. N. (2007). A dimerization hierarchy in the transmembrane domains of the HER receptor family. *Biochemistry*, 46(7):2010–9.

Eckstein, N., Servan, K., Girard, L., Cai, D., von Jonquieres, G., Jaehde, U., Kassack, M. U., Gazdar, A. F., Minna, J. D., and Royer, H. D. (2008). Epidermal growth factor receptor pathway analysis identifies amphiregulin as a key factor for cisplatin resistance of human breast cancer cells. *J Biol Chem*, 283(2):739–50.

Eichhorn, P. J., Gili, M., Scaltriti, M., Serra, V., Guzman, M., Nijkamp, W., Beijersbergen, R. L., Valero, V., Seoane, J., Bernards, R., and Baselga, J. (2008). Phosphatidylinositol 3-kinase hyperactivation results in lapatinib resistance that is reversed by the mTOR/phosphatidylinositol 3-kinase inhibitor NVP-BEZ235. *Cancer Res*, 68(22):9221–30.

Engelman, J. A., Chen, L., Tan, X., Crosby, K., Guimaraes, A. R., Upadhyay, R., Maira, M., McNamara, K., Perera, S. A., Song, Y., Chirieac, L. R., Kaur, R., Lightbown, A., Simendinger, J., Li, T., Padera, R. F., Garcia-Echeverria, C., Weissleder, R., Mahmood, U., Cantley, L. C., and Wong, K. K. (2008). Effective use of PI3K and MEK inhibitors to treat mutant Kras G12D and PIK3CA H1047R murine lung cancers. *Nat Med*, 14(12):1351–6.

Engelman, J. A., Zejnullahu, K., Mitsudomi, T., Song, Y., Hyland, C., Park, J. O., Lindeman, N., Gale, C. M., Zhao, X., Christensen, J., Kosaka, T., Holmes, A. J., Rogers, A. M., Cappuzzo, F., Mok, T., Lee, C., Johnson, B. E., Cantley, L. C., and Janne, P. A. (2007). MET amplification leads to gefitinib resistance in lung cancer by activating ERBB3 signaling. *Science*, 316(5827):1039–43.

Esteva, F. J., Valero, V., Booser, D., Guerra, L. T., Murray, J. L., Pusztai, L., Cristofanilli, M., Arun, B., Esmaeli, B., Fritsche, H. A., Sneige, N., Smith, T. L., and Hortobagyi, G. N. (2002). Phase II study of weekly docetaxel and trastuzumab for patients with HER-2-overexpressing metastatic breast cancer. *J Clin Oncol*, 20(7):1800–8.

Faber, A. C., Li, D., Song, Y., Liang, M. C., Yeap, B. Y., Bronson, R. T., Lifshits, E., Chen, Z., Maira, S. M., Garcia-Echeverria, C., Wong, K. K., and Engelman, J. A. (2009). Differential induction of apoptosis in HER2 and EGFR addicted cancers following PI3K inhibition. *Proc Natl Acad Sci U S A*, 106(46):19503–8.

Ferguson, K. M., Berger, M. B., Mendrola, J. M., Cho, H. S., Leahy, D. J., and Lemmon, M. A. (2003). EGF activates its receptor by removing interactions that autoinhibit ectodomain dimerization. *Mol Cell*, 11(2):507–17.

Ferguson, K. M., Darling, P. J., Mohan, M. J., Macatee, T. L., and Lemmon, M. A. (2000). Extracellular domains drive homo- but not hetero-dimerization of erbB receptors. *EMBO J*, 19(17):4632–43.

Franco, R. and Rosenfeld, M. G. (1990). Hormonally inducible phosphorylation of a nuclear pool of ribosomal protein S6. *J Biol Chem*, 265(8):4321–5.

Franklin, M. C., Carey, K. D., Vajdos, F. F., Leahy, D. J., de Vos, A. M., and Sliwkowski, M. X. (2004). Insights into ErbB signaling from the structure of the ErbB2-pertuzumab complex. *Cancer Cell*, 5(4):317–28.

Friess, T., Scheuer, W., and Hasmann, M. (2005). Combination treatment with erlotinib and pertuzumab against human tumor xenografts is superior to monotherapy. *Clin Cancer Res*, 11(14):5300–9.

Frolov, A., Schuller, K., Tzeng, C. W., Cannon, E. E., Ku, B. C., Howard, J. H., Vickers, S. M., Heslin, M. J., Buchsbaum, D. J., and Arnoletti, J. P. (2007). ErbB3 expression and dimerization with EGFR influence pancreatic cancer cell sensitivity to erlotinib. *Cancer Biol Ther*, 6(4):548–54.

Futreal, P. A., Coin, L., Marshall, M., Down, T., Hubbard, T., Wooster, R., Rahman, N., and Stratton, M. R. (2004). A census of human cancer genes. *Nat Rev Cancer*, 4(3):177–83.

Gamett, D. C., Pearson, G., Cerione, R. A., and Friedberg, I. (1997). Secondary dimerization between members of the epidermal growth factor receptor family. *J Biol Chem*, 272(18):12052–6.

Garrett, T. P., McKern, N. M., Lou, M., Elleman, T. C., Adams, T. E., Lovrecz, G. O., Kofler, M., Jorissen, R. N., Nice, E. C., Burgess, A. W., and Ward, C. W. (2003). The crystal structure of a truncated ErbB2 ectodomain reveals an active conformation, poised to interact with other ErbB receptors. *Mol Cell*, 11(2):495–505.

Garrett, T. P., McKern, N. M., Lou, M., Elleman, T. C., Adams, T. E., Lovrecz, G. O., Zhu, H. J., Walker, F., Frenkel, M. J., Hoyne, P. A., Jorissen, R. N., Nice, E. C., Burgess, A. W., and Ward, C. W. (2002). Crystal structure of a truncated epidermal growth factor receptor extracellular domain bound to transforming growth factor alpha. *Cell*, 110(6):763–73.

Ginestier, C., Adelaide, J., Goncalves, A., Repellini, L., Sircoulomb, F., Letessier, A., Finetti, P., Geneix, J., Charafe-Jauffret, E., Bertucci, F., Jacquemier, J., Viens, P., and Birnbaum, D. (2007). ERBB2 phosphorylation and trastuzumab sensitivity of breast cancer cell lines. *Oncogene*, 26(50):7163–9.

Graus-Porta, D., Beerli, R. R., Daly, J. M., and Hynes, N. E. (1997). ErbB-2, the preferred heterodimerization partner of all ErbB receptors, is a mediator of lateral signaling. *EMBO J*, 16(7):1647–55.

Greenman, C., Stephens, P., Smith, R., Dalgliesh, G. L., Hunter, C., Bignell, G., Davies, H., Teague, J., Butler, A., Stevens, C., Edkins, S., O'Meara, S., Vastrik, I., Schmidt, E. E., Avis, T., Barthorpe, S., Bhamra, G., Buck, G., Choudhury, B., Clements, J., Cole, J., Dicks, E., Forbes, S., Gray, K., Halliday, K., Harrison, R., Hills, K., Hinton, J., Jenkinson, A., Jones, D., Menzies, A., Mironenko, T., Perry, J., Raine, K., Richardson, D., Shepherd, R., Small, A., Tofts, C., Varian, J., Webb, T., West, S., Widaa, S., Yates, A., Cahill, D. P., Louis, D. N., Goldstraw, P., Nicholson, A. G., Brasseur, F., Looijenga, L., Weber, B. L., Chiew, Y. E., DeFazio, A., Greaves, M. F., Green, A. R., Campbell, P., Birney, E., Easton, D. F.,

Chenevix-Trench, G., Tan, M. H., Khoo, S. K., Teh, B. T., Yuen, S. T., Leung, S. Y., Wooster, R., Futreal, P. A., and Stratton, M. R. (2007). Patterns of somatic mutation in human cancer genomes. *Nature*, 446(7132):153–8.

Grubb, R. L., Calvert, V. S., Wulkuhle, J. D., Paweletz, C. P., Linehan, W. M., Phillips, J. L., Chuaqui, R., Valasco, A., Gillespie, J., Emmert-Buck, M., Liotta, L. A., and Petricoin, E. F. (2003). Signal pathway profiling of prostate cancer using reverse phase protein arrays. *Proteomics*, 3(11):2142–6.

Guy, P. M., Platko, J. V., Cantley, L. C., Cerione, R. A., and Carraway, K. L., r. (1994). Insect cell-expressed p180erbB3 possesses an impaired tyrosine kinase activity. *Proc Natl Acad Sci U S A*, 91(17):8132–6.

Gymnopoulos, M., Elsliger, M. A., and Vogt, P. K. (2007). Rare cancer-specific mutations in PIK3CA show gain of function. *Proc Natl Acad Sci U S A*, 104(13):5569–74.

Hall, J. M., Lee, M. K., Newman, B., Morrow, J. E., Anderson, L. A., Huey, B., and King, M. C. (1990). Linkage of early-onset familial breast cancer to chromosome 17q21. *Science*, 250(4988):1684–9.

Hanahan, D. and Weinberg, R. A. (2000). The hallmarks of cancer. *Cell*, 100(1):57–70.

Harris, R. C., Chung, E., and Coffey, R. J. (2003). EGF receptor ligands. *Exp Cell Res*, 284(1):2–13.

Hartwell, L. H., Szankasi, P., Roberts, C. J., Murray, A. W., and Friend, S. H. (1997). Integrating genetic approaches into the discovery of anticancer drugs. *Science*, 278(5340):1064–8.

Hastie, T. (2010). *gam: Generalized Additive Models*. R package version 1.03.

Henjes, F. (2006). Quantifizierung der MAPK (Mitogen-aktivierte Proteinkinase) in humanen Brustkrebszelllinien mit Hilfe von miniaturisierten Immunoassays. Diploma thesis, University Bielefeld.

Holbro, T., Civenni, G., and Hynes, N. E. (2003). The ErbB receptors and their role in cancer progression. *Exp Cell Res*, 284(1):99–110.

Hommelgaard, A. M., Lerdrup, M., and van Deurs, B. (2004). Association with membrane protrusions makes ErbB2 an internalization-resistant receptor. *Mol Biol Cell*, 15(4):1557–67.

Hudelist, G., Kostler, W. J., Attems, J., Czerwenka, K., Muller, R., Manavi, M., Steger, G. G., Kubista, E., Zielinski, C. C., and Singer, C. F. (2003). Her-2/neu-triggered intracellular tyrosine kinase activation: in vivo relevance of ligand-independent activation mechanisms and impact upon the efficacy of trastuzumab-based treatment. *Br J Cancer*, 89(6):983–91.

Hudelist, G., Kostler, W. J., Czerwenka, K., Kubista, E., Attems, J., Muller, R., Gschwantler-Kaulich, D., Manavi, M., Huber, I., Hoschutzky, H., Zielinski, C. C., and Singer, C. F. (2006). Her-2/neu and EGFR tyrosine kinase activation predict the efficacy of trastuzumab-based therapy in patients with metastatic breast cancer. *Int J Cancer*, 118(5):1126–34.

Hughes, J. B., Berger, C., Rodland, M. S., Hasmann, M., Stang, E., and Madshus, I. H. (2009). Pertuzumab increases epidermal growth factor receptor downregulation by counteracting epidermal growth factor receptor-ErbB2 heterodimerization. *Mol Cancer Ther*, 8(7):1885–92.

Hutcheson, I. R., Knowlden, J. M., Hiscox, S. E., Barrow, D., Gee, J. M., Robertson, J. F., Ellis, I. O., and Nicholson, R. I. (2007). Heregulin beta1 drives gefitinib-resistant growth and invasion in tamoxifen-resistant MCF-7 breast cancer cells. *Breast Cancer Res*, 9(4):R50.

Hynes, N. E. and Lane, H. A. (2005). ERBB receptors and cancer: the complexity of targeted inhibitors. *Nat Rev Cancer*, 5(5):341–54.

Isakoff, S. J., Engelman, J. A., Irie, H. Y., Luo, J., Brachmann, S. M., Pearline, R. V., Cantley, L. C., and Brugge, J. S. (2005). Breast cancer-associated PIK3CA mutations are oncogenic in mammary epithelial cells. *Cancer Res*, 65(23):10992–1000.

Izumi, Y., Xu, L., di Tomaso, E., Fukumura, D., and Jain, R. K. (2002). Tumour biology: herceptin acts as an anti-angiogenic cocktail. *Nature*, 416(6878):279–80.

Jackson, J. G., St Clair, P., Sliwkowski, M. X., and Brattain, M. G. (2004). Blockade of epidermal growth factor- or heregulin-dependent ErbB2 activation with the anti-ErbB2 monoclonal antibody 2C4 has divergent downstream signaling and growth effects. *Cancer Res*, 64(7):2601–9.

Jimeno, A. and Hidalgo, M. (2006). Multitargeted therapy: can promiscuity be praised in an era of political correctness? *Crit Rev Oncol Hematol*, 59(2):150–8.

Joecker, A., Sonntag, J., Henjes, F., Goetschel, F., Tresch, A., Beissbarth, T., Wiemann, S., and Korf, U. (2010). QuantProReloaded: Quantitative Analysis of Microspot Immunoassays. *Bioinformatics*.

Jones, R. B., Gordus, A., Krall, J. A., and MacBeath, G. (2006). A quantitative protein interaction network for the ErbB receptors using protein microarrays. *Nature*, 439(7073):168–74.

Junttila, T. T., Akita, R. W., Parsons, K., Fields, C., Lewis Phillips, G. D., Friedman, L. S., Sampath, D., and Sliwkowski, M. X. (2009). Ligand-independent HER2/HER3/PI3K complex is disrupted by trastuzumab and is effectively inhibited by the PI3K inhibitor GDC-0941. *Cancer Cell*, 15(5):429–40.

Kaminski, R., Zagozdzon, R., Fu, Y., Mroz, P., Fu, W., Seng, S., Avraham, S., and Avraham, H. K. (2006). Role of SRC kinases in Neu-induced tumorigenesis: challenging the paradigm using Csk homologous kinase transgenic mice. *Cancer Res*, 66(11):5757–62.

Karaman, M. W., Herrgard, S., Treiber, D. K., Gallant, P., Atteridge, C. E., Campbell, B. T., Chan, K. W., Ciceri, P., Davis, M. I., Edeen, P. T., Faraoni, R., Floyd, M., Hunt, J. P., Lockhart, D. J., Milanov, Z. V., Morrison, M. J., Pallares, G., Patel, H. K., Pritchard, S., Wodicka, L. M., and Zarrinkar, P. P. (2008). A quantitative analysis of kinase inhibitor selectivity. *Nat Biotechnol*, 26(1):127–32.

Karunagaran, D., Tzahar, E., Beerli, R. R., Chen, X., Graus-Porta, D., Ratzkin, B. J., Seger, R., Hynes, N. E., and Yarden, Y. (1996). ErbB-2 is a common auxiliary subunit of NDF and EGF receptors: implications for breast cancer. *EMBO J*, 15(2):254–64.

Kataoka, Y., Mukohara, T., Shimada, H., Saijo, N., Hirai, M., and Minami, H. (2009). Association between gain-of-function mutations in PIK3CA and resistance to HER2-targeted agents in HER2-amplified breast cancer cell lines. *Ann Oncol*, 21(2):255–62.

Kauraniemi, P., Barlund, M., Monni, O., and Kallioniemi, A. (2001). New amplified and highly expressed genes discovered in the ERBB2 amplicon in breast cancer by cDNA microarrays. *Cancer Res*, 61(22):8235–40.

Kinkade, C. W., Castillo-Martin, M., Puzio-Kuter, A., Yan, J., Foster, T. H., Gao, H., Sun, Y., Ouyang, X., Gerald, W. L., Cordon-Cardo, C., and Abate-Shen, C. (2008). Targeting AKT/mTOR and ERK MAPK signaling inhibits hormone-refractory prostate cancer in a preclinical mouse model. *J Clin Invest*, 118(9):3051–64.

Klos, K. S., Wyszomierski, S. L., Sun, M., Tan, M., Zhou, X., Li, P., Yang, W., Yin, G., Hittelman, W. N., and Yu, D. (2006). ErbB2 increases vascular endothelial growth factor protein synthesis via activation of mammalian target of rapamycin/p70S6K leading to increased angiogenesis and spontaneous metastasis of human breast cancer cells. *Cancer Res*, 66(4):2028–37.

Kokai, Y., Myers, J. N., Wada, T., Brown, V. I., LeVea, C. M., Davis, J. G., Dobashi, K., and Greene, M. I. (1989). Synergistic interaction of p185c-neu and the EGF receptor leads to transformation of rodent fibroblasts. *Cell*, 58(2):287–92.

Korf, U., Derdak, S., Tresch, A., Henjes, F., Schumacher, S., Schmidt, C., Hahn, B., Lehmann, W. D., Poustka, A., Beissbarth, T., and Klingmuller, U. (2008a). Quantitative protein microarrays for time-resolved measurements of protein phosphorylation. *Proteomics*, 8(21):4603–12.

Korf, U., Henjes, F., Schmidt, C., Tresch, A., Mannsperger, H., Lobke, C., Beissbarth, T., and Poustka, A. (2008b). Antibody microarrays as an experimental platform for the analysis of signal transduction networks. *Adv Biochem Eng Biotechnol*, 110:153–75.

Kraus, M. H., Issing, W., Miki, T., Popescu, N. C., and Aaronson, S. A. (1989). Isolation and characterization of ERBB3, a third member of the ERBB/epidermal growth factor receptor family: evidence for overexpression in a subset of human mammary tumors. *Proc Natl Acad Sci U S A*, 86(23):9193–7.

Kriegs, M., Kasten-Pisula, U., Rieckmann, T., Holst, K., Saker, J., Dahm-Daphi, J., and Dikomey, E. (2010). The epidermal growth factor receptor modulates DNA double-strand break repair by regulating non-homologous end-joining. *DNA Repair (Amst)*.

Krop, I. E., Beeram, M., Modi, S., Jones, S. F., Holden, S. N., Yu, W., Girish, S., Tibbitts, J., Yi, J. H., Sliwkowski, M. X., Jacobson, F., Lutzker, S. G., and Burris, H. A. (2010). Phase I study of trastuzumab-DM1, an HER2 antibody-drug conjugate, given every 3 weeks to patients with HER2-positive metastatic breast cancer. *J Clin Oncol*, 28(16):2698–704.

Laemmli, U. K. (1970). Cleavage of structural proteins during the assembly of the head of bacteriophage T4. *Nature*, 227(5259):680–5.

Lane, H. A., Beuvink, I., Motoyama, A. B., Daly, J. M., Neve, R. M., and Hynes, N. E. (2000). ErbB2 potentiates breast tumor proliferation through modulation of p27(Kip1)-Cdk2 complex formation: receptor overexpression does not determine growth dependency. *Mol Cell Biol*, 20(9):3210–23.

Le, X. F., Vadlamudi, R., McWatters, A., Bae, D. S., Mills, G. B., Kumar, R., and Bast, R. C., J. (2000). Differential signaling by an anti-p185(HER2) antibody and heregulin. *Cancer Res*, 60(13):3522–31.

Leary, A. F., Hanna, W. M., van de Vijver, M. J., Penault-Llorca, F., Ruschoff, J., Osamura, R. Y., Bilous, M., and Dowsett, M. (2009). Value and limitations of measuring HER-2 extracellular domain in the serum of breast cancer patients. *J Clin Oncol*, 27(10):1694–705.

Lehman, J. A., Calvo, V., and Gomez-Cambronero, J. (2003). Mechanism of ribosomal p70S6 kinase activation by granulocyte macrophage colony-stimulating factor in neutrophils: cooperation of a MEK-related, THR421/SER424 kinase and a rapamycin-sensitive, m-TOR-related THR389 kinase. *J Biol Chem*, 278(30):28130–8.

Lemmon, M. A. (2009). Ligand-induced ErbB receptor dimerization. *Exp Cell Res*, 315(4):638–48.

Lenferink, A. E., Pinkas-Kramarski, R., van de Poll, M. L., van Vugt, M. J., Klapper, L. N., Tzahar, E., Waterman, H., Sela, M., van Zoelen, E. J., and Yarden, Y. (1998). Differential endocytic routing of homo- and hetero-dimeric ErbB tyrosine kinases confers signaling superiority to receptor heterodimers. *EMBO J*, 17(12):3385–97.

Liu, W., Zhou, Y., Reske, S. N., and Shen, C. (2008). PTEN mutation: many birds with one stone in tumorigenesis. *Anticancer Res*, 28(6A):3613–9.

Liu, X., Robinson, G. W., and Hennighausen, L. (1996). Activation of Stat5a and Stat5b by tyrosine phosphorylation is tightly linked to mammary gland differentiation. *Mol Endocrinol*, 10(12):1496–506.

Loebke, C., Sueltmann, H., Schmidt, C., Henjes, F., Wiemann, S., Poustka, A., and Korf, U. (2007). Infrared-based protein detection arrays for quantitative proteomics. *Proteomics*, 7(4):558–64.

Longva, K. E., Pedersen, N. M., Haslekas, C., Stang, E., and Madshus, I. H. (2005). Herceptin-induced inhibition of ErbB2 signaling involves reduced phosphorylation of Akt but not endocytic down-regulation of ErbB2. *Int J Cancer*, 116(3):359–67.

Lu, Y., Zi, X., Zhao, Y., Mascarenhas, D., and Pollak, M. (2001). Insulin-like growth factor-I receptor signaling and resistance to trastuzumab (Herceptin). *J Natl Cancer Inst*, 93(24):1852–7.

Maira, S. M., Stauffer, F., Brueggen, J., Furet, P., Schnell, C., Fritsch, C., Brachmann, S., Chene, P., De Pover, A., Schoemaker, K., Fabbro, D., Gabriel, D., Simonen, M., Murphy, L., Finan, P., Sellers, W., and Garcia-Echeverria, C. (2008). Identification and characterization of NVP-BEZ235, a new orally available dual phosphatidylinositol 3-kinase/mammalian target of rapamycin inhibitor with potent in vivo antitumor activity. *Mol Cancer Ther*, 7(7):1851–63.

Mallon, R., Hollander, I., Feldberg, L., Lucas, J., Soloveva, V., Venkatesan, A., Dehnhardt, C., Delos Santos, E., Chen, Z., Dos Santos, O., Ayral-Kaloustian, S., and Gibbons, J. (2010). Antitumor efficacy profile of PKI-402, a dual phosphatidylinositol 3-kinase/mammalian target of rapamycin inhibitor. *Mol Cancer Ther*, 9(4):976–84.

Mannsperger, H. A., Gade, S., Henjes, F., Beissbarth, T., and Korf, U. (2010). RPPanalyzer: Analysis of reverse-phase protein array data. *Bioinformatics*, 26(17):2202–3.

Ming, X. F., Burgering, B. M., Wennstrom, S., Claesson-Welsh, L., Heldin, C. H., Bos, J. L., Kozma, S. C., and Thomas, G. (1994). Activation of p70/p85 S6 kinase by a pathway independent of p21ras. *Nature*, 371(6496):426–9.

Molina, M. A., Codony-Servat, J., Albanell, J., Rojo, F., Arribas, J., and Baselga, J. (2001). Trastuzumab (herceptin), a humanized anti-Her2 receptor monoclonal antibody, inhibits basal and activated Her2 ectodomain cleavage in breast cancer cells. *Cancer Res*, 61(12):4744–9.

Moulder, S. L., Yakes, F. M., Muthuswamy, S. K., Bianco, R., Simpson, J. F., and Arteaga, C. L. (2001). Epidermal growth factor receptor (HER1) tyrosine kinase inhibitor ZD1839 (Iressa) inhibits HER2/neu (erbB2)-overexpressing breast cancer cells in vitro and in vivo. *Cancer Res*, 61(24):8887–95.

Mullen, P., Cameron, D. A., Hasmann, M., Smyth, J. F., and Langdon, S. P. (2007). Sensitivity to pertuzumab (2C4) in ovarian cancer models: cross-talk with estrogen receptor signaling. *Mol Cancer Ther*, 6(1):93–100.

Nagata, Y., Lan, K. H., Zhou, X., Tan, M., Esteva, F. J., Sahin, A. A., Klos, K. S., Li, P., Monia, B. P., Nguyen, N. T., Hortobagyi, G. N., Hung, M. C., and Yu, D. (2004). PTEN activation contributes to tumor inhibition by trastuzumab, and loss of PTEN predicts trastuzumab resistance in patients. *Cancer Cell*, 6(2):117–27.

Nahta, R., Takahashi, T., Ueno, N. T., Hung, M. C., and Esteva, F. J. (2004). P27(kip1) down-regulation is associated with trastuzumab resistance in breast cancer cells. *Cancer Res*, 64(11):3981–6.

Nahta, R., Yuan, L. X., Zhang, B., Kobayashi, R., and Esteva, F. J. (2005). Insulin-like growth factor-I receptor/human epidermal growth factor receptor 2 heterodimerization contributes to trastuzumab resistance of breast cancer cells. *Cancer Res*, 65(23):11118–28.

Nevalainen, M. T., Xie, J., Torhorst, J., Bubendorf, L., Haas, P., Kononen, J., Sauter, G., and Rui, H. (2004). Signal transducer and activator of transcription-5 activation and breast cancer prognosis. *J Clin Oncol*, 22(11):2053–60.

O'Brien, N. A., Browne, B. C., Chow, L., Wang, Y., Ginther, C., Arboleda, J., Duffy, M. J., Crown, J., O'Donovan, N., and Slamon, D. J. (2010). Activated Phosphoinositide 3-Kinase/AKT Signaling Confers Resistance to Trastuzumab but not Lapatinib. *Mol Cancer Ther*, 9(6):1489–502.

O'Reilly, K. E., Rojo, F., She, Q. B., Solit, D., Mills, G. B., Smith, D., Lane, H., Hofmann, F., Hicklin, D. J., Ludwig, D. L., Baselga, J., and Rosen, N. (2006). mTOR inhibition induces upstream receptor tyrosine kinase signaling and activates Akt. *Cancer Res*, 66(3):1500–8.

Paweletz, C. P., Charboneau, L., Bichsel, V. E., Simone, N. L., Chen, T., Gillespie, J. W., Emmert-Buck, M. R., Roth, M. J., Petricoin, I. E., and Liotta, L. A. (2001). Reverse phase protein microarrays which capture disease progression show activation of pro-survival pathways at the cancer invasion front. *Oncogene*, 20(16):1981–9.

Pennell, N. A. and Lynch, T. J., J. (2009). Combined inhibition of the VEGFR and EGFR signaling pathways in the treatment of NSCLC. *Oncologist*, 14(4):399–411.

Perez-Tenorio, G., Alkhori, L., Olsson, B., Waltersson, M. A., Nordenskjold, B., Rutqvist, L. E., Skoog, L., and Stal, O. (2007). PIK3CA mutations and PTEN loss correlate with similar prognostic factors and are not mutually exclusive in breast cancer. *Clin Cancer Res*, 13(12):3577–84.

Perou, C. M., Sorlie, T., Eisen, M. B., van de Rijn, M., Jeffrey, S. S., Rees, C. A., Pollack, J. R., Ross, D. T., Johnsen, H., Akslen, L. A., Fluge, O., Pergamenschikov, A., Williams, C., Zhu, S. X., Lonning, P. E., Borresen-Dale, A. L., Brown, P. O., and Botstein, D. (2000). Molecular portraits of human breast tumours. *Nature*, 406(6797):747–52.

Pinkas-Kramarski, R., Soussan, L., Waterman, H., Levkowitz, G., Alroy, I., Klapper, L., Lavi, S., Seger, R., Ratzkin, B. J., Sela, M., and Yarden, Y. (1996). Diversification of Neu differentiation factor and epidermal growth factor signaling by combinatorial receptor interactions. *EMBO J*, 15(10):2452–67.

Pleasance, E. D., Cheetham, R. K., Stephens, P. J., McBride, D. J., Humphray, S. J., Greenman, C. D., Varela, I., Lin, M. L., Ordonez, G. R., Bignell, G. R., Ye, K., Alipaz, J., Bauer, M. J., Beare, D., Butler, A., Carter, R. J., Chen, L., Cox, A. J., Edkins, S., Kokko-Gonzales, P. I., Gormley, N. A., Grocock, R. J., Haudenschild, C. D., Hims, M. M., James, T., Jia, M., Kingsbury, Z., Leroy, C., Marshall, J., Menzies, A., Mudie, L. J., Ning, Z., Royce, T., Schulz-Trieglaff, O. B., Spiridou, A., Stebbings, L. A., Szajkowski, L., Teague, J., Williamson, D., Chin, L., Ross, M. T., Campbell, P. J., Bentley, D. R., Futreal, P. A., and Stratton, M. R. (2010). A comprehensive catalogue of somatic mutations from a human cancer genome. *Nature*, 463(7278):191–6.

Plowman, G. D., Culouscou, J. M., Whitney, G. S., Green, J. M., Carlton, G. W., Foy, L., Neubauer, M. G., and Shoyab, M. (1993). Ligand-specific activation of HER4/p180erbB4, a fourth member of the epidermal growth factor receptor family. *Proc Natl Acad Sci U S A*, 90(5):1746–50.

Plowman, G. D., Whitney, G. S., Neubauer, M. G., Green, J. M., McDonald, V. L., Todaro, G. J., and Shoyab, M. (1990). Molecular cloning and expression of an additional epidermal growth factor receptor-related gene. *Proc Natl Acad Sci U S A*, 87(13):4905–9.

Pohl, M., Stricker, I., Schoeneck, A., Schulmann, K., Klein-Scory, S., Schwarte-Waldhoff, I., Hasmann, M., Tannapfel, A., Schmiegel, W., and Reinacher-Schick, A. (2009). Antitumor activity of the HER2 dimerization inhibitor pertuzumab on human colon cancer cells in vitro and in vivo. *J Cancer Res Clin Oncol*, 135(10):1377–86.

R Development Core Team (2010). *R: A Language and Environment for Statistical Computing*. R Foundation for Statistical Computing, Vienna, Austria. ISBN 3-900051-07-0.

Reinhard, C., Fernandez, A., Lamb, N. J., and Thomas, G. (1994). Nuclear localization of p85s6k: functional requirement for entry into S phase. *EMBO J*, 13(7):1557–65.

Riese, D. J., n., van Raaij, T. M., Plowman, G. D., Andrews, G. C., and Stern, D. F. (1995). The cellular response to neuregulins is governed by complex interactions of the erbB receptor family. *Mol Cell Biol*, 15(10):5770–6.

Rotin, D., Margolis, B., Mohammadi, M., Daly, R. J., Daum, G., Li, N., Fischer, E. H., Burgess, W. H., Ullrich, A., and Schlessinger, J. (1992). SH2 domains prevent tyrosine dephosphorylation of the EGF receptor: identification of Tyr992 as the high-affinity binding site for SH2 domains of phospholipase C gamma. *EMBO J*, 11(2):559–67.

Roux, P. P., Shahbazian, D., Vu, H., Holz, M. K., Cohen, M. S., Taunton, J., Sonenberg, N., and Blenis, J. (2007). RAS/ERK signaling promotes site-specific ribosomal protein S6 phosphorylation via RSK and stimulates cap-dependent translation. *J Biol Chem*, 282(19):14056–64.

Ryan, A. J. and Wedge, S. R. (2005). ZD6474–a novel inhibitor of VEGFR and EGFR tyrosine kinase activity. *Br J Cancer*, 92 Suppl 1:S6–13.

Saal, L. H., Holm, K., Maurer, M., Memeo, L., Su, T., Wang, X., Yu, J. S., Malmstrom, P. O., Mansukhani, M., Enoksson, J., Hibshoosh, H., Borg, A., and Parsons, R. (2005). PIK3CA mutations correlate with hormone receptors, node metastasis, and ERBB2, and are mutually exclusive with PTEN loss in human breast carcinoma. *Cancer Res*, 65(7):2554–9.

Sahin, O., Frohlich, H., Lobke, C., Korf, U., Burmester, S., Majety, M., Mattern, J., Schupp, I., Chaouiya, C., Thieffry, D., Poustka, A., Wiemann, S., Beissbarth, T., and Arlt, D. (2009). Modeling ERBB receptor-regulated G1/S transition to find novel targets for de novo trastuzumab resistance. *BMC Syst Biol*, 3:1.

Sakai, K., Yokote, H., Murakami-Murofushi, K., Tamura, T., Saijo, N., and Nishio, K. (2007). Pertuzumab, a novel HER dimerization inhibitor, inhibits the growth of human lung cancer cells mediated by the HER3 signaling pathway. *Cancer Sci*, 98(9):1498–503.

Santen, R. J., Song, R. X., McPherson, R., Kumar, R., Adam, L., Jeng, M. H., and Yue, W. (2002). The role of mitogen-activated protein (MAP) kinase in breast cancer. *J Steroid Biochem Mol Biol*, 80(2):239–56.

Sarbassov, D. D., Guertin, D. A., Ali, S. M., and Sabatini, D. M. (2005). Phosphorylation and regulation of Akt/PKB by the rictor-mTOR complex. *Science*, 307(5712):1098–101.

Sarup, J. C., Johnson, R. M., King, K. L., Fendly, B. M., Lipari, M. T., Napier, M. A., Ullrich, A., and Shepard, H. M. (1991). Characterization of an anti-p185HER2 monoclonal antibody that stimulates receptor function and inhibits tumor cell growth. *Growth Regul*, 1(2):72–82.

Scheuer, W., Friess, T., Burtscher, H., Bossenmaier, B., Endl, J., and Hasmann, M. (2009). Strongly enhanced antitumor activity of trastuzumab and pertuzumab combination treatment on HER2-positive human xenograft tumor models. *Cancer Res*, 69(24):9330–6.

Schulze, W. X., Deng, L., and Mann, M. (2005). Phosphotyrosine interactome of the ErbB-receptor kinase family. *Mol Syst Biol*, 1:2005 0008.

Scott, G. K., Dodson, J. M., Montgomery, P. A., Johnson, R. M., Sarup, J. C., Wong, W. L., Ullrich, A., Shepard, H. M., and Benz, C. C. (1991). p185HER2 signal transduction in breast cancer cells. *J Biol Chem*, 266(22):14300–5.

Sergina, N. V., Rausch, M., Wang, D., Blair, J., Hann, B., Shokat, K. M., and Moasser, M. M. (2007). Escape from HER-family tyrosine kinase inhibitor therapy by the kinase-inactive HER3. *Nature*, 445(7126):437–41.

Serra, V., Markman, B., Scaltriti, M., Eichhorn, P. J., Valero, V., Guzman, M., Botero, M. L., Llonch, E., Atzori, F., Di Cosimo, S., Maira, M., Garcia-Echeverria, C., Parra, J. L., Arribas, J., and Baselga, J. (2008). NVP-BEZ235, a dual PI3K/mTOR inhibitor, prevents PI3K signaling and inhibits the growth of cancer cells with activating PI3K mutations. *Cancer Res*, 68(19):8022–30.

Shattuck, D. L., Miller, J. K., Carraway, K. L., r., and Sweeney, C. (2008). Met receptor contributes to trastuzumab resistance of Her2-overexpressing breast cancer cells. *Cancer Res*, 68(5):1471–7.

She, Q. B., Chandarlapaty, S., Ye, Q., Lobo, J., Haskell, K. M., Leander, K. R., DeFeo-Jones, D., Huber, H. E., and Rosen, N. (2008). Breast tumor cells with PI3K mutation or HER2 amplification are selectively addicted to Akt signaling. *PLoS One*, 3(8):e3065.

Shi, F., Telesco, S. E., Liu, Y., Radhakrishnan, R., and Lemmon, M. A. (2010). ErbB3/HER3 intracellular domain is competent to bind ATP and catalyze autophosphorylation. *Proc Natl Acad Sci U S A*, 107(17):7692–7.

Slamon, D. J., Clark, G. M., Wong, S. G., Levin, W. J., Ullrich, A., and McGuire, W. L. (1987). Human breast cancer: correlation of relapse and survival with amplification of the HER-2/neu oncogene. *Science*, 235(4785):177–82.

Sorlie, T. (2004). Molecular portraits of breast cancer: tumour subtypes as distinct disease entities. *Eur J Cancer*, 40(18):2667–75.

Sorlie, T., Perou, C. M., Tibshirani, R., Aas, T., Geisler, S., Johnsen, H., Hastie, T., Eisen, M. B., van de Rijn, M., Jeffrey, S. S., Thorsen, T., Quist, H., Matese, J. C., Brown, P. O., Botstein, D., Eystein Lonning, P., and Borresen-Dale, A. L. (2001). Gene expression patterns of breast carcinomas distinguish tumor subclasses with clinical implications. *Proc Natl Acad Sci U S A*, 98(19):10869–74.

Stein, R. A. and Staros, J. V. (2000). Evolutionary analysis of the ErbB receptor and ligand families. *J Mol Evol*, 50(5):397–412.

Stratton, M. R., Campbell, P. J., and Futreal, P. A. (2009). The cancer genome. *Nature*, 458(7239):719–24.

Szabó, V. (2009). Impact of targeted therapeutics on ERBB receptor network activation in the human breast cancer cell line BT474 applying quantitative microarrays. Master's thesis, Ruprecht-Karls-Universität Heidelberg.

Tai, Y. C. and Speed, T. P. (2009). On gene ranking using replicated microarray time course data. *Biometrics*, 65(1):40–51.

Takai, N., Jain, A., Kawamata, N., Popoviciu, L. M., Said, J. W., Whittaker, S., Miyakawa, I., Agus, D. B., and Koeffler, H. P. (2005). 2C4, a monoclonal antibody against HER2, disrupts the HER kinase signaling pathway and inhibits ovarian carcinoma cell growth. *Cancer*, 104(12):2701–8.

Tan, M., Li, P., Klos, K. S., Lu, J., Lan, K. H., Nagata, Y., Fang, D., Jing, T., and Yu, D. (2005). ErbB2 promotes Src synthesis and stability: novel mechanisms of Src activation that confer breast cancer metastasis. *Cancer Res*, 65(5):1858–67.

Thor, A. D., Liu, S., Edgerton, S., Moore, D., n., Kasowitz, K. M., Benz, C. C., Stern, D. F., and DiGiovanna, M. P. (2000). Activation (tyrosine phosphorylation) of ErbB-2 (HER-2/neu): a study of incidence and correlation with outcome in breast cancer. *J Clin Oncol*, 18(18):3230–9.

Tibes, R., Qiu, Y., Lu, Y., Hennessy, B., Andreeff, M., Mills, G. B., and Kornblau, S. M. (2006). Reverse phase protein array: validation of a novel proteomic technology and utility for analysis of primary leukemia specimens and hematopoietic stem cells. *Mol Cancer Ther*, 5(10):2512–21.

Tikhomirov, O. and Carpenter, G. (2004). Ligand-induced, p38-dependent apoptosis in cells expressing high levels of epidermal growth factor receptor and ErbB-2. *J Biol Chem*, 279(13):12988–96.

Tzahar, E., Waterman, H., Chen, X., Levkowitz, G., Karunagaran, D., Lavi, S., Ratzkin, B. J., and Yarden, Y. (1996). A hierarchical network of interreceptor interactions determines signal transduction by Neu differentiation factor/neuregulin and epidermal growth factor. *Mol Cell Biol*, 16(10):5276–87.

Ueno, Y., Sakurai, H., Tsunoda, S., Choo, M. K., Matsuo, M., Koizumi, K., and Saiki, I. (2008). Heregulin-induced activation of ErbB3 by EGFR tyrosine kinase activity promotes tumor growth and metastasis in melanoma cells. *Int J Cancer*, 123(2):340–7.

Ullrich, A., Coussens, L., Hayflick, J. S., Dull, T. J., Gray, A., Tam, A. W., Lee, J., Yarden, Y., Libermann, T. A., Schlessinger, J., and et al. (1984). Human epidermal growth factor receptor cDNA sequence and aberrant expression of the amplified gene in A431 epidermoid carcinoma cells. *Nature*, 309(5967):418–25.

Valabrega, G., Montemurro, F., Sarotto, I., Petrelli, A., Rubini, P., Tacchetti, C., Aglietta, M., Comoglio, P. M., and Giordano, S. (2005). TGFalpha expression impairs Trastuzumab-induced HER2 downregulation. *Oncogene*, 24(18):3002–10.

van der Heijden, M. S. and Bernards, R. (2010). Inhibition of the PI3K pathway: hope we can believe in? *Clin Cancer Res*, 16(12):3094–9.

Vogel, C. L., Cobleigh, M. A., Tripathy, D., Gutheil, J. C., Harris, L. N., Fehrenbacher, L., Slamon, D. J., Murphy, M., Novotny, W. F., Burchmore, M., Shak, S., Stewart, S. J., and Press, M. (2002). Efficacy and safety of trastuzumab as a single agent in first-line treatment of HER2-overexpressing metastatic breast cancer. *J Clin Oncol*, 20(3):719–26.

Wallasch, C., Weiss, F. U., Niederfellner, G., Jallal, B., Issing, W., and Ullrich, A. (1995). Heregulin-dependent regulation of HER2/neu oncogenic signaling by heterodimerization with HER3. *EMBO J*, 14(17):4267–75.

Wang, S. E., Xiang, B., Guix, M., Olivares, M. G., Parker, J., Chung, C. H., Pandiella, A., and Arteaga, C. L. (2008). Transforming growth factor beta engages TACE and ErbB3 to activate phosphatidylinositol-3 kinase/Akt in ErbB2-overexpressing breast cancer and desensitizes cells to trastuzumab. *Mol Cell Biol*, 28(18):5605–20.

Wang, Z., Zhang, L., Yeung, T. K., and Chen, X. (1999). Endocytosis deficiency of epidermal growth factor (EGF) receptor-ErbB2 heterodimers in response to EGF stimulation. *Mol Biol Cell*, 10(5):1621–36.

Ward, H. W. (1973). Anti-oestrogen therapy for breast cancer: a trial of tamoxifen at two dose levels. *Br Med J*, 1(5844):13–4.

Wehrman, T. S., Raab, W. J., Casipit, C. L., Doyonnas, R., Pomerantz, J. H., and Blau, H. M. (2006). A system for quantifying dynamic protein interactions defines a role for Herceptin in modulating ErbB2 interactions. *Proc Natl Acad Sci U S A*, 103(50):19063–8.

Weng, Q. P., Kozlowski, M., Belham, C., Zhang, A., Comb, M. J., and Avruch, J. (1998). Regulation of the p70 S6 kinase by phosphorylation in vivo. Analysis using site-specific anti-phosphopeptide antibodies. *J Biol Chem*, 273(26):16621–9.

Worthylake, R., Opresko, L. K., and Wiley, H. S. (1999). ErbB-2 amplification inhibits down-regulation and induces constitutive activation of both ErbB-2 and epidermal growth factor receptors. *J Biol Chem*, 274(13):8865–74.

Wulfkuhle, J. D., Speer, R., Pierobon, M., Laird, J., Espina, V., Deng, J., Mammano, E., Yang, S. X., Swain, S. M., Nitti, D., Esserman, L. J., Belluco, C., Liotta, L. A., and Petricoin, E. F., r. (2008). Multiplexed cell signaling analysis of human breast cancer applications for personalized therapy. *J Proteome Res*, 7(4):1508–17.

Xia, W., Liu, L. H., Ho, P., and Spector, N. L. (2004). Truncated ErbB2 receptor (p95ErbB2) is regulated by heregulin through heterodimer formation with ErbB3 yet remains sensitive to the dual EGFR/ErbB2 kinase inhibitor GW572016. *Oncogene*, 23(3):646–53.

Yakes, F. M., Chinratanalab, W., Ritter, C. A., King, W., Seelig, S., and Arteaga, C. L. (2002). Herceptin-induced inhibition of phosphatidylinositol-3 kinase and Akt Is required for antibody-mediated effects on p27, cyclin D1, and antitumor action. *Cancer Res*, 62(14):4132–41.

Yamamoto, T., Ikawa, S., Akiyama, T., Semba, K., Nomura, N., Miyajima, N., Saito, T., and Toyoshima, K. (1986). Similarity of protein encoded by the human c-erb-B-2 gene to epidermal growth factor receptor. *Nature*, 319(6050):230–4.

Yang, C., Liu, Y., Lemmon, M. A., and Kazanietz, M. G. (2006). Essential role for Rac in heregulin beta1 mitogenic signaling: a mechanism that involves epidermal growth factor receptor and is independent of ErbB4. *Mol Cell Biol*, 26(3):831–42.

Yang, Q. and Guan, K. L. (2007). Expanding mTOR signaling. *Cell Res*, 17(8):666–81.

Yarden, Y. and Sliwkowski, M. X. (2001). Untangling the ErbB signalling network. *Nat Rev Mol Cell Biol*, 2(2):127–37.

Ye, D., Mendelsohn, J., and Fan, Z. (1999). Augmentation of a humanized anti-HER2 mAb 4D5 induced growth inhibition by a human-mouse chimeric anti-EGF receptor mAb C225. *Oncogene*, 18(3):731–8.

Zhang, D. J., Ward, A., Tschulena, U., Bechtel, S., Uhlmann, S., Sahin, O., and Wiemann, S. (2010). *flowDeconvolutor: open-source solution to flow cytometry cell cycle analysis in R and Bioconductor*. submitted.

Zurita, A. J., Troncoso, P., Cardo-Vila, M., Logothetis, C. J., Pasqualini, R., and Arap, W. (2004). Combinatorial screenings in patients: the interleukin-11 receptor alpha as a candidate target in the progression of human prostate cancer. *Cancer Res*, 64(2):435–9.

Die hier vorgelegte Dissertation habe ich eigenständig und ohne unerlaubte Hilfe angefertigt. Die Dissertation wurde in der vorgelegten oder ähnlicher Form bei keiner anderen Institution eingereicht. Ich habe bisher keine erfolglosen Promotionsversuche unternommen.

Heidelberg, den 14.09.2010

Frauke Henjes